Channel Estimation and Equalization for Cooperative Communication

by

Hakam Mheidat

A thesis

presented to the University of Waterloo

in fulfillment of the

thesis requirement for the degree of

Doctor of Philosophy

in

Electrical and Computer Engineering

Waterloo, Ontario, Canada, 2006

I hereby declare that I am the sole author of this thesis. This is a true copy of the thesis, including any required final revisions, as accepted by my examiners.

I understand that my thesis may be made electronically available to the public.

Abstract

The revolutionary concept of space-time coding introduced in the last decade has demonstrated that the deployment of multiple antennas at the transmitter allows for simultaneous increase in throughput and reliability because of the additional degrees of freedom offered by the spatial dimension of the wireless channel. However, the use of antenna arrays is not practical for deployment in some practical scenarios, e.g., sensor networks, due to space and power limitations.

A new form of realizing transmit diversity has been recently introduced under the name of *user* cooperation or *cooperative* diversity. The basic idea behind cooperative diversity rests on the observation that in a wireless environment, the signal transmitted by the source node is overheard by other nodes, which can be defined as “partners” or “relays”. The source and its partners can jointly process and transmit their information, creating a “*virtual antenna array*” and therefore emulating transmit diversity.

Most of the ongoing research efforts in cooperative diversity assume frequency flat channels with perfect channel knowledge. However, in practical scenarios, e.g. broadband wireless networks, these assumptions do not apply. Frequency-selective fading and imperfect channel knowledge should be considered as a more realistic channel model. The development of equalization and channel estimation algorithms play a crucial element in the design of digital receivers as their accuracy determine the overall performance.

This dissertation creates a framework for designing and analyzing various time and frequency domain equalization schemes, i.e. distributed time reversal (D-TR) STBC, distributed single carrier frequency domain (D-SC-FDE) STBC, and distributed orthogonal frequency division multiplexing (D-OFDM) STBC schemes, for broadband cooperative communication systems. Exploiting the orthogonally embedded in D-STBCs, we were able

to maintain low-decoding complexity for all underlying schemes, thus, making them excellent candidates for practical scenarios, such as multi-media broadband communication systems.

Furthermore, we propose and analyze *various* non-coherent and channel estimation algorithms to improve the quality and reliability of wireless communication networks. Specifically, we derive a non-coherent decoding rule which can be implemented in practice by a Viterbi-type algorithm. We demonstrate through the derivation of a pairwise error probability expression that the proposed non-coherent detector guarantees full diversity. Although this decoding rule has been derived assuming quasi-static channels, its inherent channel tracking capability allows its deployment over time-varying channels with a promising performance as a sub-optimal solution. As a possible alternative to non-coherent detection, we also investigate the performance of mismatched-coherent receiver, i.e., coherent detection with imperfect channel estimation. Our performance analysis demonstrates that the mismatched-coherent receiver is able to collect the full diversity as its non-coherent competitor over quasi-static channels.

Finally, we investigate and analyze the effect of multiple antennas deployment at the cooperating terminals assuming different relaying techniques. We derive pairwise error probability expressions quantifying analytically the impact of multiple antenna deployment at the source, relay and/or destination terminals on the diversity order for each of the relaying methods under consideration.

Acknowledgments

I would like to express my sincere gratitude to my supervisor Professor Murat Uysal whose valuable support, advice and comments made this work possible. Murat is truly an endless source of creative ideas. His tireless efforts, advice and guidance helped me learn valuable lessons which would definitely help me greatly in my future career.

Many thanks are due to the members of my doctoral committee, Prof. Amir K. Khandani, Prof. Samir Elhedhli, Prof. M. Oussama Damen, and Prof. Liang-Liang Xie for their valuable time and efforts. It has been a great honor and pleasure to have Prof. Ravi Adve from the University of Toronto as my external committee member. I am truly honored to have such a great examining committee.

I would like to thank my family, my parents, my brothers and sisters and their families for all of the love, support, and encouragement they have given me throughout this process. I would also like to thank my mother in law Ae ok Chun for treating me like her own son and supporting me. Special thanks to Y. J. Kim, C. D. Park, and Silver Mirror Kim for their support. I have been truly blessed and am extremely grateful to have the family that I have.

Finally, I would like to thank my wife, Hyunjoo Kim, who has been my life glory and motivation. I would like to thank her for her support, help and patience in the process of this work. No one could ask for more than she gives me everyday; she is truly God's miracle in my life.

Dedication

To my parents: *Mohammed and Hekmat*

and

To my beloved wife: *Hyunjoo*

Contents

List of Tables

List of Figures

Abbreviations

AaF	Amplify-and-forward
AWGN	Additive white Gaussian noise
BER	Bit error rate
CP	Cyclic prefix
CSI	Channel state information
DaF	Decode-and-forward
DFT	Discrete Fourier Transform
EDO	The effective diversity order
EGC	Equal gain combining
FFT	Fast Fourier Transform
IFFT	Inverse Fast Fourier Transform
i.i.d	Identical independent distribution
LMMSE	Linear minimum mean square error
MIMO	Multiple-input-multiple-output
MISO	Multi-input-single-output
MRC	Maximal-ratio-combining
ML	Maximum-likelihood
MLSE	Maximum likelihood sequence estimation
OFDM	Orthogonal frequency division multiplexing
PEP	Pairwise error probability
PIR	Pilot insertion rate
PSK	Phase shift keying
QAM	Quadrature amplitude modulation
SC	Selection combining
SC-FDE	Single-carrier frequency domain equalization

SER	Symbol error rate
SIMO	Single-input-multi-output
SNR	Signal-to-Noise Ratio
STBC	Space-time block coding
STTC	Space-time trellis coding
TCM	Trellis-coded modulation
TR	Time reversal
ZP	Zero-padding

Notations

$(.)^*$	Conjugate operation
$(.)^{\mathrm{T}}$	Transpose operation
$(.)^{\mathrm{H}}$	Conjugate transpose operation
$E[.]$	Expectation operation
$tr\{.\}$	Trace operation
$[.]_{k,l}$	The $(k,l)^{th}$ entry of a matrix
$[.]_k$	The k^{th} entry of a vector
$\lvert . \rvert$	The absolute value
$\lVert . \rVert$	Euclidean norm of a vector
$\otimes$	Kronecker product
$*$	Convolution operation
$\mathbf{I}_J$	The identity matrix of size J
$\mathbf{0}_{V\times V}$	All-zero matrix of size $V \times V$.
$\mathbf{Q}$	$J \times J$ FFT matrix whose (l,k) element is given by $\mathbf{Q}(l,k) = 1/\sqrt{J}\exp(-j2\pi l k / J)$ where $0 \le l,k \le J-1$
$\Gamma(.)$	The gamma function
$E_i(.)$	The exponential-integral function
$\lceil . \rceil$	The ceiling function
$\Phi_Y(\omega)$	The characteristic functions of Y
$Q(.)$	The Gaussian-Q function
$\det(.)$	The determinant of a matrix
$\mathrm{diag}(.)$	The diagonal of a matrix
$\Gamma(.,.)$	The incomplete gamma function
$\ln(.)$	The Natural logarithm

Chapter 1

Introduction

A quick glimpse of recent technological history reveals out that mobile communication systems create a new generation roughly every 10 years. First-generation analogue systems were introduced in the early 1980's, then second-generation (2G) digital systems came in the early 1990's. Now third-generation (3G) systems are slowly unfolding all over the world while intensive conceptual and research work toward the definition of a future system has been already started.

2G systems, such as GSM and IS-95, were essentially designed for voice and low data rate applications. In an effort to address customer demands for high-speed data communication, telecommunication companies have been launching 3G systems where the business focus has shifted from voice services to multimedia communication applications over the Internet. Despite the increasing penetration rate of 3G systems in the wireless market, 3G networks are challenged primarily in meeting the requirements imposed by the ever-increasing demands of high-throughput multimedia and internet applications. Additionally, 3G systems consist primarily of wide area networks and thus fall short of supporting heterogeneous networks, including wireless local area networks (LANs) and wireless personal area networks (WPANs).

Several wireless technologies co-exist in the current market customized for different service types, data rates, and users. The next generation systems also known as the fourth gen-

eration (4G) systems are envisioned to accommodate and integrate all existing and future technologies in a single standard. The key feature of the 4G systems would be “high usability” [1]; that is the user would be able to use the system at anytime, anywhere, and with any technology. Users carrying an integrated wireless terminal would have access to a variety of multimedia applications in a reliable environment at lower cost. To meet these demands, next generation wireless communication systems must support high capacity and variable bit rate information (adaptive) transmission with high bandwidth efficiency to conserve limited spectrum resources.

1.1 Diversity Techniques for Fading Channels

The characteristics of wireless channel impose fundamental limitations on the performance of wireless communication systems. The wireless channel can be investigated by composing it into two parts, i.e., large-scale (long-term) impairments including path loss, shadowing and small-scale (short-term) impairment which is commonly referred as fading. The former component is used to predict the average signal power at the receiver side and the transmission coverage area. The latter is due to the multipath propagation which causes random fluctuations in the received signal level and affects the instantaneous signal-to-noise ratio (SNR).

For a typical mobile wireless channel in urban areas where there is no line of sight propagation and the number of scatters is considerably large, the application of central limit theory indicates that the complex fading channel coefficient has two quadrature components which are zero-mean Gaussian random processes. As a result, the amplitude of the fading envelope follows a Rayleigh distribution. In terms of error rate performance, Rayleigh fading converts the exponential dependency of the bit-error probability on the SNR for the classical additive

white Gaussian noise (AWGN) channel into an approximately inverse linear one, resulting in a large SNR penalty.

A common approach to mitigate the degrading effects of fading is the use of diversity techniques. Diversity improves transmission performance by making use of more than one independently faded version of the transmitted signal. If several replicas of the signals are transmitted over multiple channels that exhibit independent fading with comparable strengths, the probability that all the independently faded signal components experience deep fading simultaneously is significantly reduced.

There are various approaches to extract diversity from the wireless channel. The most common methods are briefly summarized as follows [2], [3], [4]:

1.1.1 Time Diversity

In this form of diversity, the same signal is transmitted in different time slots separated by an interval longer than the coherence time of the channel. Channel coding in conjunction with interleaving is an efficient technique to provide time diversity. In fast fading environments where the mobility is high, time diversity becomes very efficient. However, for slow-fading channel (e.g., low mobility environments, fixed-wireless applications), it offers little protection unless significant interleaving delays can be tolerated.

1.1.2 Frequency Diversity

In this form of diversity, the same signal is sent over different frequency carriers, whose separation must be larger than the coherence bandwidth of the channel to ensure independence among diversity channels. Since multiple frequencies are needed, this is generally not a bandwidth-efficient solution. A natural way of frequency diversity, which is sometimes referred to as path diversity, arises for frequency-selective channels. When the multipath delay spread is a significant fraction of the symbol period, the received signal can be interpreted as

a linear combination of the transmitted signal weighted by independent fading coefficients. Therefore, path diversity is obtained by resolving the multipath components at different delays using a RAKE correlator [2], which is the optimum receiver in the MMSE sense designed for this type of channels.

1.1.3 Space Diversity

In this form of diversity, which is also sometimes called as antenna diversity, the receiver and/or transmitter uses multiple antennas. This technique is especially attractive since it does not require extra bandwidth. To extract full diversity advantages, the spacing between antenna elements should be wide enough with respect to the carrier wavelength. The required antenna separation depends on the local scattering environment as well as on the carrier frequency. For a mobile station which is near the ground with many scatters around, the channel decorrelates over shorter distances, and typical antenna separation of half to one carrier wavelength is sufficient. For base stations on high towers, a larger antenna separation of several to tens of wavelengths may be required.

1.1.4 Diversity Combining Techniques

There exist different combining techniques, each of which can be used in conjunction with any of the aforemetioned diversity forms. The most common diversity combining techniques are *selection*, *equal gain* and *maximal ratio* combining [2]. Selection combining (SC) is conceptually the simplest; it consists of selecting at each time, among the available diversity branches (channels), the one with the largest value of SNR. Since it requires only a measure of the powers received from each branch and a switch to choose among the branches, it is relatively easy to implement. However, the fact that it disregards the information obtained from all branches except the selected one indicates its non-optimality. In equal gain combining (EGC), the signals at the output of diversity branches are combined linearly

and the phase of the linear combination are selected to maximize the SNR disregarding the amplitude differences. Since each branch is combined linearly, compared to SC, EGC performs better. In maximal-ratio-combining (MRC), the signals at the output of diversity branches are again combined linearly and the coefficients of the linear combination are selected to maximize the SNR regarding both the phase and the amplitude. The MRC outperforms the other two, since it makes use of the both fading amplitude and phase information. However, the difference between EGC and MRC is not considerably large in terms of power efficiency; therefore, EGC can be preferred where implementation costs are crucial. It should be emphasized that the effectiveness of any diversity scheme rests on the availability of independently faded versions of the transmitted signal so that the probability of two or more relevant versions of the signal undergoing a deep fade is minimum. The reader can refer to [2]-[4] and references therein for a broad overview of diversity combining systems.

1.2 Transmit Diversity

Space diversity, in the form of multiple antenna deployment at the receive side, has been successfully used in uplink transmission (i.e., from mobile station to base station) of the cellular communication systems. However, the use of multiple receive antennas at the mobile handset in the downlink transmission (i.e., from base station to mobile station) is more difficult to implement because of size limitations and the expense of multiple down-conversion of RF paths. This motivates the use of multiple transmit antennas at the base station in the downlink. Since a base station often serves many mobile stations, it is also more economical to add hardware and additional signal processing burden to base stations rather than the mobile handsets. Despite its obvious advantages, transmit diversity has traditionally been viewed as more difficult to exploit, in part because the transmitter is assumed to know less about the channel than the receiver and in part because of the challenging signaling design

problem. Within the last decade, transmit diversity has attracted a great attention and practical solutions to realize transmit diversity advantages have been proposed [4].

The transmit diversity techniques can be classified into two broad categories based on the need for channel state information at the transmit side: Close loop schemes and open loop schemes. The first category uses feedback, either explicitly or implicitly, from the receiver to the transmitter to configure the transmitter. Close loop transmit diversity has more power efficiency compared to open loop transmit diversity. However, it increases the overhead of transmission and therefore is not bandwidth-efficient. Moreover, in practice, vehicle movements or interference causes a mismatch between the state of the channel perceived by the transmitter and that perceived by the receiver, making the feedback unreliable in some situations.

In open loop transmit diversity schemes feedback is not required. They use linear processing at the transmitter to spread the information across multiple antennas. At the receive side, information is recovered by either linear processing or maximum-likelihood decoding techniques. The first of such schemes was proposed by Wittneben [5], [6] where the operating frequency-flat fading channel is converted intentionally into a frequency-selective channel to exploit *artificial* path diversity by means of a maximum-likelihood decoder. It was later shown in [7] that delay diversity schemes are optimal in providing diversity in the sense that the diversity advantage experienced by an optimal receiver is equal to the number of transmit antennas.

The linear filtering used to create delay diversity at the transmitter can be viewed as a channel code which takes binary or integer input and creates real-valued output. Therefore, from a coding perspective, delay diversity schemes correspond to repetition codes and lead to the natural question as to whether more sophisticated codes might be designed. The challenge

of designing channel codes for multiple-antenna systems has led to the introduction of so-called *space-time trellis codes* by Tarokh, Seshadri and Calderbank [8].

1.3 Space-Time Coding

Space-time trellis codes (STTCs) combine the channel code design with symbol mapping onto multiple transmit antennas. The data symbols are cleverly coded across space and time to extract diversity advantages [8]. Figure 1.1 illustrates a space-time coded system. Let space-time code be represented as a $W \times M_S$ matrix, where M_S is the number of transmit antennas and W is the codeword length. Each entry of **X** represents the modulation symbol transmitted from the m_S^{th} ($m_S = 1,2,...M_S$) antenna during the w^{th} ($w = 1,2,...W$) symbol period.

$$\mathbf{X} = \begin{bmatrix} x_1^1 & x_2^1 & \dots & x_{M_S}^1 \\ x_1^2 & \dots & \dots & x_{M_S}^2 \\ \vdots & \dots & \dots & \vdots \\ x_1^W & x_2^W & \dots & x_{M_S}^W \end{bmatrix} \tag{1.1}$$

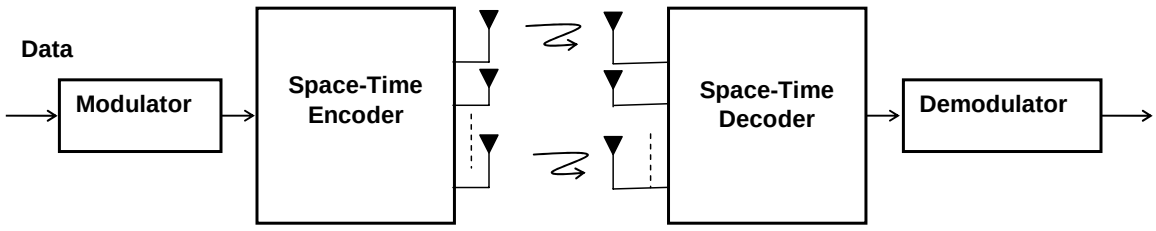

Figure 1.1: Block diagram of a space-time coded system.

The signal at each receive antenna is a superposition of the M_S transmitted signals corrupted by fading. The received signal at the n^{th} antenna within the w^{th} symbol period is given by

$$r_n^w = \sum_{m_S=1}^{M_S} h_{m_S}^n x_{m_S}^w + n_n^w \tag{1.2}$$

where $h_{m_S}^n$ denotes the frequency flat fading coefficient from the $m_S{}^{th}$ transmit antenna to the n^{th} receive antenna. It is modeled as a complex Gaussian random variable with variance 0.5 per dimension leading to the well-known Rayleigh fading channel model. In (1.2), n_n^w models the additive noise term and is zero-mean complex Gaussian random variable with variance $N_0/2$ per dimension. In matrix notation, the received signal can be written as

$$\mathbf{R} = \mathbf{XH} + \mathbf{N} \tag{1.3}$$

where $\mathbf{R}$ is the received signal matrix of size $W \times N$, $\mathbf{H}$ is the channel matrix of size $M_S \times N$, and $\mathbf{N}$ is the additive noise matrix of size $W \times N$.

Assuming coherent detection with perfect channel state information (CSI), i.e., the fading coefficients are perfectly estimated and made available to the receiver, the maximum likelihood (ML) receiver depends on the minimization of the metric

$$\hat{\mathbf{X}} = \arg\min_{\mathbf{X}} \left\| \mathbf{R} - \mathbf{XH} \right\|^2. \tag{1.4}$$

Assume that the ML receiver decodes in favor of another codeword $\hat{\mathbf{X}}$ and let $P\left(\mathbf{X}, \hat{\mathbf{X}}\right)$ denote the pairwise error probability (PEP) which represents the probability of choosing $\hat{\mathbf{X}}$ when indeed $\mathbf{X}$ was transmitted. PEP is the building block for the derivation of union bounds to the error probability. It is widely used in the literature to predict the attainable diversity order where the closed-form error probability expressions are unavailable. In [8], Tarokh et al. derive a Chernoff bound on the PEP for space-time coded systems given by

$$P(\mathbf{X}, \hat{\mathbf{X}}) \le \left(\prod_{j=0}^{r} \lambda_j \right) \left(\frac{E_S}{4N_0} \right)^{-rN} \tag{1.5}$$

where E_S is the average symbol energy, r is the rank of the codeword difference matrix defined by $\mathbf{E} = \left(\mathbf{X} - \hat{\mathbf{X}}\right)\left(\mathbf{X} - \hat{\mathbf{X}}\right)^{\mathrm{H}}$, and λ_j denote the non-zero eigenvalues of $\mathbf{E}$. In (1.5), rN

represents the diversity advantage, (i.e., the slope of the performance curve), while the product of the non-zero eigen values of **E** denotes the coding advantage, (i.e., the horizontal shift of the performance curve). The design criteria for space-time codes are further given in [8]:

Rank criterion: The code difference matrix, taken over all possible combinations of code matrices, should be full rank. This criterion maximizes the diversity gain obtained from the space-time code. The maximum diversity order that can be achieved is $r = \min(W, M_S)$. Therefore, in order to achieve the maximum diversity of $M_S \times N$, **E** must be full rank.

Determinant criterion: The minimum determinant of **E**, taken over all possible combinations of code matrices, should be maximized. This maximizes the coding gain. From (1.5), it can be seen that the diversity gain term dominates the error probability at high SNR. Therefore, the diversity gain should be maximized before the coding gain in the design of a space-time code.

Based on the above criteria, Tarokh et al. [8] proposed some handcrafted codes which perform very well, within the 2-3 dB of the outage capacity derived in [9] for multiple antenna systems. Since Tarokh's pioneering work, there has been an extensive research effort in this area for the design of optimized space-time trellis codes, a few to name are [10]-[12] among many others.

Since every STTC has a well-defined trellis structure, standard soft decision techniques, such as a Viterbi decoder, can be used at the receiver. For a fixed number of transmit antennas, the decoding complexity of STTCs (measured by the number of trellis states at the decoder) increases exponentially with the transmission rate. Space-time block codes (STBCs) [13]-[15] were proposed as an attractive alternative to its trellis counterpart with a much lower decoding complexity. These codes are defined by a mapping operation of a block of input symbols into the space and time domains, transmitting the resulting sequences from different antennas simultaneously. Tarokh et al.'s work in [13] was inspired by Alamouti's

early work [15], where a simple two-branch transmit diversity scheme was presented and shown to provide the same diversity order as MRC with two receive antennas. Alamouti's scheme is appealing in terms of its performance and simplicity. It requires a very simple decoding algorithm based only on linear processing at the receiver. STBCs based on orthogonal designs [13] generalizes Alamouti's scheme to an arbitrary number of transmit antennas still preserving the decoding simplicity and are able to achieve the full diversity at full transmission rate for real signal constellations and at half rate for complex signal constellations such as QAM or PSK. Over the last few years several contributions have been made to further improve the data rate of STBCs, e.g., [16], [17] and the references therein.

Super-orthogonal space-time trellis coding (SO-STTC) [18] is another class of space-time code family. It combines set-partitioning with a super set of orthogonal STBC. While providing full-diversity and full-rate, the structure of these new codes allows the coding gain to be improved over traditional STTC constructions. The underlying orthogonal structure of these codes can be further exploited to decrease the decoding complexity in comparison to original STTC designs. Another class of space-time codes is linear dispersion codes (LDC) [19]. Original LDCs have been original designed to maximize capacity gains and subsume spatial multiplexing, which is a transmission technique offers a linear (in the number of transmit-receive antenna pairs) increase in the transmission rate (or capacity) for the same bandwidth and with no additional power expenditure, and STBCs as special cases. This code family is able to provide an efficient trade-off between multiplexing and diversity gains for arbitrary numbers of transmit and receive antennas [20].

As evidenced by the literal explosion of research papers on the topic, space-time coding and its various combinations are becoming well understood in the research community. A detailed treatment of space-time coding can be found in recently published text-books, e.g., [21], [22], [23].

1.4 Cooperative Diversity

Space-time coding techniques are quite attractive for deployment in the cellular applications at base stations and have been already included in the 3rd generation wireless standards. Although transmit diversity is clearly advantageous on a cellular base station, it may not be practical for other scenarios. Specifically, due to size, cost, or hardware limitations, a wireless device may not be able to support multiple transmit antennas. Examples include mobile terminals and wireless sensor networks which are gaining popularity in the recent years.

In order to overcome these limitations, yet still emulate transmit antenna diversity, a new form of realizing spatial diversity has been recently introduced under the name of user cooperation or cooperative diversity [24]-[28]. The basic idea behind cooperative diversity rests on the observation that in a wireless environment, the signal transmitted by the source node is overheard by other nodes, which can be defined as “partners” or “relays”. The source and its partners can jointly process and transmit their information, creating a virtual antenna array although each of them is equipped with only one antenna. Similar to physical antenna arrays, these virtual antenna arrays combat multipath fading in wireless channels by providing receivers with essentially redundant signals over independent channels that can be combined to average individual channel effects. The recent surge of interest in cooperative communication was subsequent to the works of Sendonaris et al. [24], [25] and Laneman et al. [26-28]. However, the basic ideas behind user cooperation can be traced back to Meulen’s early work on the relay channel [29]. A first rigorous information theoretical analysis of the relay channel has been introduced in [30] by Cover and Gamal for AWGN channels. Extending the work of [30] for fading channels, Sendonaris et al. [24]-[25] have investigated the achievable rate region for relay-assisted transmission and coined the term “user cooperation”.

In an independent work by Laneman et al. [26], [27] it is demonstrated that full spatial diversity can be achieved through user cooperation. Their proposed user cooperation protocol

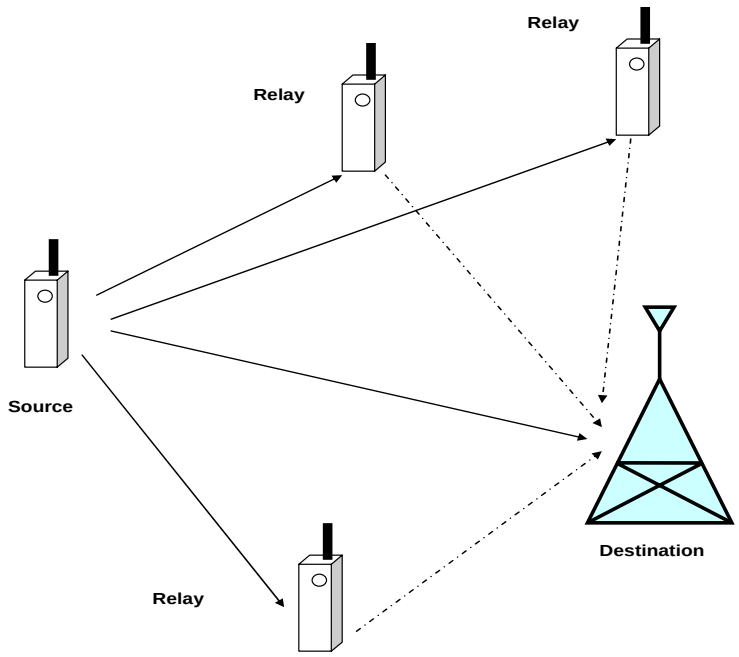

Figure 1.2: Relay assisted transmission.

is built upon a two-phase transmission scheme. In the first phase (i.e., broadcasting phase), the source broadcasts to the destination and relay terminals. In the second phase (i.e., relaying phase), the relays transmit processed version of their received signals to the destination using either orthogonal subchannels, i.e., repetition based cooperative diversity, or the same subchannel, i.e., space-time coded cooperative diversity. The latter relies on the implementation of conventional orthogonal space-time block coding [13] in a distributed fashion among the relay nodes.

Two main relaying techniques are studied in [26]: Amplify-and-Forward (AaF) and Decode-and-Forward (DaF). In DaF relaying, the relay node fully decodes, re-encodes and retransmits the source node's message. In AaF relaying, the relay retransmits a scaled version of the received signal without any attempt to decode it. AaF relaying can be furthered categorized based on the availability of channel state information (CSI) at the relay terminal. In CSI-assisted AaF scheme [26], the relay uses instantaneous CSI of the source to relay

($S \rightarrow R$) link to scale its received noisy signal before re-transmission. This ensures that the same output power is maintained for each realization. On the hand, the "blind" AaF scheme does not have access to CSI and employs fixed power constraint. This ensures that an average output power is maintained, but allows for the instantaneous output power to be much larger than the average. Although blind AaF is not expected to perform as well as CSI-assisted AaF relaying, the elimination of channel estimation at the relay terminal promises low complexity and makes it attractive from a practical point of view.

Another classification for relaying is also proposed in [26]. In the so-called "fixed" relaying, the relay always forwards the message that it receives from the source. The performance of fixed DaF relaying is limited by direct transmission between the source and relay. An alternative to fixed relaying is "selection" relaying (SR) which is, in nature, adaptive to the channel conditions. In this type of relaying, the source reverts to non-cooperation mode at times when the measured instantaneous SNR falls below a certain threshold and continues its own direct transmission to the destination. The work in [31]-[32] can be considered as a systematic realization of such adaptive relaying through powerful channel coding techniques. In so-called "coded cooperation" of [31], [32], Hunter et al. realize the concept of user cooperation through the distributed implementation of existing channel coding methods such as convolutional and turbo codes. The basic idea is that each user tries to transmit incremental redundancy for its partner. Whenever that is not possible, the users automatically revert to a non-cooperative mode.

The user cooperation protocol proposed by Laneman et al. in [28] effectively implements transmit diversity in a distributed manner. In [33], Nabar et al. establish a unified framework of cooperation protocols for single-relay wireless networks. They quantify achievable performance gains for distributed schemes in an analogy to conventional co-located multi-antenna configurations. Specifically, they consider three TDMA-based protocols named Pro-

tocol I, Protocol II, and Protocol III which correspond to traditional MIMO (multi-input-multi-output), SIMO (single-input-multi-output) and MISO (multi-input -single-output) schemes, respectively (Table 1.1). In the following, we describe these cooperation protocols which will be also a main focus of our work.

- **Protocol I:** During the first time slot, the source terminal communicates with the relay and destination. During the second time slot, both the relay and source terminals communicate with the destination terminal. This protocol realizes maximum degrees of broadcasting and receive collision. In an independent work by Azarian et al. [34], it has been demonstrated that this protocol is optimum in terms of diversity-multiplexing tradeoff. Protocol I is referred as "non-orthogonal amplify and forward (NAF) protocol" in [34].
- **Protocol II:** The source terminal communicates with the relay and destination terminals in first time slot. In the second time slot, only the relay terminal communicates with the destination. This protocol realizes a maximum degree of broadcasting and exhibits no receive collision. This is the same cooperation protocol proposed by Laneman et al. in [26].
- **Protocol III:** This is essentially similar to Protocol I except that the destination terminal does not receive from the source during the first time slot. This protocol does not implement broadcasting but realizes receive collision.

Table 1.1: Cooperation protocols for single-relay networks [33].

Protocol / **Terminal**	**Protocol I**		**Protocol II**		**Protocol III**	
	Time 1	Time 2	Time 1	Time 2	Time 1	Time 2
Source	●	●	●	-	●	●
Relay	○	●	○	●	○	●
Destination	○	○	○	○	-	○

(● : Transmitting, ○ : Receiving, - : Idle)

It can be noticed from the descriptions of protocols that the signal transmitted to both the relay and destination terminals is the same over the two time slots in Protocol II. Therefore, classical space-time code construction does not apply to Protocol II. On the other hand, Protocol I and Protocol III can transmit different signals to the relay and destination terminals. Hence, the conventional STBC can be easily applied to these protocols in a distributed fashion. It should be noted that the use of STBC has been also proposed by Laneman et al. in [28, p.2421] for Protocol II. Their proposed use of STBC however implements coding across the relay nodes assuming a scenario with more than one relay and differs from the STBC setup in [33] which involves the source terminal in a single-relay scenario.

1.5 Thesis Motivation and Contributions

Although cooperative diversity has recently garnered much attention, research in this field is still in its infancy. The pioneering works in this area address mainly information-theoretic aspects, deriving fundamental performance bounds. However, practical implementation of cooperative diversity requires an in-depth investigation of several physical layer issues such as channel estimation, equalization, and synchronization integrating the underlying cooperation protocols and relaying modes. In this dissertation, we design and analyze equalization and channel estimation schemes for cooperative communication and further investigate the mutiple-antenna deployment in cooperative networks.

1.5.1 Equalization for Cooperative Communication

Most of the existing research efforts in cooperative communications consider frequency-flat fading channels and assume perfect synchronization. The assumption of prefect synchronization simplifies the performance analysis and allows the exploitation of the virtual antenna analogy for distributed nodes. However, in a practical scenario, the source and its relays are

subject to different time delays typically much larger than those that co-located antenna elements can experience. This would, in effect, convert the operating flat-fading channel into a frequency-selective channel. This channel model would be also appropriate for broadband sensor network applications such as video surveillance which are supposed to handle huge traffic volume of real-time video. The dispersive nature of frequency-selective channels causes inter-symbol interference leading to unavoidable performance degradation for conventional symbol-by-symbol decoders.

In the literature, there have been significant research efforts on broadband space-time coded systems. Specific attention has been paid to STBCs (particularly Alamouti code) can be extended to frequency-selective channels. Among the several techniques studied for STBC, three of those deserve particular attention with their low-complexity structures, namely single-carrier frequency domain equalization for STBC (SC-FDE-STBC) [35], OFDM-STBC [36], and time-reversal STBC (TR-STBC) [37]. An overview and comparison of these schemes can be found in [38]-[40].

Although there is a relatively rich literature on how to design space-time coded systems for frequency-selective channels, the same problem has not yet received much attention in the context of user cooperation. During the period of my research, only few results have been reported on broadband cooperative transmission systems. Yatawatta and Petropulu [41] study an OFDM cooperative diversity system assuming AaF relaying and derive upper bounds on the channel capacity. They also investigate the achievable diversity order for cooperative OFDM, however their results are limited to the non-fading interuser channel. Building upon their previous work on distributed STBC [42], Anghel and Kaveh [43] study the performance of a relay-assisted uplink OFDM-STBC scheme and derive an expression for symbol error probability. Their transmission model assumes DaF, however they ignore the error propagation effect to simplify their analysis. Li et al. [44] have studied a blind

equalization technique for a cooperative space-time coded scenario over frequency selective channels. The transmission model in [44] only considers the relaying phase and assumes that the relays have made correct decisions, i.e., the effect of error propagation is ignored. In another work on distributed OFDM-STBC with DaF relaying, Scutari and Barbarossa [45] propose a ML detector at the destination terminal for binary phase-shift keying (BPSK) transmission. The derived detector however assumes perfect knowledge of the source-to-relay error probabilities, which comes at the cost of increasing complexity and transmission overhead.

As revealed by the literature search, most of the previous works on broadband cooperative communication focus on multi-carrier communications and the analysis in some of these works are oversimplified due to the underlying assumptions, i.e., non-fading inter user channel, ignoring the effect of error propagation etc. Chapter 2 of this dissertation aims to provide a comprehensive treatment of time-domain and frequency-domain equalization techniques for cooperative networks with AaF relaying. Specifically, we consider distributed STBC for a single-relay assisted transmission scenario in which the source-to-relay ($S \rightarrow R$), relay-to-destination ($R \rightarrow D$), and source-to-destination ($S \rightarrow D$) links experience possibly different channel delay spreads. The key contributions, which have been already published by the author [46-50] during the course of this research, are summarized as follows:

- We propose three broadband cooperative transmission techniques for distributed STBC (D-STBC). The proposed schemes, so-called D-TR-STBC, D-SC-STBC and D-OFDM-STBC, implement either time-domain or frequency-domain equalization and are able to preserve low-decoding complexity carefully exploiting the underlying orthogonality of distributed STBC.
- We present a diversity gain analysis of the proposed schemes over frequency-selective channels through the PEP derivation. Our performance analysis for D-TR-STBC

and D-SC-STBC schemes demonstrates that both schemes are able to achieve a maximum diversity order of $\min(L_1, L_3) + L_2 + 2$ where L_1, L_2, and L_3 are the channel memory lengths for $S \to R$, $R \to D$, and $S \to D$ links, respectively. This illustrates that the smaller multi-path diversity order experienced in and links becomes performance limiting for the relaying path.

- Our performance analysis of uncoded D-OFDM-STBC demonstrates that uncoded D-OFDM-STBC is not able to exploit multipath diversity and achieves only a diversity order of two. We further consider D-OFDM-STBC concatenated with TCM (trellis coded modulation). The achievable diversity order for D-OFDM-TCM-STBC is given by $\min(\lceil ECL/2 \rceil, L_1 + 1, L_3 + 1) + \min(\lceil ECL/2 \rceil, L_2 + 1)$ where $\lceil . \rceil$ denotes the ceiling function and *ECL* stands for the effective code length of the outer trellis code. Our derivations point out that with an appropriate design of an outer TCM code, i.e., with sufficiently large *ECL*, coded D-OFDM-STBC achieves the same diversity order as D-TR-STBC and D-SC-STBC.
- We present a comprehensive Monte Carlo simulation study to confirm the analytical observations on diversity gains and to further investigate several practical issues within the considered relay-assisted transmission scenario.

1.5.2 Non-Coherent and Mismatched-Coherent Detection for Cooperative Communication

The coherent scenario, utilized in majority of the works on cooperative diversity so far, assumes the availability of perfect CSI at the receiver. In practice, the fading channel coefficients are estimated and then used in the detection process at the destination terminal. Relay terminals operating in DaF mode also require this information for the decoding process. For AaF relaying, the knowledge of CSI is required for appropriately scaling the received signal to satisfy relay power constraints. The quality of channel estimation thus affects the overall performance of cooperative transmission and might become a performance limiting factor

In the past few years, there have been only sporadic research efforts which investigate non-coherent detection in the context of cooperative scenarios. In [51], Chen and Laneman [51] propose a non-coherent demodulator with a piecewise-linear combiner that accurately approximates the ML detector for cooperative diversity schemes with BFSK (binary frequency shift keying) modulation. In [52], Tarasak et al. develop a differential modulation scheme for a two-user cooperative diversity system with BPSK transmission which avoids channel estimation. This scheme can achieve a diversity order of two with DaF relaying and a sufficiently high SNR in the inter-user channel. Wang et al. [53] develop different distributed space-time processing schemes for a cooperative scenario which do not require CSI. They study so-called DaF, SR, incremental DaF (IDaF) and incremental SR (ISR) for non-coherent scenarios. In incremental relaying, they assume that the relaying phase is eliminated, if the destination terminal determines from the CRC bits that the signal received through the direct link during the broadcasting phase has been decoded correctly. If the relays use SR, this protocol is called incremental SR (ISR), otherwise, if the relays use DaF, it is called incremental DaF (IDaF). At the price of increasing complexity, they demonstrate that ISR outperforms other competing schemes. Yiu et al. [54], [55] have proposed non-coherent distributed STBCs where each node in the network is assigned a unique signature vector. The signal transmitted by each cooperating node consists of the product of a unitary matrix, which carries the information to be sent, and the signature vector of that node. It is shown that the non-coherent STBCs designed for co-located antennas are favorable choices for the information carrying matrices in a cooperative scenario as well. In a recent work by Annavajjala et al. [56], the performance of non-coherent detection with BFSK is investigated assuming AaF relaying. However, their transmission model is oversimplified due to the underlying assumption of non-fading link in the $R \rightarrow D$ link.

The works in [51]-[55] build upon the assumption of DaF relaying and focus on only quasi-static fading channels. So far, there has not been a comprehensive treatment of non-coherent detection and coherent detection with imperfect channel estimation assuming AaF relaying. Considering the wide range applications of cooperative communications, channel estimation over time-varying fading channels should be further explored. A typical example is mobile sensor applications which involve simultaneous tracking of multiple targets and identification of their coordinated movements, e.g., intelligent highway scenarios. Chapter 3 of this dissertation investigates non-coherent and mismatched-coherent detection over quasi-static and time varying channels for distributed STBC schemes assuming AaF relaying. Our main contributions, which have already been accepted/submitted for publication [57], [58], can be summarized as follows:

- We derive non-coherent ML detection for distributed STBCs. The form of the ML rule for time-varying channels does not lend itself to a practical implementation other than exhaustive search over all possible sequences. Under the assumption of quasi-static fading channel and by exploiting the inherent orthogonality of STBCs, we illustrate that the likelihood function reduces to a simple form which can be implemented in practice by a Viterbi-type algorithm. We further demonstrate that the derived decoding rule can be deployed over time-varying channels as a low-complexity sub-optimal solution.
- As a competing scheme to non-coherent detection, we investigate the deployment of mismatched-coherent receiver for distributed STBCs. For channel estimation purposes, we employ pilot symbols (i.e., a set of symbols whose location and values are known to the receiver) multiplexed with the information-bearing data. Both ML and minimum mean square error (MMSE) type of channel estimators are considered.
- We present a diversity gain analysis of the non-coherent and mismatched-coherent receivers through the PEP derivation. Our PEP analysis demonstrates that both receivers are

able to collect the maximum diversity order over quasi-static channels. Our results further indicate that the non-coherent receiver is able to outperform mismatched-coherent receiver for low Doppler spreads while the mismatched receiver becomes a better choice for relatively higher Doppler spreads.

1.5.3 Cooperative Communication with Multiple-Antenna Nodes

A particular application area of cooperative communication is infrastructure-based cooperative networks with fixed relays [61]. For such scenarios, relay nodes may have the capability to support multiple antennas. Therefore, due to low cost and complexity reduction, it can be readily argued that the deployment of fewer fixed relay nodes each of which is equipped with multiple antennas is a promising alternative to large scale relay networks [59], [60].

While most of the current literature on user cooperation is built upon the assumption that user nodes are equipped with a single antenna, there have been some recent results which exploit further the benefits of multiple antenna deployment. An information theoretical analysis of a MIMO relay channel has been first exposed by [62]. In [63], Wang et al. derive upper and lower bounds on the capacity of MIMO relay channels and demonstrate significant gains. Jing et al. [64] investigate the application of linear dispersion space-time codes across multiple-antenna nodes and discuss optimal power allocation rules assuming Protocol II and AaF relaying. Specifically, they demonstrate that the optimal power allocation is for the source to expand half the power and for the relays to share the other half such that the power used by each relay is proportional to its number of antennas. Extending their own work in [65], Yiu et al. [66] consider distributed STBC with multiple antennas at the relay and destination terminals assuming Protocol II and DaF relaying. Under the assumption that there are F active relays each of which is equipped with M_T antennas and a destination node with N receive antennas, it has been shown in [66] that existing STBCs designed for $N_C \geq 2$ co-located anten-

nas can guarantee a diversity order of $\min(N_C N, M_T FN)$. The transmission model in [66] is however oversimplified as it only considers the relaying phase ignoring effect of error propagation.

Although the topic of MIMO relaying has just started to attract attention, the amount of contributions so far is scarce. With this in mind, it is the aim of Chapter 4 is to provide an end-to-end comprehensive performance analysis to demonstrate the effect of multiple antenna deployment assuming different relaying techniques. Specifically, we consider Protocol II with blind AaF, CSI-assisted AaF, DaF relaying and quantify analytically the impact of multiple antenna deployment at the source, relay and/or destination terminals on the diversity order for each of the relaying methods under consideration. In the consider user cooperation scenario, the source and destination are equipped with M_S and N antennas, respectively. The relay terminal is equipped with M_R receive and M_T transmit antennas. Our diversity gain analysis through PEP derivations demonstrates that both CSI-assisted AaF and DaF schemes achieve a diversity order of $N(M_S + M_T)$. On the other hand, the diversity order of blind AaF relaying is limited to $\min(M_S, N) + NM_S$. Therefore, the smaller diversity order experienced in source-to-relay and relay-to-destination links becomes the bottleneck for the relaying path in blind AaF relaying. Under the assumption of $M_S = M_R = M_T = M$, both DaF and CSI-assisted AaF schemes are able to always perform better than blind AaF relaying. The key results of this chapter are reported in [67], [68].

Chapter 2
Equalization for Cooperative Communication

Introduction

Since space-time codes (conventional ones as well as its distributed versions) were developed originally for frequency-flat channels, applying them over frequency-selective channels becomes a challenging design problem. The dispersive nature of such channels causes inter-symbol interference, leading to unavoidable performance degradation. Although there is a relatively rich literature on how to design space-time coded systems for frequency-selective channels, the same problem has not yet received much attention in the context of user cooperation. In this chapter, we investigate various equalization methods for cooperative diversity schemes over frequency-selective fading channels. Specifically, we consider three equalization schemes proposed originally for conventional STBCs [13-15] and extend them to distributed STBC in a cooperative transmission scenario with AaF relaying. The distributed STBC equalization schemes are named after their original (non-cooperative) counterparts as Distributed Time-Reversal (D-TR) STBC, Distributed Single-Carrier (D-SC) STBC and Distributed Orthogonal Frequency Division Multiplexed (D-OFDM) STBC. We carry out a detailed performance analysis for each scheme through PEP derivations to obtain the achiev-

able diversity orders. We further present a comprehensive Monte Carlo simulation study to compare the performance of compteing schemes.

2.1 Transmission Model

A wireless communication scenario is considered where the source terminal transmits information to the destination terminal with the assistance of a relay terminal (See Figure 2.1). The channel impulse responses (CIRs) for $S \to R$, $S \to D$ and $R \to D$ links for the t^{th} transmission block are given by $\mathbf{h}_1^t = \left[h_{SR}^t[0],...,h_{SR}^t[L_1]\right]^{\mathrm{T}}$, $\mathbf{h}_2^t = \left[h_{SD}^t[0],...,h_{SD}^t[L_2]\right]^{\mathrm{T}}$, and $\mathbf{h}_3^t = \left[h_{RD}^t[0],...,h_{RD}^t[L_3]\right]^{\mathrm{T}}$, respectively, where L_1, L_2 and L_3 denote the corresponding channel memory lengths. The random vectors $\mathbf{h}_1^t$, $\mathbf{h}_2^t$ and $\mathbf{h}_3^t$ are assumed to be independent zero-mean complex Gaussian with power delay profile vectors denoted by $\mathbf{v}_1 = [\sigma_1^2(0),...,\sigma_1^2(L_1)]$, $\mathbf{v}_2 = [\sigma_2^2(0),...,\sigma_2^2(L_2)]$, and $\mathbf{v}_3 = [\sigma_3^2(0),...,\sigma_3^2(L_3)]$, respectively, and are normalized such that $\sum_{l_i=0}^{L_i} \sigma_i^2(l_i) = 1$, $i = 1,2,3$. The CIRs are assumed to be constant over two consecutive blocks and vary independently every two blocks.

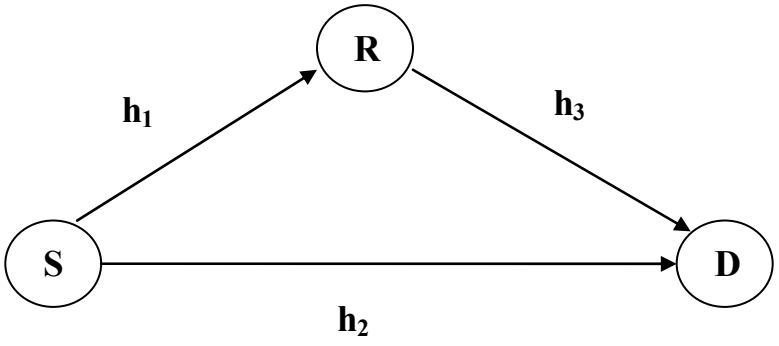

Figure 2.1: Relay-assisted transmission over frequency-selective channels. $\mathbf{h}_1^t$, $\mathbf{h}_2^t$ and $\mathbf{h}_3^t$ represent CIRs of underlying frequency-selective channels.

As for the user cooperation protocol, we adopt Protocol III of [33]. For the $R \to D$ link, AaF relaying is used, in which the relay terminal amplifies and re-transmits the signal received from the source terminal in the first signaling interval. All terminals are equipped with a single transmit and receive antenna. Any linear modulation technique such as QAM or PSK modulation can be used.

Information symbols are first parsed to two streams of $V \times 1$ blocks x_i^t, $i = 1,2$ and then multiplied by a zero-padding (ZP) matrix[1] $\mathbf{\Psi} = \left[\mathbf{I}_V, \mathbf{0}_{V \times \ell}\right]^{\mathrm{T}}$ of size $J \times V$, where $\ell = \max\left(L_1 + L_3, L_2\right)$ and J is the frame length. As explained in [69], the use of zero-padding as the precoding method in a single-carrier transmission scenario ensures that the available multipath diversity is fully exploited. To further remove inter-block interference and make the channel matrix circulant, a cyclic prefix (CP) with length ℓ is added between adjacent information blocks. Due to the adopted precoding form (i.e., zero padding), we simply insert additional zeros at the start of the frame as CP. In a practical implementation, the block of all-zeros at the end of the current frame can also be used as the next frame's block of all-zeros to be inserted at its beginning, avoiding unnecessary additional overhead.

Let E_{SD}, E_{SR}, and E_{RD} represent the average energies available at the destination and relay terminals taking into account possibly different path loss and shadowing effects in $S \to D$, $S \to R$, and $R \to D$ links, respectively. The signal received at the relay terminal during the first signaling interval is

$$\mathbf{r}_R^j = \sqrt{E_{SR}}\,\mathbf{H}_1^t \mathbf{\Psi} \mathbf{x}_1^t + \mathbf{n}_R^t \tag{2.1}$$

where $\mathbf{H}_1^t$ is a $J \times J$ circulant matrix with entries $[\mathbf{H}_1^t]_{k,l} = \mathbf{h}_1^t((k-l) \bmod J)$ and $\mathbf{n}_R^t$ is the AWGN vector with each entry having zero-mean and variance of $N_0/2$ per dimension. The

[1] The structure of the precoding matrix has the zero-padding form for D-TR-STBC and D-SC-STBC. For D-OFDM-STBC the precoding matrix is given by $\mathbf{\Psi} = \mathbf{Q}^{\mathrm{H}}$, i.e., Inverse Fourier Transform (IFFT).

relay terminal normalizes each entry of the received signal $[\mathbf{r}_R^t]_q$, $q = 1,2,...,J$, by a factor of $\sqrt{\mathrm{E}\left(|[\mathbf{r}_R^t]_q|^2\right)} = \sqrt{E_{SR} + N_0}$ to ensure unit average energy and re-transmits the signal during the second time slot. Therefore, the received signal at the destination terminal in the second time slot is given by

$$\mathbf{r}^t = \sqrt{E_{RD}}\mathbf{H}_3^t\tilde{\mathbf{r}}_R^t + \sqrt{E_{SD}}\mathbf{H}_2^t\boldsymbol{\Psi}\mathbf{x}_2^t + \mathbf{n}_D^t \tag{2.2}$$

where $\tilde{\mathbf{r}}_R^t$ is the normalized received signal and $\mathbf{n}_D^t$ is the additive white Gaussian noise vector with each entry having zero-mean and variance of $N_0/2$ per dimension. $\mathbf{H}_2^t$ and $\mathbf{H}_3^t$ are $J \times J$ circulant matrices with entries $[\mathbf{H}_2^t]_{k,l} = \mathbf{h}_2^t((k-l) \bmod J)$ and $[\mathbf{H}_3^t]_{k,l} = \mathbf{h}_3^t((k-l) \bmod J)$, respectively. Combining (2.1) and (2.2), we obtain

$$\mathbf{r}^t = \sqrt{\frac{E_{RD}E_{SR}}{E_{SR}+N_0}}\mathbf{H}_3^t\mathbf{H}_1^t\boldsymbol{\Psi}\mathbf{x}_1^t + \sqrt{E_{SD}}\mathbf{H}_2^t\boldsymbol{\Psi}\mathbf{x}_2^t + \tilde{\mathbf{n}}^t, \tag{2.3}$$

where we define the *effective* noise term as

$$\tilde{\mathbf{n}}_t = \sqrt{\frac{E_{RD}}{E_{SR}+N_0}}\mathbf{H}_3\mathbf{n}_R^t + \mathbf{n}_D^t. \tag{2.4}$$

Each entry of $\tilde{\mathbf{n}}_t$ (conditioned on $\mathbf{h}_3$) has zero mean and a variance of

$$E\left[\left|\tilde{\mathbf{n}}^t\right|_n^2 \middle| \mathbf{h}_3\right] = N_0\left(1 + \frac{E_{RD}}{E_{SR}+N_0}\sum_{m=0}^{L_3}|\mathbf{h}_3(m)|^2\right). \tag{2.5}$$

The destination terminal normalizes the received signal by a factor of $\sqrt{1+\sum_{m=0}^{L_3}|\mathbf{h}_3(m)|^2 E_{RD}/(E_{SR}+N_0)}$. This does not affect SNR, but simplifies the analytical derivation [33]. After normalization, we obtain

$$\mathbf{r}^t = \sqrt{\gamma_1}\mathbf{H}_3^t\mathbf{H}_1^t\boldsymbol{\Psi}\mathbf{x}_1^t + \sqrt{\gamma_2}\mathbf{H}_2^t\boldsymbol{\Psi}\mathbf{x}_2^t + \mathbf{n}^t \tag{2.6}$$

where $\mathbf{n}^t$ is complex Gaussian with zero mean and variance of $N_0/2$ per dimension and γ_1, γ_2 are defined as

$$\gamma_1 = \frac{(E_{SR}/N_0)E_{RD}}{1+E_{SR}/N_0+\sum_{m=0}^{L_3}\left|\mathbf{h}_3(m)\right|^2 E_{RD}/N_0}, \tag{2.7}$$

$$\gamma_2 = \frac{(1+E_{SR}/N_0)E_{SD}}{1+E_{SR}/N_0+\sum_{m=0}^{L_3}\left|\mathbf{h}_3(m)\right|^2 E_{RD}/N_0}. \tag{2.8}$$

2.2 Distributed Time-Reversal STBC

TR-STBC was introduced in [37] as an extension of the Alamouti STBC scheme [15] to frequency-selective channels by imposing the Alamouti orthogonal structure at a block level rather than the original symbol-level implementation used for frequency-flat fading channels. We consider TR-STBC in a distributed fashion where the transmitted blocks for $S \to R \to D$ and $S \to D$ links are generated by the encoding rule

$$\mathbf{d}_1^{k+1} = -\mathbf{J}\left(\mathbf{d}_2^{k}\right)^*,\ \mathbf{d}_2^{k+1} = \mathbf{J}\left(\mathbf{d}_1^{k}\right)^*\ k = 0,2,4,6,... \tag{2.9}$$

Here, $\mathbf{d}_i = \mathbf{\Psi}\mathbf{x}_i$, $i = 1,2$ are the zero-padded information vectors, $\mathbf{J} = \mathbf{P}_J^V$ is a $J \times J$ partial permutation matrix [69].

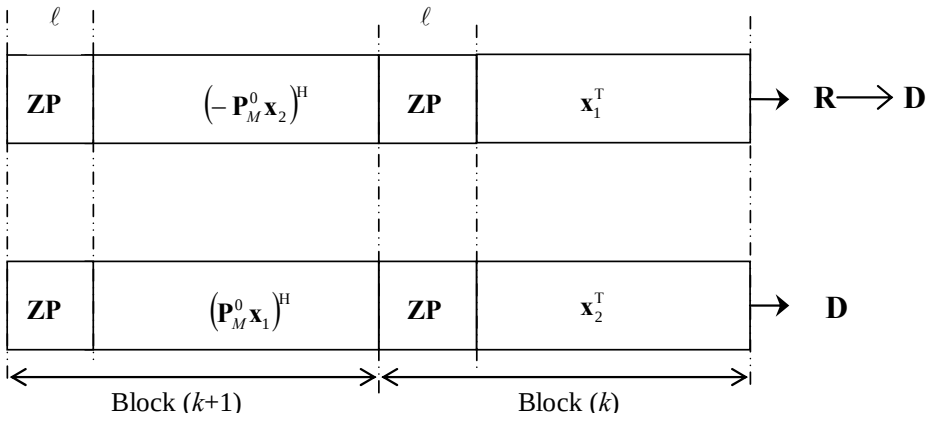

Figure 2.2: Transmission block format for D-TR-STBC.

During the k^{th} block, the source transmits $\mathbf{d}_1^k$ to the relay terminal in the broadcasting phase. In the relaying phase, both the relay and source terminals transmit $\mathbf{d}_1^k$ and $\mathbf{d}_2^k$ to the destination terminal, respectively. As for block k+1, the source transmits $-\mathbf{J}\left(\mathbf{d}_2^k\right)$ to the relay in the broadcasting phase. In the relaying phase, both the relay and source terminals transmit $-\mathbf{J}\left(\mathbf{d}_2^k\right)$ and $\mathbf{J}\left(\mathbf{d}_1^k\right)^*$ to the destination terminal (c.f. Figure 2.2).

Assuming that the channel coefficients remain constant over blocks k and k+1, i.e. $\mathbf{H}_i^k = \mathbf{H}_i^{k+1} = \mathbf{H}_i$, for $i = 1,2,3,$ the received signals are given by

$$\mathbf{r}^k = \sqrt{\gamma_1}\mathbf{H}_3\mathbf{H}_1\mathbf{d}_1^k + \sqrt{\gamma_2}\mathbf{H}_2\mathbf{d}_2^k + \mathbf{n}^k, \tag{2.10}$$

$$\mathbf{r}^{k+1} = -\sqrt{\gamma_1}\mathbf{H}_3\mathbf{H}_1\mathbf{J}\left(\mathbf{d}_2^k\right)^* + \sqrt{\gamma_2}\mathbf{H}_2\mathbf{J}\left(\mathbf{d}_1^k\right)^* + \mathbf{n}^{k+1} \tag{2.11}$$

Taking the conjugate of $\mathbf{r}^{k+1}$ and then multiplying by the time-reversal matrix **J**, we have

$$\mathbf{J}\left(\mathbf{r}^{k+1}\right)^* = -\sqrt{\gamma_1}\mathbf{H}_3^{\mathrm{H}}\mathbf{H}_1^{\mathrm{H}}\mathbf{d}_2^k + \sqrt{\gamma_2}\mathbf{H}_2^{\mathrm{H}}\mathbf{d}_1^k + \mathbf{J}\left(\mathbf{n}^{k+1}\right)^* \tag{2.12}$$

where we use the identities $\mathbf{J}\mathbf{H}_3^*\mathbf{H}_1^*\mathbf{J} = \mathbf{H}_3^{\mathrm{H}}\mathbf{H}_1^{\mathrm{H}}$ and $\mathbf{J}\mathbf{H}_2^*\mathbf{J} = \mathbf{H}_2^{\mathrm{H}}$. Combining (2.10) and (2.12) in matrix form yields

$$\begin{bmatrix} \mathbf{r}^k \\ \mathbf{J}\left(\mathbf{r}^{k+1}\right)^* \end{bmatrix} = \underbrace{\begin{bmatrix} \sqrt{\gamma_1}\mathbf{H}_3\mathbf{H}_1 & \sqrt{\gamma_2}\mathbf{H}_2 \\ \sqrt{\gamma_2}\mathbf{H}_2^{\mathrm{H}} & -\sqrt{\gamma_1}\mathbf{H}_3^{\mathrm{H}}\mathbf{H}_1^{\mathrm{H}} \end{bmatrix}}_{\mathbf{H}_{eq}} \begin{bmatrix} \mathbf{d}_1^k \\ \mathbf{d}_2^k \end{bmatrix} + \begin{bmatrix} \mathbf{n}^k \\ \mathbf{J}\left(\mathbf{n}^{k+1}\right)^* \end{bmatrix}. \tag{2.13}$$

Multiplying (2.13) by $\mathbf{Y} = \left(\mathbf{I}_2 \otimes \left(\sqrt{\gamma_1\left|\mathbf{H}_3\right|^2\left|\mathbf{H}_1\right|^2 + \gamma_2\left|\mathbf{H}_2\right|^2}\right)^{-1}\right)\mathbf{H}_{eq}^{\mathrm{H}}$, we observe that the data streams are decoupled (due to orthogonality of $\mathbf{H}_{eq}$) allowing us to write

$$\mathbf{r}_{out,i}^k = \sqrt{\gamma_1\left|\mathbf{H}_3\right|^2\left|\mathbf{H}_1\right|^2 + \gamma_2\left|\mathbf{H}_2\right|^2}\,\mathbf{d}_i^k + \mathbf{n}_{out,i}^k, \; i = 1,2 \tag{2.14}$$

where $\mathbf{n}_{out,i}^k$ represents the filtered noise vector which is still Gaussian with each entry having zero-mean and a variance of $N_0/2$ per dimension. Since the two data streams $\mathbf{d}_1^k$ and $\mathbf{d}_2^k$ are now decoupled, each can be detected by applying standard equalization techniques such as MMSE or MLSE (maximum likelihood sequence estimation) equalizers [70].

2.2.1 Diversity Gain Analysis for D-TR-STBC

In this sub-section, we investigate the achievable diversity gain for the D-TR-STBC scheme through the derivation of the PEP expression. First, we assume that $S \to R$ and $S \to D$ links experience frequency-selectivity while the channel between the relay and the destination terminals is AWGN, i.e., $\mathbf{h}_3[0] = 1$. Physically, this assumption corresponds to the case where the destination and relay terminals have a very strong line-of-sight connection [33]. We should emphasize that this rather unrealistic assumption of static (i.e., non-fading) $R \to D$ link is made only to simplify performance analysis and to provide a benchmark for the general case where all underlying links experience fading.

Defining the transmitted codeword vector and the erroneously-decoded codeword vector as $\mathbf{x}$ and $\hat{\mathbf{x}}$, respectively, the conditional PEP is given as

$$P(\mathbf{x}, \hat{\mathbf{x}} \,|\, \mathbf{h}_1, \mathbf{h}_2) = Q\left(\sqrt{\frac{d^2(\mathbf{x}, \hat{\mathbf{x}})}{2N_0}} \right), \tag{2.15}$$

assuming ML decoding with perfect knowledge of the CSI at the receiver side. Here, $Q(.)$ is the Gaussian-Q function and $d^2(\mathbf{x}, \hat{\mathbf{x}})$ denotes the Euclidean distance between $\mathbf{x}$ and $\hat{\mathbf{x}}$. Applying the standard Chernoff bound to (2.15), we obtain

$$P(\mathbf{x}, \hat{\mathbf{x}} \,|\, \mathbf{h}_1, \mathbf{h}_2) \le \exp\left(-\frac{d^2(\mathbf{x}, \hat{\mathbf{x}})}{4N_0} \right). \tag{2.16}$$

Noting that $\mathbf{d}_i = \mathbf{\Psi}_i \mathbf{x}_i$, we can write $d^2(\mathbf{x}, \hat{\mathbf{x}})$ as follows

$$d^2(\mathbf{x}, \hat{\mathbf{x}}) = \gamma_1 \left\| \mathbf{H}_1 (\mathbf{d} - \hat{\mathbf{d}}) \right\|^2 + \gamma_2 \left\| \mathbf{H}_2 (\mathbf{d} - \hat{\mathbf{d}}) \right\|^2 \tag{2.17}$$

where γ_1 and γ_2 in (2.7) and (2.8) now reduce to

$$\gamma_1 = \frac{(E_{SR} / N_0) E_{RD}}{1 + E_{SR} / N_0 + E_{RD} / N_0}, \tag{2.18}$$

$$\gamma_2 = \frac{(1 + E_{SR} / N_0) E_{SD}}{1 + E_{SR} / N_0 + E_{RD} / N_0} \tag{2.19}$$

under the non-fading $R \to D$ link assumption. By further defining $\mathbf{h}_i^{\mathrm{T}} = [\mathbf{h}_i(0),...,\mathbf{h}_i(L_i)]$ and

$$\boldsymbol{\chi}_i = \begin{bmatrix} [\mathbf{d}]_0 & [\mathbf{d}]_1 & \cdots & [\mathbf{d}]_{J-1} \\ [\mathbf{d}]_{J-1} & [\mathbf{d}]_0 & \cdots & [\mathbf{d}]_{J-2} \\ \vdots & \vdots & \cdots & \vdots \\ [\mathbf{d}]_{J-L_i} & [\mathbf{d}]_{J-L_i+1} & \cdots & [\mathbf{d}]_{J-L_i-1} \end{bmatrix}, \quad i = 1,2 \tag{2.20}$$

(2.17) can be rewritten as

$$d^2(\mathbf{x}, \hat{\mathbf{x}}) = \gamma_1 \left\| \mathbf{h}_1^{\mathrm{T}} (\boldsymbol{\chi} - \hat{\boldsymbol{\chi}}) \right\|^2 + \gamma_2 \left\| \mathbf{h}_2^{\mathrm{T}} (\boldsymbol{\chi} - \hat{\boldsymbol{\chi}}) \right\|^2 . \tag{2.21}$$

Substituting (2.21) in (2.16) and following the steps detailed in Appendix A.1, we obtain the final PEP form as

$$P(\mathbf{x}, \hat{\mathbf{x}}) \le \left(1 + \frac{\gamma_1}{4N_0} \right)^{-(L_1+1)} \left(1 + \frac{\gamma_2}{4N_0} \right)^{-(L_2+1)} \prod_{l_1=0}^{L_1} \frac{1}{\boldsymbol{\lambda}_1(l_1)} \prod_{l_2=0}^{L_2} \frac{1}{\boldsymbol{\lambda}_2(l_2)} \tag{2.22}$$

where $\boldsymbol{\lambda}_i$, $i = 1,2$ denote the eigenvalues of the codeword difference matrix defined by $\mathbf{A}_i = \boldsymbol{\Omega}_i^{1/2} \boldsymbol{\chi}_i \boldsymbol{\Omega}_i^{1/2}$ with $\boldsymbol{\Omega}_i = diag(\mathbf{v}_i)$ and $\boldsymbol{\chi}_i = (\boldsymbol{\chi}_i - \hat{\boldsymbol{\chi}}_i)(\boldsymbol{\chi}_i - \hat{\boldsymbol{\chi}}_i)^{\mathrm{H}}$. In the following, we discuss various aspects on the performance of D-TR-STBC.

Maximum Achievable Diversity for D-TR-STBC: We assume perfect power control where $S \to D$ and $R \to D$ links are balanced and high SNRs for all underlying links, i.e., $E_{SD}/N_0 = E_{RD}/N_0 >> 1$. It is also assumed that SNR in $S \to R$ is large enough, i.e., $E_{SR}/N_0 > E_{SD}/N_0$. Under these assumptions, we have $\gamma_1 / N_0 = \gamma_2 / N_0 >> 1$, simplifying (2.22) to

$$P(\mathbf{x}, \hat{\mathbf{x}}) \le \left(\frac{E_{SD}}{4N_0} \right)^{-(L_1+L_2+2)} \prod_{l_1=0}^{L_1} \frac{1}{\boldsymbol{\lambda}_1(l_1)} \prod_{l_2=0}^{L_2} \frac{1}{\boldsymbol{\lambda}_2(l_2)} . \tag{2.23}$$

Since $\mathbf{A}_i$ is full rank, the maximum achievable diversity order is given by $L_1 + L_2 + 2$. Under the assumption of non-fading $S \to R$ link, the maximum achievable diversity order can

be similarly found and is given by $L_3 + L_2 + 2$. If we further assume that L_1=L_2=L in (2.23) (or similarly L_2=L_3=L for the scenario with non-fading $S \to R$ link), we obtain

$$P(\mathbf{x}, \hat{\mathbf{x}}) \le \left(\frac{E_{SD}}{4N_0} \right)^{-2(L+1)} \prod_{l=0}^{L} \left(\frac{1}{\boldsymbol{\lambda}_1(l)} \right)^2 \tag{2.24}$$

which is the PEP expression for non-distributed TR-STBC.

Existence of Error Floor: In the investigation of the maximum achievable diversity order, we have assumed that SNR in $S \to R$ link is sufficiently large, i.e., $E_{SR}/N_0 > E_{SD}/N_0$. Now we consider the limiting case of $E_{SD}/N_0 \to \infty$. For this case, (2.22) takes the following form

$$P(\mathbf{x}, \hat{\mathbf{x}}) \le \left(\frac{E_{SR}}{4N_0} \right)^{-(L_1+L_2+2)} \prod_{l_1=0}^{L_1} \frac{1}{\boldsymbol{\lambda}_1(l_1)} \prod_{l_2=0}^{L_2} \frac{1}{\boldsymbol{\lambda}_2(l_2)}. \tag{2.25}$$

It is observed that the performance becomes independent of E_{SD}/N_0 and is now governed by E_{SR}/N_0. Therefore, the performance is expected to deteriorate for low E_{SR}/N_0 resulting in error floors, which is an inherent disadvantage of the employed Protocol III of [33]. It should be noted that such error floors can be avoided if Protocol I of [33] is used as the user cooperation protocol where the source-to-destination transmission is allowed within the first signaling interval.

Effect of Power Imbalance: Now we consider the case of no power control and assume $E_{SD} = nE_{RD}$ where n is a positive number. Then, (2.22) becomes

$$P(\mathbf{x}, \hat{\mathbf{x}}) \le \left(1 + \frac{\frac{1}{n}\frac{E_{SR}}{N_0}\frac{E_{SD}}{4N_0}}{1 + \frac{E_{SR}}{N_0} + \frac{1}{n}\frac{E_{SD}}{N_0}} \right)^{-(L_1+1)} \left(1 + \frac{\left(1 + \frac{E_{SR}}{N_0}\right)\frac{E_{SD}}{4N_0}}{1 + \frac{E_{SR}}{N_0} + \frac{1}{n}\frac{E_{SD}}{N_0}} \right)^{-(L_2+1)} \prod_{l_1=0}^{L_1} \frac{1}{\boldsymbol{\lambda}_1(l_1)} \prod_{l_2=0}^{L_2} \frac{1}{\boldsymbol{\lambda}_2(l_2)} \tag{2.26}$$

For large n, we obtain

$$P(\mathbf{x}, \hat{\mathbf{x}}) \le \left(\frac{1}{n}\frac{E_{SD}}{4N_0} \right)^{-(L_1+1)} \left(\frac{E_{SD}}{4N_0} \right)^{-(L_2+1)} \prod_{l_1=0}^{L_1} \frac{1}{\boldsymbol{\lambda}_1(l_1)} \prod_{l_2=0}^{L_2} \frac{1}{\boldsymbol{\lambda}_2(l_2)} \tag{2.27}$$

where the performance is governed by E_{SD}/N_0 which means that the $S \to D$ link is the dominant link. On the other hand, for small values of *n*, (2.26) reduces to

$$P(\mathbf{x},\hat{\mathbf{x}}) \le \left(\frac{E_{SR}}{4N_0}\right)^{-(L_1+1)} \left(\frac{n}{4}\left(1+\frac{E_{SR}}{N_0}\right)\right)^{-(L_2+1)} \prod_{l_1=0}^{L_1} \frac{1}{\boldsymbol{\lambda}_1(l_1)} \prod_{l_2=0}^{L_2} \frac{1}{\boldsymbol{\lambda}_2(l_2)} \tag{2.28}$$

where the performance is once again dominated by E_{SR}/N_0.

Extension to fading $R \to D$ **link:** Now, we return our attention on the general case where all three underlying links experience frequency-selective fading. Due to the presence of $|\mathbf{h}_3(m)|^2$ terms in (2.7) and (2.8), the derivation of PEP becomes analytically intractable without any assumptions imposed on the SNR in the underlying links. However, for the asymptotic case of $E_{SD}/N_0 = E_{RD}/N_0 >> 1$ with perfect power control and sufficiently large $E_{SR}/N_0 > E_{SD}/N_0$ values, the scaling factors in (2.7) and (2.8) reduce to $\gamma_1 = \gamma_2 = E_{SD}$. Then, we can obtain the following PEP expressions (See Appendix A.2 for detailed steps of the derivations)

Case 1: $L_3 > L_1$

$$P(\mathbf{x},\hat{\mathbf{x}}) \le (L_3+1)^{L_1} \frac{\Gamma(L_3-L_1+1)}{\Gamma(L_3+1)} \left(\frac{E_{SD}}{4N_0}\right)^{-(L_1+L_2+2)} \prod_{l_1=0}^{L_1} (\boldsymbol{\lambda}_1(l_1))^{-1} \prod_{l_2=0}^{L_2} (\boldsymbol{\lambda}_2(l_2))^{-1} \tag{2.29}$$

Case 2: $L_1 > L_3$

$$P(\mathbf{x},\hat{\mathbf{x}}) \le (L_1+1)^{L_3} \frac{\Gamma(L_1-L_3+1)}{\Gamma(L_1+1)} \left(\frac{E_{SD}}{4N_0}\right)^{-(L_3+L_2+2)} \prod_{l_3=0}^{L_3} (\boldsymbol{\lambda}_1(l_3))^{-1} \prod_{l_2=0}^{L_2} (\boldsymbol{\lambda}_2(l_2))^{-1} \tag{2.30}$$

Case 3: $L_1 = L_3$

$$P(\mathbf{x},\hat{\mathbf{x}}) \le \frac{(L_3+1)^{L_3+1}}{\Gamma(L_3+1)} (-1)^{L_3-1} \left(\frac{E_{SD}}{4N_0}\right)^{-(L_3+L_2+2)} \prod_{l_2=0}^{L_2} (\boldsymbol{\lambda}_2(l_2))^{-1}$$
$$\times \sum_{l_1=1}^{L_1+1} \frac{p_{l_1}}{(\boldsymbol{\lambda}_1(l_1))^{L_3+1}} e^{\frac{4N_0(L_3+1)}{\boldsymbol{\lambda}_1(l_1)E_{SD}}} E_i\left(-\frac{4N_0(L_3+1)}{\boldsymbol{\lambda}_1(l_1)E_{SD}}\right) \tag{2.31}$$

where $\Gamma(.)$ and $E_i(.)$ represent the gamma function and the exponential-integral function, respectively [71].

It is observed from (2.29)-(2.31) that the maximum achievable diversity order is given by $\min(L_1, L_3) + L_2 + 2$. This illustrates that the smaller of the multipath diversity orders experienced in $S \to R$ and $R \to D$ links becomes the performance bottleneck for the relaying path. In other words, it is not possible to extract the full multipath diversity for D-TR-STBC in a cooperative scenario. For the convenience of the reader, we further consider all possible scenarios where the underlying links experience either non-fading or fading channels and present the achievable diversity order for each case in Table 2.1. The term "fading" in the Table is used to refer to both frequency-flat and frequency-selective channels since the derived expressions in (2.29)-(2.31) cover frequency-flat fading as a special case.

Table 2.1: Achievable Diversity Orders for Distributed TR-STBC.

S → R	**R → D**	**S → D**	**Diversity Order**
Fading	Fading	Fading	$\min(L_1, L_3) + L_2 + 2$
Fading	Non-fading	Fading	$L_1 + L_2 + 2$
Non-fading	Fading	Fading	$L_3 + L_2 + 2$

2.3 Distributed Single-Carrier STBC

Single-carrier frequency domain equalization is an attractive equalization scheme for broadband wireless channels which are characterized by their long impulse response memory [72]. An Alamouti-based scheme for frequency-selective channels which relies on frequency-domain equalization was proposed in [35]. Here, we consider its distributed version within the context of our relay-assisted transmission scenario (Figure 2.1). Assuming that the chan-

nel coefficients remain constant over two consecutive blocks, i.e. $\mathbf{H}_i^k = \mathbf{H}_i^{k+1} = \mathbf{H}_i$ for $i = 1,2,3$, the received signals for blocks k and k+1

$$\mathbf{r}^k = \sqrt{\gamma_1}\mathbf{H}_3\mathbf{H}_1\mathbf{d}_1^k + \sqrt{\gamma_2}\mathbf{H}_2\mathbf{d}_2^k + \mathbf{n}^k, \tag{2.32}$$

$$\mathbf{r}^{k+1} = -\sqrt{\gamma_1}\mathbf{H}_3\mathbf{H}_1\mathbf{J}\left(\mathbf{d}_2^k\right)^* + \sqrt{\gamma_2}\mathbf{H}_2\mathbf{J}\left(\mathbf{d}_1^k\right)^* + \mathbf{n}^{k+1}, \tag{2.33}$$

which are identical to (2.10)-(2.11) and repeated here for convenience. Next, we transform the received signals to the frequency domain by applying the DFT (Discrete Fourier Transform), i.e., multiplying (2.32) by the **Q** matrix and the conjugate of (2.33) by **QJ**

$$\mathbf{Q}\mathbf{r}^k = \sqrt{\gamma_1}\mathbf{Q}\mathbf{H}_3\mathbf{H}_1\mathbf{d}_1^k + \sqrt{\gamma_2}\mathbf{Q}\mathbf{H}_2\mathbf{d}_2^k + \mathbf{Q}\mathbf{n}^k, \tag{2.34}$$

$$\mathbf{Q}\mathbf{J}\left(\mathbf{r}^{k+1}\right)^* = -\sqrt{\gamma_1}\mathbf{Q}\mathbf{H}_3^{\mathrm{H}}\mathbf{H}_1^{\mathrm{H}}\mathbf{d}_2^k + \sqrt{\gamma_2}\mathbf{Q}\mathbf{H}_2^{\mathrm{H}}\mathbf{d}_1^k + \mathbf{Q}\mathbf{J}\left(\mathbf{n}^{k+1}\right)^* . \tag{2.35}$$

Exploiting the circulant structure of the channel matrices, we have

$$\mathbf{H}_i^t = \mathbf{Q}^{\mathrm{H}}\mathbf{\Lambda}_i^t\mathbf{Q} \tag{2.36}$$

where $\mathbf{\Lambda}_i^t,\ i = 1,2,3$ is a diagonal matrix whose (j,j) element is equal to the j^{th} DFT coefficient of $\mathbf{h}_i^t$. Using (2.36), we can write (2.34) and (2.35) in matrix form as

$$\begin{bmatrix} \mathbf{Q}\mathbf{r}^k \\ \mathbf{Q}\mathbf{J}\left(\mathbf{r}^{k+1}\right)^* \end{bmatrix} = \begin{bmatrix} \sqrt{\gamma_1}\mathbf{\Lambda}_3\mathbf{\Lambda}_1 & \sqrt{\gamma_2}\mathbf{\Lambda}_2 \\ \sqrt{\gamma_2}\mathbf{\Lambda}_2^* & -\sqrt{\gamma_1}\mathbf{\Lambda}_3^*\mathbf{\Lambda}_1^* \end{bmatrix}\begin{bmatrix} \mathbf{Q}\mathbf{d}_1^k \\ \mathbf{Q}\mathbf{d}_2^k \end{bmatrix} + \begin{bmatrix} \mathbf{Q}\mathbf{n}^k \\ \mathbf{Q}\mathbf{J}\left(\mathbf{n}^{k+1}\right)^* \end{bmatrix} = \tilde{\mathbf{\Lambda}}\mathbf{U} + \tilde{\mathbf{N}} \tag{2.37}$$

Since $\tilde{\mathbf{\Lambda}}$ is an orthogonal matrix of size $2J \times 2J$, we can multiply (2.37) (without loss of optimality) by

$$\mathbf{K} = \left(\mathbf{I}_2 \otimes \left(\gamma_1\left|\mathbf{\Lambda}_3\right|^2\left|\mathbf{\Lambda}_1\right|^2 + \gamma_2\left|\mathbf{\Lambda}_2\right|^2\right)^{-1/2}\right)\tilde{\mathbf{\Lambda}}^H . \tag{2.38}$$

The resulting output streams are now decoupled allowing us to write each output sequence as

$$\mathbf{r}_{out,i}^k = \sqrt{\gamma_1\left|\mathbf{\Lambda}_3\right|^2\left|\mathbf{\Lambda}_1\right|^2 + \gamma_2\left|\mathbf{\Lambda}_2\right|^2}\,\mathbf{Q}\mathbf{d}_i^k + \mathbf{n}_{out,i}^k \tag{2.39}$$

where $\mathbf{n}_{out,i}^{k}$ is a noise vector with each entry still Gaussian with zero-mean and variance of $N_0/2$ per dimension. After the decoupling, standard SISO equalizers can be used for the detection of data streams $\mathbf{x}_i^k$, $i = 1,2$.

2.3.1 Diversity Gain Analysis for D-SC-STBC

In this sub-section, we investigate the achievable diversity order for D-SC-STBC scheme through the derivation of the PEP expression. For a given channel realization, the Chernoff bound on PEP is given by (2.16) where $d^2(\mathbf{x},\hat{\mathbf{x}})$ is given in this case by

$$d^2(\mathbf{x},\hat{\mathbf{x}}) = \left\|\mathbf{YQ}\left(\mathbf{d}-\hat{\mathbf{d}}\right)\right\|^2 \tag{2.40}$$

with $\mathbf{Y} = \sqrt{\gamma_1|\mathbf{\Lambda}_1|^2 + \gamma_2|\mathbf{\Lambda}_2|^2}$. Then, (2.40) can be rewritten as

$$\begin{aligned} d^2(\mathbf{x},\hat{\mathbf{x}}) &= (\mathbf{d}-\hat{\mathbf{d}})^{\mathrm{H}}\mathbf{Q}^{\mathrm{H}}\mathbf{Y}^{\mathrm{H}}\mathbf{YQ}(\mathbf{d}-\hat{\mathbf{d}}) \\ &= \gamma_1(\mathbf{d}-\hat{\mathbf{d}})^{\mathrm{H}}\mathbf{Q}^{\mathrm{H}}|\mathbf{\Lambda}_1|^2\mathbf{Q}(\mathbf{d}-\hat{\mathbf{d}}) + \gamma_2(\mathbf{d}-\hat{\mathbf{d}})^{\mathrm{H}}\mathbf{Q}^{\mathrm{H}}|\mathbf{\Lambda}_2|^2\mathbf{Q}(\mathbf{d}-\hat{\mathbf{d}}). \end{aligned} \tag{2.41}$$

Using the property $\mathbf{Q}^{\mathrm{H}}|\mathbf{\Lambda}_i|^2\mathbf{Q} = \mathbf{H}_i\mathbf{H}_i^{\mathrm{H}}$, we write (2.41) as

$$d^2(\mathbf{x},\hat{\mathbf{x}}) = \gamma_1\left\|\mathbf{H}_1\left(\mathbf{d}-\hat{\mathbf{d}}\right)\right\|^2 + \gamma_2\left\|\mathbf{H}_2\left(\mathbf{d}-\hat{\mathbf{d}}\right)\right\|^2 \quad . \tag{2.42}$$

Interestingly, comparing (2.17) and (2.42), we notice that distance metrics for TR-STBC and SC-STBC are identical. Thus, following the same steps of the previous section, we obtain the same PEP expressions for D-TR-STBC, i.e., (2.22) and (2.29)-(2.31). We should emphasize here that the equivalence between these two schemes (assuming maximum likelihood detection) has not been reported before in the literature even for the non-cooperative case to the best of our knowledge.

For a sanity check, we compare our results with [69] which provides a PEP expression for non-distributed (conventional) SC-STBC. Under the following assumptions

- Non-fading $R \to D$ link
- Perfect power control employed, i.e., $E_{SD} = E_{RD}$ and $E_{SR}/N_0 >> E_{RD}/N_0$

- High SNR, i.e., $\gamma_1 / N_0 = \gamma_2 / N_0 = E_{SD} / N_0 >> 1$,
- Equal channel memory lengths, i.e., $L = L_1 = L_2$,

it can be easily shown that (2.22) reduces to

$$P(\mathbf{x}, \hat{\mathbf{x}}) \le \left(\frac{E_{SD}}{4N_0} \right)^{-2(L+1)} \prod_{l=0}^{L} \left(\frac{1}{\boldsymbol{\lambda}_1(l)} \right)^2 \tag{2.43}$$

which was earlier reported in [69].

2.4 Distributed OFDM-STBC

In OFDM, the high-rate input stream is demultiplexed and transmitted over a number of low-rate independent frequency sub-carriers. This multicarrier transmission scheme can be efficiently implemented in practice using the Fast Fourier Transform (FFT). An elegant scheme for combining OFDM and STBC by implementing the Alamouti orthogonal structure at a block level was first reported in [36]. In this paper, we consider a similar transmission format as illustrated in Figure 2.3. Since we assume one relay, the information data symbols are parsed to two streams of $J \times 1$ blocks $\mathbf{x}_i^t \;\; i = 1,2$ and then precoded by $\boldsymbol{\Psi}_i = \mathbf{Q}^{\mathrm{H}}$ matrix where $\mathbf{Q}$ represents the inverse FFT (IFFT) matrix. The CP symbols here are the last $\tilde{L} = \max(L_1 + L_3, L_2)$ symbols of the transmission blocks.

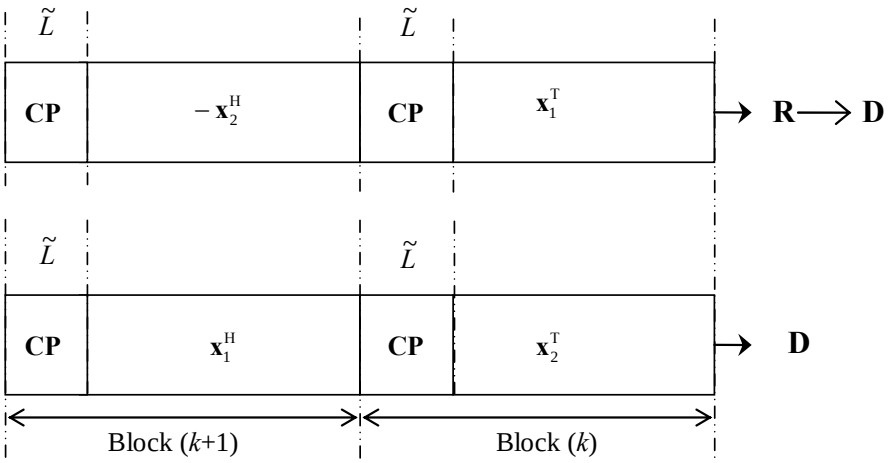

Figure 2.3: Transmission block format for D-OFDM-STBC.

The received signals at the destination terminal can be written as

$$\mathbf{r}^k = \sqrt{\gamma_1}\mathbf{H}_3\mathbf{H}_1\mathbf{Q}^{\mathrm{H}}\mathbf{x}_1^k + \sqrt{\gamma_2}\mathbf{H}_2\mathbf{Q}^{\mathrm{H}}\mathbf{x}_2^k + \mathbf{n}^k, \tag{2.44}$$

$$\mathbf{r}^{k+1} = -\sqrt{\gamma_1}\mathbf{H}_3\mathbf{H}_1\mathbf{Q}^{\mathrm{H}}\left(\mathbf{x}_2^k\right)^* + \sqrt{\gamma_2}\mathbf{H}_2\mathbf{Q}^{\mathrm{H}}\left(\mathbf{x}_1^k\right)^* + \mathbf{n}^{k+1}. \tag{2.45}$$

Applying the DFT[2] operation to (2.44) and (2.45) and using (2.36), we have

$$\mathbf{Q}\mathbf{r}^k = \sqrt{\gamma_1}\mathbf{\Lambda}_3\mathbf{\Lambda}_1\mathbf{x}_1^k + \sqrt{\gamma_2}\mathbf{\Lambda}_2\mathbf{x}_2^k + \mathbf{Q}\mathbf{n}^k, \tag{2.46}$$

$$\mathbf{Q}\mathbf{r}^{k+1} = -\sqrt{\gamma_1}\mathbf{\Lambda}_3\mathbf{\Lambda}_1\left(\mathbf{x}_2^k\right)^* + \sqrt{\gamma_2}\mathbf{\Lambda}_2\left(\mathbf{x}_1^k\right)^* + \mathbf{Q}\mathbf{n}^{k+1}. \tag{2.47}$$

Combining (2.46) and the conjugated version of (2.47) in a matrix form, we obtain

$$\begin{bmatrix} \mathbf{Q}\mathbf{r}^k \\ \left(\mathbf{Q}\mathbf{r}^{k+1}\right)^* \end{bmatrix} = \begin{bmatrix} \sqrt{\gamma_1}\mathbf{\Lambda_3}\mathbf{\Lambda}_1 & \sqrt{\gamma_2}\mathbf{\Lambda_2} \\ \sqrt{\gamma_2}\mathbf{\Lambda}_2^* & -\sqrt{\gamma_1}\mathbf{\Lambda}_3^*\mathbf{\Lambda}_1^* \end{bmatrix} \begin{bmatrix} \mathbf{x}_1^k \\ \mathbf{x}_2^k \end{bmatrix} + \begin{bmatrix} \mathbf{Q}\mathbf{n}^k \\ \left(\mathbf{Q}\mathbf{n}^{k+1}\right)^* \end{bmatrix} = \tilde{\mathbf{\Lambda}}\mathbf{x} + \tilde{\mathbf{N}}. \tag{2.48}$$

Multiplying (2.48) by (2.38) yields the decoupled streams

$$\mathbf{r}_{out,i}^k = \sqrt{\gamma_1\left|\mathbf{\Lambda}_3\right|^2\left|\mathbf{\Lambda}_1\right|^2 + \gamma_2\left|\mathbf{\Lambda}_2\right|^2}\,\mathbf{x}_i^k + \mathbf{n}_{out,i}^k,\ i = 1,2 \tag{2.49}$$

[2] We assume that the DFT size J is a power of 2, thus, the terms FFT and DFT are interchangeable.

where $\mathbf{n}_{out,i}^{k}$ is complex Gaussian noise with zero-mean and variance of $N_0/2$ per-dimension.

It is clear from the above descriptions that both OFDM and SC-FDE rely on FFT/IFFT operations. However, SC-FDE is distinct from OFDM in that the IFFT block is moved to the receiver end and placed before the decision device. This causes the effects of deep nulls in the channel frequency response (caused by the destructive addition of multipath) to spread out by the IFFT operation over all symbols, thus reducing their effect and improving the overall performance compared to uncoded OFDM.

As it will be demonstrated in the next section, uncoded OFDM fails to exploit the underlying rich multipath diversity. Outer coding with frequency interleaving can be combined with OFDM to extract the multipath diversity available in the considered cooperative scenario and, therefore, to further improve the performance. Although different outer codes can be employed, we consider trellis-coded modulation (TCM) [73] since it does not result in additional bandwidth expansion from the uncoded case. Previous works on the concatenation of TCM-STBC for the flat-fading channel case should also be noted [74]-[78].

2.4.1 Diversity Gain Analysis for D-OFDM-STBC

In this sub-section, we derive the PEP expression for the D-OFDM-STBC scheme. Under the assumptions of non-fading $R \to D$ link (i.e., $L_3 = 0$ and $\mathbf{h}_3[0] = 1$), perfect power control where $S \to D$ and $R \to D$ links are balanced, high SNRs for all underlying links (i.e., $E_{SD}/N_0 = E_{RD}/N_0 >> 1$ and $E_{SR}/N_0 > E_{SD}/N_0$), we follow the steps detailed in Appendix A.3 and obtain the PEP for D-OFDM-STBC as

$$P(\mathbf{x}, \hat{\mathbf{x}}) \le \left(\frac{E_{SD}}{4N_0}\right)^{-2} \frac{1}{\lambda_{\Sigma_1}} \frac{1}{\lambda_{\Sigma_2}} \tag{2.50}$$

where $\lambda_{\Sigma_1}, \lambda_{\Sigma_2}$ are, respectively, the eigenvalues of $\mathbf{\Sigma}_1$ and $\mathbf{\Sigma}_2$ which are functions of the codeword difference matrices. From (2.50), we conclude that uncoded D-OFDM-STBC achieves only a diversity order of two and fails to exploit the underlying multi-path diversity. For the general case where all underlying links experience frequency-selectivity and under similar assumptions on SNRs, we obtain the PEP expression as (see Appendix A.4)

$$P(\mathbf{x}, \hat{\mathbf{x}}) \le \left(\frac{E_{SD}}{4N_0}\right)^{-2} \frac{\Gamma(L_3)(L_3+1)}{\Gamma(L_3+1)} \frac{1}{\lambda_{\Sigma_1}} \frac{1}{\lambda_{\Sigma_2}}. \tag{2.51}$$

It is seen from (2.51) that the diversity order of uncoded D-OFDM-STBC is limited by two and is independent of the channel memory lengths L_1, L_2, and L_3. In other words, it extracts only the available spatial diversity, but fails to exploit the multipath diversity.

For non-fading $R \to D$ link, the PEP for trellis coded D-OFDM-STBC is given by (see Appendix A.5)

$$P(\mathbf{x}, \hat{\mathbf{x}}) \le \left(\frac{E_{SD}}{4N_0}\right)^{-\delta} \prod_{j_1=1}^{r_1} \left(\frac{1}{\boldsymbol{\lambda}_{\mathbf{\Theta}_1}(j_1)}\right)^{-1} \prod_{j_2=1}^{r_2} \left(\frac{1}{\boldsymbol{\lambda}_{\mathbf{\Theta}_2}(j_2)}\right)^{-1}. \tag{2.52}$$

Following a similar argument as in [78], it can be shown that the diversity order is

$$\delta = \min(\lceil ECL/2 \rceil, L_1 + 1) + \min(\lceil ECL/2 \rceil, L_2 + 1) \tag{2.53}$$

where ECL is the effective code length of the outer TCM code and $\lceil . \rceil$ denotes the ceiling function. For the general case where all links experience frequency-selectivity, it can be shown that the diversity order is

$$\delta = \min(\lceil ECL/2 \rceil, L_1 + 1, L_3 + 1) + \min(\lceil ECL/2 \rceil, L_2 + 1). \tag{2.54}$$

Our derivation points out that with an appropriate choice of underlying TCM code (i.e., with sufficiently large ECL), coded D-OFDM-STBC achieves the same diversity order as D-TR-STBC and D-SC-STBC. Therefore, using judiciously-designed outer codes with frequency-interleaving, both spatial and multipath diversity gains can be achieved in a coded D-OFDM-

STBC scheme[3]. For the convenience of the reader, we further consider various scenarios and present the achievable diversity order for each case in Table 2.2.

Table 2.2: Achievable Diversity Orders for Distributed OFDM-STBC.

$\mathbf{S \rightarrow R}$	$\mathbf{R \rightarrow D}$	$\mathbf{S \rightarrow D}$	**Coded**
Fading	Fading	Fading	$\min\left(\lceil ECL/2 \rceil, L_3+1, L_1+1\right)+\min\left(\lceil ECL/2 \rceil, L_2+1\right)$
Fading	Non-fading	Fading	$\min\left(\lceil ECL/2 \rceil, L_1+1\right)+\min\left(\lceil ECL/2 \rceil, L_2+1\right)$
Non-fading	Fading	Fading	$\min\left(\lceil ECL/2 \rceil, L_3+1\right)+\min\left(\lceil ECL/2 \rceil, L_2+1\right)$

2.5 Numerical Results

In this section, we present Monte-Carlo simulation results for distributed STBC systems which have been described and analyzed in the previous sections. We assume a quasi-static Rayleigh fading channel and employ 4-PSK modulation. First, we consider a scenario with a non-fading $R \rightarrow D$ link which can be justified in a practical scenario by the existence of a strong line-of-sight path [33]. $S \rightarrow D$ and $S \rightarrow R$ links are modeled as frequency-selective channels with memory lengths $L_1 = L_2 = 3$ and a uniform delay power profile. We further assume perfect power control, i.e., the $S \rightarrow D$ and $R \rightarrow D$ links are balanced. Under this scenario, Figure 2.4 illustrates the symbol error rate (SER) performance of D-TR-STBC, D-SC-STBC and uncoded D-OFDM-STBC for $E_{SR}/N_0 = 25\text{dB}$. D-TR-STBC and D-SC-STBC yield identical performance and both schemes (with MLSE decoding) are able to provide a diversity order of $L_1 + L_2 + 2 = 8$, confirming our conclusions from the PEP analysis,

[3] Besides the employment of outer coding, another alternative to extract multipath diversity is to use space-time-frequency (STF) codes proposed in [79] which exploit subgrouping technique to design low-complexity STF block codes.

c.f. (2.23). Although MLSE is able to collect the maximum achievable diversity gain, its complexity might be prohibitive for some cases. Therefore, we also consider MMSE in our simulations as an alternative suboptimum equalizer. Our simulation results indicate that the MLSE equalizer outperforms the MMSE equalizer by $\approx 2.7\text{dB}$ at $SER = 10^{-4}$. This loss can be further reduced, if multiple antennas are employed at the destination [80]. It is also observed from Figure 2.4 that both schemes outperform uncoded D-OFDM-STBC significantly since the latter scheme is not able to exploit the underlying multipath diversity without channel coding and frequency interleaving as previously discussed. We notice from the figure that both D-TR-STBC and D-SC-STBC outperform D-OFDM-STBC by $\approx 4\text{dB}$ and 6dB at $SER = 10^{-3}$ for MMSE and MLSE implementations, respectively.

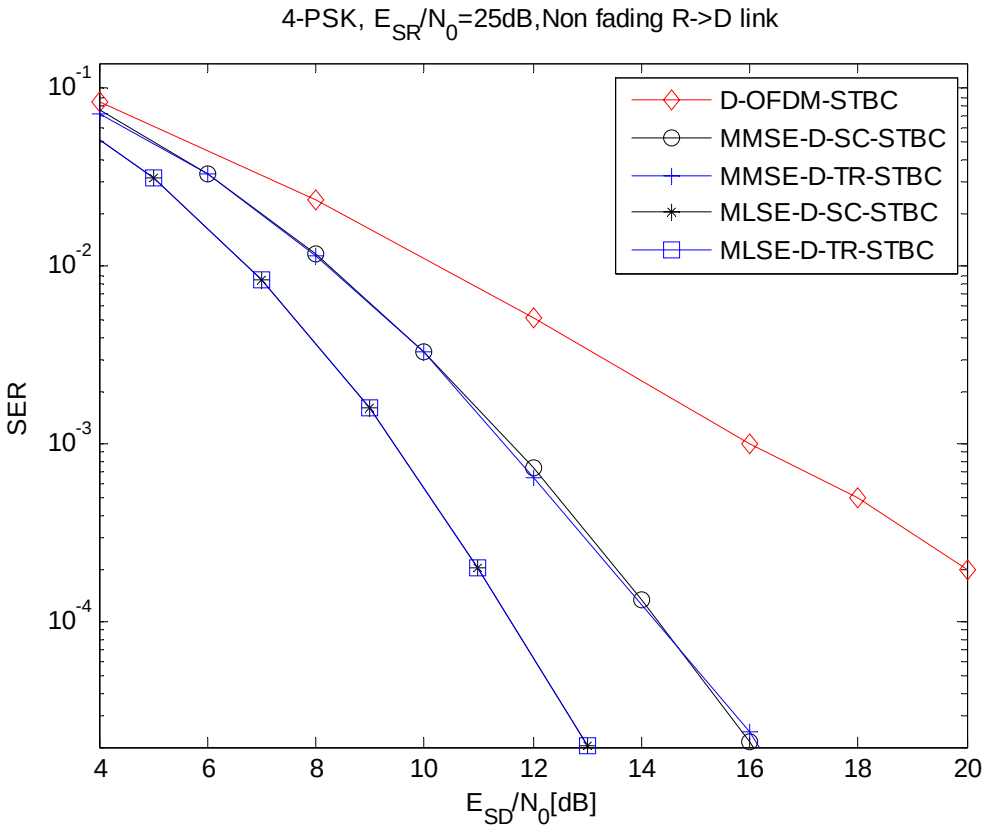

Figure 2.4: SER performances of D-TR-STBC, D-SC-STBC and D-OFDM STBC for non-fading $R \rightarrow D$ link ($E_{SR} / N_0 = 25\text{dB}$).

Figure 2.5 illustrates the performance of D-TR-STBC, D-SC-STBC and uncoded D-OFDM-STBC for $E_{SR}/N_0 = 5\text{dB}$ and $E_{SR}/N_0 = 15\text{dB}$. The performances of all three schemes are significantly degraded as E_{SR}/N_0 decreases, confirming our observations from (2.25). As noted previously, this is an inherent disadvantage of the adopted user cooperation protocol of [33]. Relay-selection algorithms can be used to remove the error floor and to preserve the diversity order at an acceptable level [81]. Another alternative to avoid error floors is the deployment of Protocol I [33] where the source-to-destination transmission is allowed within the first signaling interval.

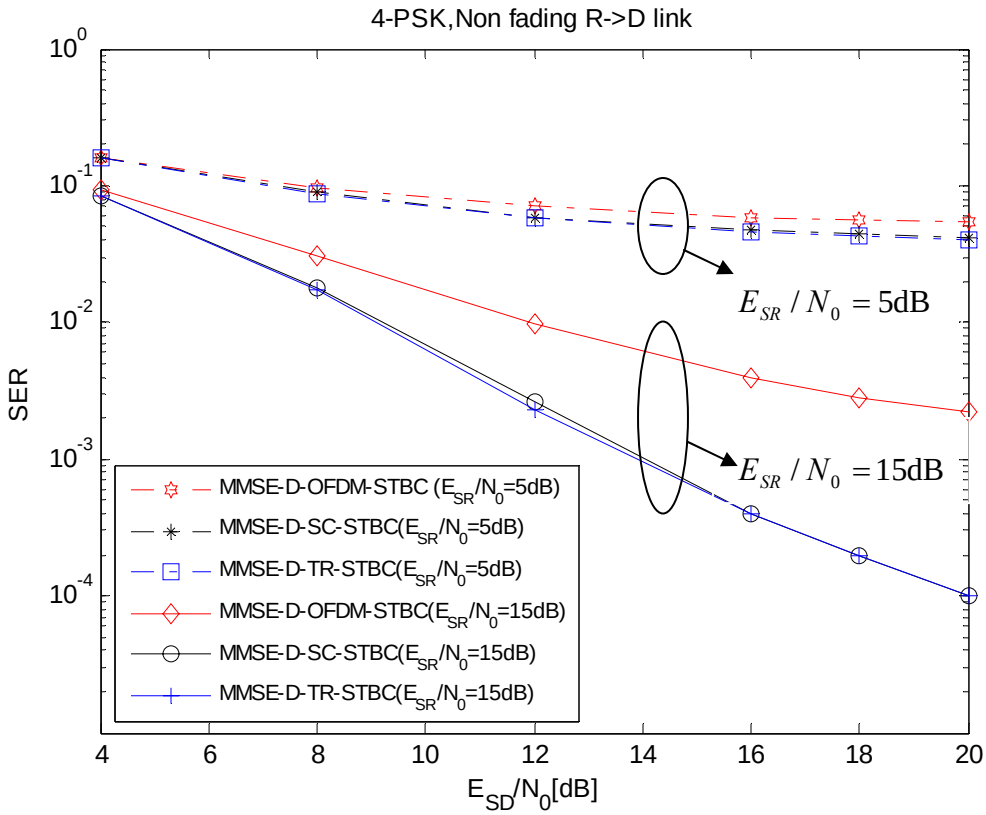

Figure 2.5: SER performances of D-TR-STBC, D-SC-STBC and D-OFDM STBC for non-fading $R \rightarrow D$ link. ($E_{SR}/N_0 = 5\text{dB},15\text{dB}$)

In Figures 2.6 and 2.7, we investigate the performance of D-TR-STBC assuming MLSE equalization and relaxing the assumption of non-fading $R \to D$ link. We assume various combinations of channel memory lengths. It should be noted here that interchanging the values of L_1 and L_3 yields identical performance and those symmetrical scenarios are omitted here for the sake of presentation simplicity. The case of non-fading $R \to D$ link (i.e., L_3=0 with $\mathbf{h}_3[0]=1$), is also included as a benchmark.

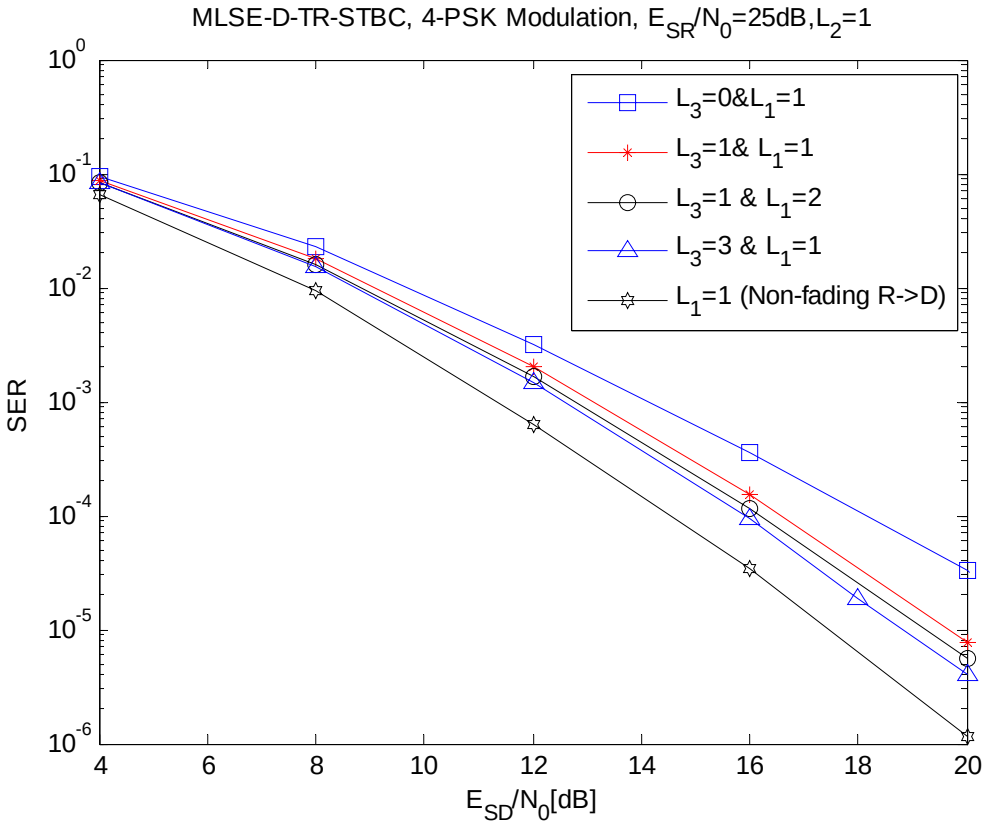

Figure 2.6: SER performance of D-TR-STBC over frequency-selective $S \to R$, $R \to D$ and $S \to D$ links for various combinations of channel lengths.

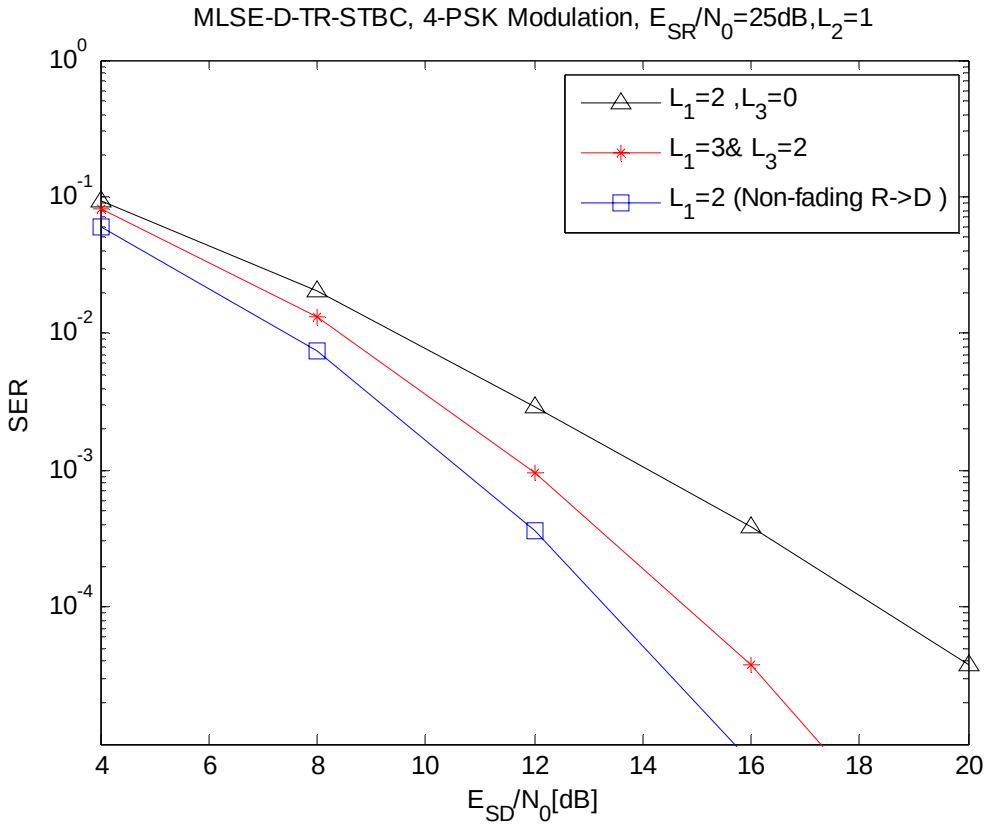

Figure 2.7: SER performance of D-TR-STBC over frequency-selective $S \to R$, $R \to D$ and $S \to D$ links for various combinations of channel lengths.

It is clear from the slopes of the error rate performance curves in Figures 2.6 and 2.7 that the maximum achievable order is $\min(L_1, L_3) + L_2 + 2$ for each case, confirming our observations from the PEP expressions in (2.29)-(2.31). For example, in Figure 2.6 for the considered scenarios of $(L_1 = 1 \text{ and } L_3 = 1)$, $(L_1 = 2 \text{ and } L_3 = 1)$ and $(L_1 = 1 \text{ and } L_3 = 3)$, all three give identical slopes achieving a diversity order of 4 as predicted through (2.29)-(2.31). For the non-fading $R \to D$ link, we observe a diversity order of 4 as predicted by (2.23). We should emphasize here that the complexity of the MLSE receiver (given by the number of trellis states in the Viterbi algorithm) is adjusted according to the channel memory length for each scenario to extract the available multipath diversity. For instance, we use a total of 4^3 states and 4^4 states for $(L_1 = 1 \text{ and } L_3 = 1)$ and $(L_1 = 2 \text{ and } L_3 = 1)$, respectively.

Figure 2.8 depicts the SER performance of D-SC-STBC scheme with power imbalance, i.e., $E_{SD} \neq E_{RD}$. We assume $E_{SD} = nE_{RD}$ and compare the error rate performance for two different ratios, i.e., n=0.1 and 10. We also include the performance of perfect power control case, i.e., n=1, as a benchmark. We observe performance improvement in the low-to-intermediate SNR range for n=0.1, i.e. $E_{RD} >> E_{SD}$ in comparison to the balanced case, i.e. n=1; however, this also results in an immediate error floor. On the other hand, larger values of n result in performance degradation in the low-to-intermediate SNR range while it results in performance improvement over the perfect power control case for asymptotically high SNR values.

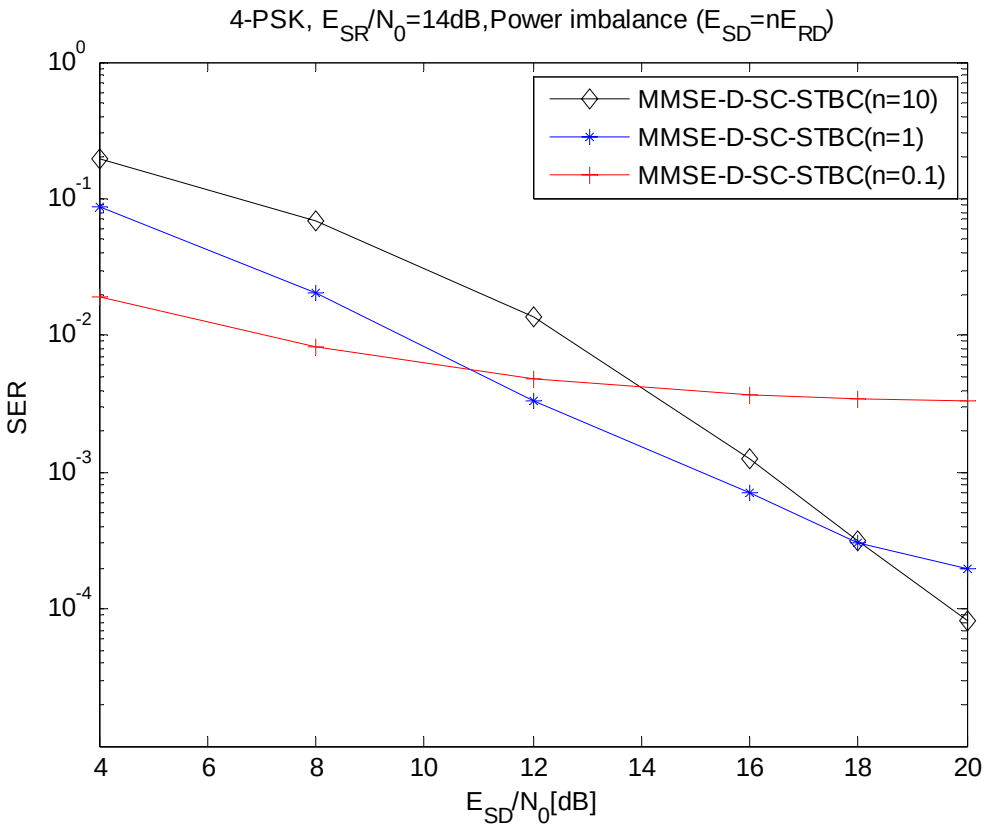

Figure 2.8: SER performance of MMSE-D-SC-STBC scheme with power imbalance.

Figure 2.9 depicts the SER performance of coded D-OFDM-STBC and compares it to that of D-TR-STBC. Taking into account the rate of TCM code, SNR has been penalized for both schemes under consideration. A 16-state 8-PSK Ungerboeck code with rate=2/3 and effective code length of 3 (labeled as U16) [73] is employed as an outer code. We assume $E_{SR}/N_0 = 35\text{dB}$ and consider the following scenarios:

1) $L_1 = L_2 = L = 1$ and non-fading $R \to D$ link, i.e. $L_3 = 0$ and $\mathbf{h}_3[0] = 1$.

2) $L_1 = L_2 = L = 1$ and frequency-flat $R \to D$ link, i.e. $L_3 = 0$

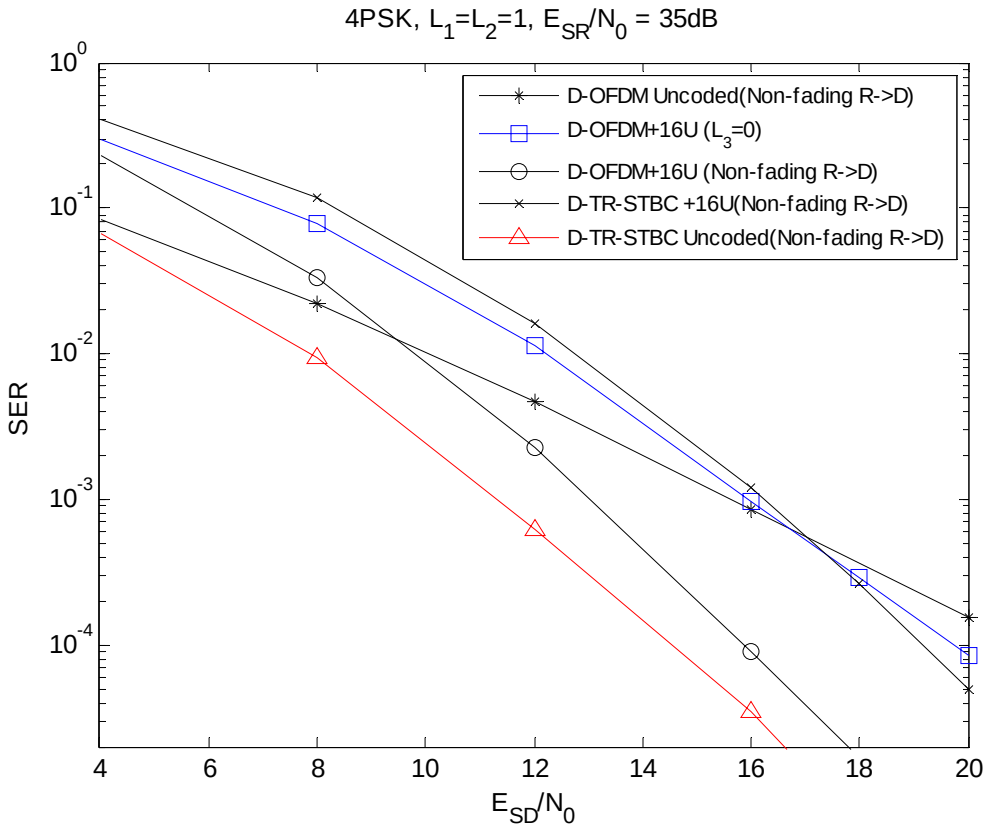

Figure 2.9: SER performances of D-TR-STBC and D-STBC-OFDM schemes with outer TCM code.

As Figure 2.9 clearly demonstrates, coded D-OFDM-STBC has comparable performance to D-TR-STBC achieving the same diversity order. Specifically, D-OFDM-STBC achieves a diversity order of 4, as predicted by (2.53), i.e., $2\times\min\left(\lceil ECL/2\rceil=2, L+1=2\right)=4$. For the second scenario, we observe a diversity order of 3 confirming (2.54), i.e., $\min\left(\lceil ECL/2\rceil=2,2,1\right)+\min\left(\lceil ECL/2\rceil=2,2\right)=3$. It is also interesting to note that the performance of the *uncoded* D-TR-STBC outperforms its *coded* version. This is a result of the fact that we assume separate decoding and equalization in our implementation. A similar observation has been reported in [82], [83] in the context of conventional TCM systems.

Appendix A

This Appendix presents the derivations of PEP expressions for D-TR-STBC, uncoded D-OFDM-STBC and TCM-D-OFDM-STBC. In the following, we drop the indices (*k*,*i*) for notational brevity.

Appendix A.1 Derivation of Eq. (2.22)

In this Appendix, we derive the PEP expression for D-TR-STBC scheme for non-fading $R \to D$ link and frequency-selective $S \to R$ and $S \to D$ links. Defining the transmitted codeword vector and erroneously decoded codeword vector as $\mathbf{x}$ and $\hat{\mathbf{x}}$, respectively, the Chernoff bound on PEP is given as

$$P(\mathbf{x}, \hat{\mathbf{x}} \,|\, \mathbf{h}_1, \mathbf{h}_2) \le \exp\left(-\frac{d^2(\mathbf{x}, \hat{\mathbf{x}})}{4N_0} \right) \tag{2.55}$$

where $d^2(\mathbf{x}, \hat{\mathbf{x}})$ is earlier defined by (2.21) and repeated below for the reader's convenience

$$d^2(\mathbf{x}, \hat{\mathbf{x}}) = \gamma_1 \left\| \mathbf{h}_1^{\mathrm{T}} (\boldsymbol{\chi} - \hat{\boldsymbol{\chi}}) \right\|^2 + \gamma_2 \left\| \mathbf{h}_2^{\mathrm{T}} (\boldsymbol{\chi} - \hat{\boldsymbol{\chi}}) \right\|^2 .$$

By introducing $\boldsymbol{\chi}_i = (\boldsymbol{\chi}_i - \hat{\boldsymbol{\chi}}_i)(\boldsymbol{\chi}_i - \hat{\boldsymbol{\chi}}_i)^{\mathrm{H}}$ with dimensions of $(L_i + 1) \times (L_i + 1)$, (2.21) can be written as

$$d^2(\mathbf{x}, \hat{\mathbf{x}}) = \gamma_1 \mathbf{h}_1^{\mathrm{T}} \boldsymbol{\chi}_1 \left(\mathbf{h}_1^{\mathrm{T}} \right)^{\mathrm{H}} + \gamma_2 \mathbf{h}_2^{\mathrm{T}} \boldsymbol{\chi}_2 \left(\mathbf{h}_2^{\mathrm{T}} \right)^{\mathrm{H}} . \tag{2.56}$$

Further defining $\boldsymbol{\Omega}_i = diag(\mathbf{v}_i)$, $\boldsymbol{\mu}_i = \boldsymbol{\Omega}_i^{-1/2} \mathbf{h}_i$, and $\mathbf{A}_i = \boldsymbol{\Omega}_i^{1/2} \boldsymbol{\chi}_i \boldsymbol{\Omega}_i^{1/2}$ $i = 1,2$, we obtain

$$d^2(\mathbf{x}, \hat{\mathbf{x}}) = \gamma_1 \boldsymbol{\mu}_1^{\mathrm{T}} \mathbf{A}_1 \left(\boldsymbol{\mu}_1^{\mathrm{T}} \right)^{\mathrm{H}} + \gamma_2 \boldsymbol{\mu}_2^{\mathrm{T}} \mathbf{A}_2 \left(\boldsymbol{\mu}_2^{\mathrm{T}} \right)^{\mathrm{H}} . \tag{2.57}$$

where $\mathbf{A}_i$, $i = 1,2$, are full rank due to zero padding [69]. Since $\mathbf{A}_i$ is Hermitian, there exists a unitary matrix $\mathbf{U}_{\mathbf{A}_i}$ such that $\mathbf{U}_{\mathbf{A}_i}^{\mathrm{H}} \mathbf{A}_i \mathbf{U}_{\mathbf{A}_i} = \boldsymbol{\Delta}_i$ where $\boldsymbol{\Delta}_i$ is a real diagonal matrix of size

$(L_i+1)(L_i+1)$ with non-negative entries. Noting that the diagonal elements of $\mathbf{\Delta}_i$ are the eigenvalues of $\mathbf{A}_i$, (2.57) can be written as

$$d^2(\mathbf{x},\hat{\mathbf{x}}) = \gamma_1 \boldsymbol{\beta}_1 \mathbf{\Delta}_1 \boldsymbol{\beta}_1^{\mathrm{H}} + \gamma_2 \boldsymbol{\beta}_2 \mathbf{\Delta}_2 \boldsymbol{\beta}_2^{\mathrm{H}} \tag{2.58}$$

where $\boldsymbol{\beta}_i = \boldsymbol{\mu}_i^{\mathrm{T}} \mathbf{U}_{\mathbf{A}_i}, i = 1,2$ is a zero-mean complex Gaussian vector with unit variance. Thus, we can express (2.58) as

$$d^2(\mathbf{x},\hat{\mathbf{x}}) = \gamma_1 \sum_{l_1=0}^{L_1} \boldsymbol{\lambda}_1(l_1) \left|\boldsymbol{\beta}_1(l_1)\right|^2 + \gamma_2 \sum_{l_2=0}^{L_2} \boldsymbol{\lambda}_2(l_2) \left|\boldsymbol{\beta}_2(l_2)\right|^2 \tag{2.59}$$

where $\lambda_i(l_i)$ denotes the l_i^{th} eigenvalue of $\mathbf{\Delta}_i$. Substituting (2.59) in (2.55) and averaging the resulting expression with respect to $\left|\boldsymbol{\beta}_1(l_1)\right|$ and $\left|\boldsymbol{\beta}_2(l_2)\right|$ which are Rayleigh distributed, we obtain the final PEP expression as

$$P(\mathbf{x},\hat{\mathbf{x}}) \le \prod_{l_1=0}^{L_1} \left(1 + \frac{\gamma_1}{4N_0} \boldsymbol{\lambda}_1(l_1)\right)^{-1} \prod_{l_2=0}^{L_2} \left(1 + \frac{\gamma_2}{4N_0} \boldsymbol{\lambda}_2(l_2)\right)^{-1}. \tag{2.60}$$

Appendix A.2 Derivation of Eqs. (2.29)-(2.31)

In this Appendix, we derive the PEP expression for the D-TR-STBC scheme assuming frequency-selective channels in $S \to R$, $S \to D$ and $R \to D$ links. The Chernoff bound on PEP is given as

$$P(\mathbf{x},\hat{\mathbf{x}} \mid \mathbf{h}_1, \mathbf{h}_2, \mathbf{h}_3) \le \exp\left(-\frac{d^2(\mathbf{x},\hat{\mathbf{x}})}{4N_0}\right). \tag{2.61}$$

The Euclidean distance between $\mathbf{x}$ and $\hat{\mathbf{x}}$ can be written as

$$d^2(\mathbf{x},\hat{\mathbf{x}}) = \gamma_1 \left\|\mathbf{H}_3 \mathbf{H}_1 \left(\mathbf{d} - \hat{\mathbf{d}}\right)\right\|^2 + \gamma_2 \left\|\mathbf{H}_2 \left(\mathbf{d} - \hat{\mathbf{d}}\right)\right\|^2 \tag{2.62}$$

where $\gamma_1 = \gamma_2 = E_{SD}$. To simplify analysis, (2.62) can be approximated[4] as

$$d^2(\mathbf{x},\hat{\mathbf{x}}) \approx \frac{\gamma_1}{J}\|\mathbf{H}_3\|^2\left\|\mathbf{H}_1\left(\mathbf{d}-\hat{\mathbf{d}}\right)\right\|^2 + \gamma_2\left\|\mathbf{H}_2\left(\mathbf{d}-\hat{\mathbf{d}}\right)\right\|^2$$

$$\approx \frac{\gamma_1}{J}\|\mathbf{H}_1\|^2\left\|\mathbf{H}_3\left(\mathbf{d}-\hat{\mathbf{d}}\right)\right\|^2 + \gamma_2\left\|\mathbf{H}_2\left(\mathbf{d}-\hat{\mathbf{d}}\right)\right\|^2. \quad (2.63)$$

where J is the frame length. Noting that $\|\mathbf{H}_i\|^2 = J\sum_{l_i=0}^{L_i}\left|\mathbf{h}_i(l_i)\right|^2$, i=1,3 , we can further write (2.63) as

$$d^2(\mathbf{x},\hat{\mathbf{x}}) \approx \gamma_1\sum_{l_3=0}^{L_3}\left|\mathbf{h}_3(l_3)\right|^2\left\|\mathbf{H}_1\left(\mathbf{d}-\hat{\mathbf{d}}\right)\right\|^2 + \gamma_2\left\|\mathbf{H}_2\left(\mathbf{d}-\hat{\mathbf{d}}\right)\right\|^2$$

$$\approx \gamma_1\sum_{l_1=0}^{L_1}\left|\mathbf{h}_1(l_1)\right|^2\left\|\mathbf{H}_3\left(\mathbf{d}-\hat{\mathbf{d}}\right)\right\|^2 + \gamma_2\left\|\mathbf{H}_2\left(\mathbf{d}-\hat{\mathbf{d}}\right)\right\|^2. \quad (2.64)$$

Following similar steps in Appendix A.1, we can write (2.64) as follows

$$d^2(\mathbf{x},\hat{\mathbf{x}}) \approx \gamma_1\sum_{l_3=0}^{L_3}\left|\mathbf{h}_3(l_3)\right|^2\sum_{l_1=0}^{L_1}\boldsymbol{\lambda}_1(l_1)\left|\boldsymbol{\beta}_1(l_1)\right|^2 + \gamma_2\sum_{l_2=0}^{L_2}\boldsymbol{\lambda}_2(l_2)\left|\boldsymbol{\beta}_2(l_2)\right|^2 \quad (2.65)$$

$$\approx \gamma_1\sum_{l_1=0}^{L_1}\left|\mathbf{h}_1(l_1)\right|^2\sum_{l_3=0}^{L_3}\boldsymbol{\lambda}_1(l_3)\left|\boldsymbol{\beta}_1(l_3)\right|^2 + \gamma_2\sum_{l_2=0}^{L_2}\boldsymbol{\lambda}_2(l_2)\left|\boldsymbol{\beta}_2(l_2)\right|^2 \quad (2.66)$$

where $\boldsymbol{\lambda}_i(l_i)$, i=1,2 denote the l_i^{th} eigenvalue of codeword difference matrixes and $\boldsymbol{\beta}_i$ are zero-mean complex Gaussian vectors with unit variance. In the following, we will derive the PEP expression under three different scenarios:

Case 1: $L_3 > L_1$

First, we define the random variables $Y_2 = \sum_{l_2=0}^{L_2}\boldsymbol{\lambda}_2(l_2)\left|\boldsymbol{\beta}_2(l_2)\right|^2$ and $Y_1 = X_1X_2$ with $X_1 = \sum_{l_3=0}^{L_3}\left|\mathbf{h}_3(l_3)\right|^2$ and $X_2 = \sum_{l_1=0}^{L_1}\boldsymbol{\lambda}_1(l_1)\left|\boldsymbol{\beta}_1(l_1)\right|^2$. Substituting (2.65) in (2.61) and averaging the resulting expression with respect to Y_1 and Y_2, we obtain

[4] Through a Monte-Carlo simulation experiment, we have observed that the mean square error (MSE) difference between (2.62) and (2.63) is only ~0.3 at $E_{SD}/N_0 = 4$dB. The approximate expression converges to the exact one as early as $E_{SD}/N_0 = 6$dB. Therefore, this approximation can be used safely for any practical purpose.

$$P(\mathbf{x},\hat{\mathbf{x}}) \le E_{Y_1}\left[\exp\left(-\frac{E_{SD}}{4N_0}Y_1\right)\right]E_{Y_2}\left[\exp\left(-\frac{E_{SD}}{4N_0}Y_2\right)\right]$$
$$= \Phi_{Y_1}(\omega)\Big|_{j\omega=-\frac{E_{SD}}{4N_0}} \times \Phi_{Y_2}(\omega)\Big|_{j\omega=-\frac{E_{SD}}{4N_0}} \quad (2.67)$$

where $\Phi_{Y_1}(\omega)$ and $\Phi_{Y_2}(\omega)$ are the characteristic functions of Y_1 and Y_2 respectively. Since the entries of $|\boldsymbol{\beta}_2|$ are Rayleigh distributed, $\Phi_{Y_2}(\omega)$ is readily found as [84]

$$\Phi_{Y_2}(\omega)\Big|_{j\omega=-\frac{E_{SD}}{4N_0}} = \prod_{l_2=0}^{L_2}\left(1+\frac{E_{SD}}{4N_0}\boldsymbol{\lambda}(l_2)\right)^{-1} . \quad (2.68)$$

$\Phi_{Y_1}(\omega)$ can be evaluated as [85]

$$\Phi_{Y1}(\omega) = \int_0^\infty f_{X_1}(x_1)\Phi_{X_2}(\omega x_1)dx_1 \quad (2.69)$$

where $f_{X_1}(x_1), x_1 \ge 0$ is the probability density function (pdf) of X_1 and $\Phi_{X_2}(\omega x_1)$ is the characteristic function of X_2. In our case, $\mathbf{h}_3$ are modeled as zero-mean complex Gaussian random variables with variance $1/2(L_3+1)$ per-dimension (i.e., uniform power profile). Therefore, X_1 is a chi-squared random variable with $2(L_3+1)$ degrees of freedom with the following pdf [86],

$$f_{X_1}(x_1) = \frac{(L_3+1)^{L_3+1}}{\Gamma(L_3+1)}x_1^{L_3}e^{-x_1(L_3+1)} . \quad (2.70)$$

Substituting (2.70) in (2.69) and also noting $\Phi_{X_2}(\omega x_1) = \prod_{l_1=0}^{L_1} 1/(1-j\omega x_1\boldsymbol{\lambda}(l_1))$ [84], (2.69) can be written as

$$\Phi_{Y_1}(\omega)\Big|_{j\omega=-\frac{E_{SD}}{4N_0}} = \frac{(L_3+1)^{L_3+1}}{\Gamma(L_3+1)}\left(\frac{E_{SD}}{4N_0}\right)^{-(L_1+1)}\prod_{l_1=0}^{L_1}(\boldsymbol{\lambda}_1(l_1))^{-1}\int_0^\infty \frac{x_1^{L_3}e^{-x_1(L_3+1)}}{\prod_{l_1}^{L_1}\left(\frac{1}{\boldsymbol{\lambda}_1(l_1)E_{SD}/4N_0}+x_1\right)}dx_1 \quad (2.71)$$

Assuming high SNR, i.e., $E_{SD}/4N_0$ >>1, (2.71) yields

$$\Phi_{Y_1}(\omega)\Big|_{j\omega=-\frac{E_{SD}}{4N_0}} = \frac{(L_3+1)^{L_3+1}}{\Gamma(L_3+1)}\left(\frac{E_{SD}}{4N_0}\right)^{-(L_1+1)} \prod_{l_1=0}^{L_1}(\boldsymbol{\lambda}_1(l_1))^{-1}\int_0^{\infty} x_1^{L_3-L_1}e^{-x_1(L_3+1)}dx_1 . \quad (2.72)$$

Using the integral form given by [71, p.382, 3.351.3], we obtain

$$\Phi_{Y_1}(\omega)\Big|_{j\omega=-\frac{E_{SD}}{4N_0}} = (L_3+1)^{L_1}\frac{\Gamma(L_3-L_1+1)}{\Gamma(L_3+1)}\left(\frac{E_{SD}}{4N_0}\right)^{-(L_1+1)} \prod_{l_1=0}^{L_1}(\boldsymbol{\lambda}_1(l_1))^{-1} . \quad (2.73)$$

Substituting (2.73) and (2.68) in (2.67), we find the final PEP expression as

$$P(\mathbf{x},\hat{\mathbf{x}}) \le (L_3+1)^{L_1}\frac{\Gamma(L_3-L_1+1)}{\Gamma(L_3+1)}\left(\frac{E_{SD}}{4N_0}\right)^{-(L_1+L_2+2)} \prod_{l_1=0}^{L_1}(\boldsymbol{\lambda}_1(l_1))^{-1}\prod_{l_2=0}^{L_2}(\boldsymbol{\lambda}_2(l_2))^{-1} \quad (2.74)$$

Case 2: $L_1 > L_3$

Using (2.66) and noting that this case is similar to Case 1 with L_1 and L_3 now interchanged, the PEP expression is found as

$$P(\mathbf{x},\hat{\mathbf{x}}) \le (L_1+1)^{L_3}\frac{\Gamma(L_1-L_3+1)}{\Gamma(L_1+1)}\left(\frac{E_{SD}}{4N_0}\right)^{-(L_3+L_2+2)} \prod_{l_3=0}^{L_3}(\boldsymbol{\lambda}_1(l_3))^{-1}\prod_{l_2=0}^{L_2}(\boldsymbol{\lambda}_2(l_2))^{-1} . \quad (2.75)$$

Case 3: $L_1 = L_3$

Following the same argument in Case 1 and using partial fraction expansion, (2.71) can be rewritten as

$$\Phi_{Y_1}(\omega)\Big|_{j\omega=-\frac{E_{SD}}{4N_0}} = \frac{(L_3+1)^{L_3+1}}{\Gamma(L_3+1)}\sum_{l_1=1}^{L_1+1}\frac{p_{l_1}}{\boldsymbol{\lambda}_1(l_1)E_{SD}/4N_0}\int_0^{\infty}\frac{x_1^{L_3}e^{-x_1(L_3+1)}}{\left(\frac{1}{\boldsymbol{\lambda}_1(l_1)E_{SD}/4N_0}+x_1\right)}dx_1 \quad (2.76)$$

where $p_{l_1} = \prod_{l=0,l\neq l_1}^{L_1}(\boldsymbol{\lambda}_1(l_1)/\boldsymbol{\lambda}_1(l_1)-\boldsymbol{\lambda}_1(l))$. Using the integral form given by [71, p.338, 3.353.5.7] and after some mathematical manipulation, we obtain

$$\Phi_{Y_1}(\omega)\Big|_{j\omega=-\frac{E_{SD}}{4N_0}} = \frac{(L_3+1)^{L_3+1}}{\Gamma(L_3+1)}(-1)^{L_3-1}(E_{SD}/4N_0)^{-(L_3+1)}\sum_{l_1=1}^{L_1+1}\frac{p_{l_1}}{(\boldsymbol{\lambda}_1(l_1))^{L_3+1}}e^{\frac{4N_0(L_3+1)}{\boldsymbol{\lambda}_1(l_1)E_{SD}}}E_i\left(-\frac{4N_0(L_3+1)}{\boldsymbol{\lambda}_1(l_1)E_{SD}}\right)$$

$$+\frac{(L_3+1)^{L_3+1}}{\Gamma(L_3+1)}\sum_{l_1=1}^{L_1+1}\sum_{k=1}^{L_3}(k-1)!(-1)^{L_3-k}(L_3+1)^{-k}\frac{p_{l_1}}{(\boldsymbol{\lambda}_1(l_1))^{L_3+1-k}}(E_{SD}/4N_0)^{-(L_3+1-k)} \tag{2.77}$$

where $\Gamma(.)$ and $E_i(.)$ represent the gamma function and the exponential-integral function, respectively [71]. Using the fact $\sum_{l_1=1}^{L_1+1} p_{l_1}/\lambda_1^r(l_1)=0\,(1\le r\le L_1)$ and noting that $L_1=L_3$, the second term in (2.77) becomes zero. Substituting (2.77) and (2.68) in (2.67) and assuming high SNR, we find the PEP expression given as

$$P(\mathbf{x},\hat{\mathbf{x}}) \le \frac{(L_3+1)^{L_3+1}}{\Gamma(L_3+1)}(-1)^{L_3-1}\left(\frac{E_{SD}}{4N_0}\right)^{-(L_3+L_2+2)}\prod_{l_2=0}^{L_2}(\boldsymbol{\lambda}_2(l_2))^{-1}\sum_{l_1=1}^{L_1+1}\frac{p_{l_1}}{(\boldsymbol{\lambda}_1(l_1))^{L_3+1}}e^{\frac{4N_0(L_3+1)}{\boldsymbol{\lambda}_1(l_1)E_{SD}}}E_i\left(-\frac{4N_0(L_3+1)}{\boldsymbol{\lambda}_1(l_1)E_{SD}}\right)$$

(2.78)

Appendix A.3 Derivation of Eq. (2.50)

In this Appendix, we derive the PEP expression for the D-OFDM-STBC scheme assuming a non-fading $R\to D$ link. For this scheme, the distance metric $d^2(\mathbf{x},\hat{\mathbf{x}})$ is given by

$$d^2(\mathbf{x},\hat{\mathbf{x}}) = \gamma_1\left\|(\mathrm{diag}(\mathbf{x}-\hat{\mathbf{x}})\mathbf{f}_1)\mathbf{h}_1\right\|^2 + \gamma_2\left\|(\mathrm{diag}(\mathbf{x}-\hat{\mathbf{x}})\mathbf{f}_2)\mathbf{h}_2\right\|^2, \tag{2.79}$$

where we define $\mathbf{f}_i = \exp(-j2\pi(p-1)(q-1)/J)$, $p=1,...J$, $q=1,...L_i+1$. This can be further simplified as

$$d^2(\mathbf{x},\hat{\mathbf{x}}) = \gamma_1\boldsymbol{\varepsilon}_1^{\mathrm{H}}\boldsymbol{\Sigma}_1\boldsymbol{\varepsilon}_1 + \gamma_2\boldsymbol{\varepsilon}_2^{\mathrm{H}}\boldsymbol{\Sigma}_2\boldsymbol{\varepsilon}_2 \tag{2.80}$$

where $\boldsymbol{\Sigma}_i = \mathbf{U}_i^{\mathrm{H}}\boldsymbol{\Omega}_i^{1/2}(\mathrm{diag}(\mathbf{x}-\hat{\mathbf{x}})\mathbf{f}_i)^{\mathrm{H}}(\mathrm{diag}(\mathbf{x}-\hat{\mathbf{x}})\mathbf{f}_i)\boldsymbol{\Omega}_i^{1/2}\mathbf{U}_i$ and $\boldsymbol{\varepsilon}_i = \mathbf{U}_i^{\mathrm{H}}\boldsymbol{\Omega}_i^{-1/2}\mathbf{h}_i$, $i=1,2$ and $\mathbf{U}_i$ is a unitary matrix. Note that $\boldsymbol{\Sigma}_i$ is a rank-one Hermitian matrix of size $(L_i+1)(L_i+1)$. Substituting (2.80) in (2.55), we follow similar steps as in Appendix A.1 to obtain the final form for PEP as

$$P(\mathbf{x},\hat{\mathbf{x}}) \le \left(\frac{E_{SD}}{4N_0}\right)^{-2} \frac{1}{\lambda_{\Sigma_1}} \frac{1}{\lambda_{\Sigma_2}} \tag{2.81}$$

where $\lambda_{\Sigma_1}, \lambda_{\Sigma_2}$ are the eigenvalues of $\mathbf{\Sigma}_1$ and $\mathbf{\Sigma}_2$, respectively.

Appendix A.4 Derivation of Eq. (2.51)

In this Appendix, we derive the PEP expression for the D-OFDM-STBC scheme given that all underlying links are frequency-selective. For this scheme, the distance metric $d^2(\mathbf{x},\hat{\mathbf{x}})$ is given by

$$d^2(\mathbf{x},\hat{\mathbf{x}}) = \gamma_1 \left\| (\text{diag}(\mathbf{x}-\hat{\mathbf{x}})\mathbf{f}_1)\mathbf{h}_1\mathbf{f}_3\mathbf{h}_3 \right\|^2 + \gamma_2 \left\| (\text{diag}(\mathbf{x}-\hat{\mathbf{x}})\mathbf{f}_2)\mathbf{h}_2 \right\|^2. \tag{2.82}$$

Using similar arguments of Appendix A.2, we can write the distance metric as

$$d^2(\mathbf{x},\hat{\mathbf{x}}) \approx \gamma_1 \sum_{l_3=0}^{L_3} \left|\mathbf{h}_3(l_3)\right|^2 \boldsymbol{\varepsilon}_1^{\mathrm{H}} \mathbf{\Sigma}_1 \boldsymbol{\varepsilon}_1 + \gamma_2 \boldsymbol{\varepsilon}_2^{\mathrm{H}} \mathbf{\Sigma}_2 \boldsymbol{\varepsilon}_2 \tag{2.83}$$

Substituting (2.83) in (2.61) and following the steps in detailed in AppendixA.2, we obtain

$$P(\mathbf{x},\hat{\mathbf{x}}) \le \left(\frac{E_{SD}}{4N_0}\right)^{-2} \frac{\Gamma(L_3)(L_3+1)}{\Gamma(L_3+1)} \frac{1}{\lambda_{\Sigma_1}} \frac{1}{\lambda_{\Sigma_2}} \tag{2.84}$$

where $\lambda_{\Sigma_1}, \lambda_{\Sigma_2}$ are the eigenvalues of $\mathbf{\Sigma}_1$ and $\mathbf{\Sigma}_2$, respectively.

Appendix A.5 Derivation of Eq. (2.52)

In this Appendix, we derive the PEP expression for trellis-coded D-OFDM-STBC scheme. Instead of the uncoded data in the original D-OFDM-STBC scheme, the TCM encoder outputs are interleaved and then precoded by the IFFT matrix $\mathbf{Q}^{\mathrm{H}}$. Denote $\mathbf{x} = [x_1[0]x_2[0]x_1[1]x_2[1].....x_1[J-1]x_2[J-1]]$ as the output of the TCM encoder. Furthermore, let the transmitted symbols be $\mathbf{x}_1 = [x_1[0]x_1[1].....x_1[J-1]]$ and $\mathbf{x}_2 = [x_2[0]x_2[1].....x_2[J-1]]$. For this scheme, assuming non-fading $R \to D$ link, we have

$$d^2(\mathbf{x},\hat{\mathbf{x}}) = \gamma_1 \boldsymbol{\varepsilon}_1^{\mathrm{H}} \mathbf{\Theta}_1 \boldsymbol{\varepsilon}_1 + \gamma_2 \boldsymbol{\varepsilon}_2^{\mathrm{H}} \mathbf{\Theta}_2 \boldsymbol{\varepsilon}_2 \tag{2.85}$$

where $\mathbf{\Theta}_i = \mathbf{U}_i^{\mathrm{H}} \mathbf{\Omega}_i^{1/2} \mathbf{f}_i^{\mathrm{H}} \mathbf{P} \mathbf{f}_i \mathbf{\Omega}_i^{1/2} \mathbf{U}_i$, $\mathbf{P} = diag\left(\left| \mathbf{x}_1 - \hat{\mathbf{x}}_1 \right|^2 + \left| \mathbf{x}_2 - \hat{\mathbf{x}}_2 \right|^2 \right)$. Replacing (2.85) in (2.55) and following similar steps as in Appendix A.1, we obtain the final PEP as

$$P(\mathbf{x}, \hat{\mathbf{x}}) \le \left(\frac{E_{SD}}{4N_0} \right)^{-\delta} \prod_{j_1=1}^{r_1} \left(\lambda_{\mathbf{\Theta}_1}(j_1) \right)^{-1} \prod_{j_2=1}^{r_2} \left(\lambda_{\mathbf{\Theta}_2}(j_2) \right)^{-1} \tag{2.86}$$

where δ is defined as $\delta = r_1 + r_2$. Here, r_i and $\lambda_{\mathbf{\Theta}_i}(j_i)$, $j_i = 1,...,r_i$ for $i = 1,2$ are the rank and the eigenvalues of the matrix $\mathbf{\Theta}_i$, respectively.

Chapter 3

Non-Coherent and Mismatched-Coherent Detection for Cooperative Communication

Introduction

The majority of the current works on cooperative diversity build upon a coherent scenario where perfect CSI is available at the destination terminal. In practice, the fading channel coefficients are first estimated and then used in the detection process. Relay terminals operating in DaF mode also require CSI in the source-to-relay link for the decoding process. For AaF relaying, the knowledge of CSI at relay terminal is essential for appropriately scaling the received signal to satisfy relay power constraints. The quality of channel estimates thus affects the overall performance of cooperative transmission and might become a performance limiting factor.

3.1 Transmission Model

We consider the wireless communication system scenario illustrated in Figure 3.1. As for the user cooperation protocol, we adopt Protocol I of [33] and assume that the relay operates in AaF mode. Perfect synchronization is assumed among the cooperating terminals.

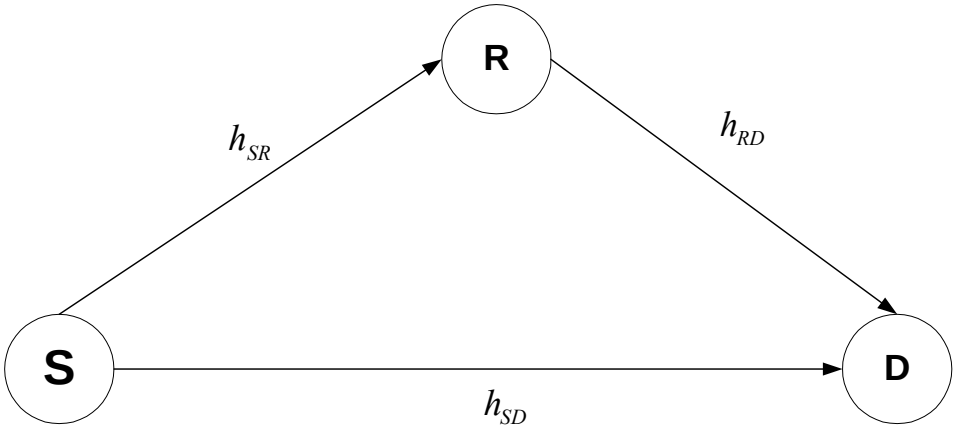

Figure 3.1: Relay-assisted transmission over frequency-flat channels.

Let E_{SD}, E_{SR}, and E_{RD} represent the average energies available at the destination and relay terminals taking into account for possibly different path loss and shadowing effects in $S \to D$, $S \to R$, and $R \to D$ links, respectively. Let two consecutive signals transmitted by the source terminal be denoted as x_1 and x_2. We assume BPSK modulation with normalized unit energy for the signals, i.e., $E[|\, x_i^2 \,|= 1]$, $i = 1,2$. In the first signaling interval, the signal received at the relay terminal is given as

$$r_R = \sqrt{E_{SR}} h_{SR} x_1 + n_R \tag{3.1}$$

where h_{SR} denotes the frequency flat fading coefficient over $S \to R$ link. It is modeled as a complex Gaussian random variable with variance 0.5 per dimension, which leads to a Rayleigh fading channel. n_R is a zero-mean complex Gaussian random variable with variance $N_0/2$ per dimension, which models the additive noise term. The signal received at the destination terminal in the first time slot is given by

$$r_{D,1} = \sqrt{E_{SD}} h_{SD} x_1 + n_{D,1} \tag{3.2}$$

where h_{SD} denotes the complex fading coefficient over $S \to D$ link modeled as a complex Gaussian random variable with variance 0.5 per dimension and $n_{D,1}$ is the additive noise term modeled as a zero-mean complex Gaussian random variable with variance $N_0/2$ per dimension. The relay terminal normalizes the received signal r_R by a factor of $\sqrt{E[|r_R|^2]}$ to ensure the unity of average energy and re-transmits the signal during the second time slot. Therefore, the received signal at the destination terminal in the second time slot is given as

$$r_{D,2} = \sqrt{E_{RD}}h_{RD}\frac{r_R}{\sqrt{E[|r_R|^2]}} + \sqrt{E_{SD}}h_{SD}x_2 + n_{D,2} \tag{3.3}$$

where $n_{D,2}$ is the additive noise term modeled as a zero-mean complex Gaussian random variable with variance $N_0/2$ per dimension. h_{RD} denotes the complex fading coefficient over the $R \to D$ link and is modeled as a complex Gaussian random variable with variance 0.5 per dimension. Replacing (3.1) and the normalization factor $E[|r_R|^2] = E_{SR} + N_0$ in (3.3), we obtain

$$r_{D,2} = \sqrt{\frac{E_{RD}E_{SR}}{E_{SR}+N_0}}h_{RD}h_{SR}x_1 + \sqrt{E_{SD}}h_{SD}x_2 + \tilde{n} \tag{3.4}$$

with

$$\tilde{n} = \sqrt{\frac{E_{RD}}{E_{SR}+N_0}}h_{RD}n_R + n_{D,2}\,. \tag{3.5}$$

In (3.5), $\tilde{n}$ (conditioned on h_{RD}) is zero-mean complex Gaussian with variance of

$$E\left[|\tilde{n}|^2 \middle| |h_{RD}|\right] = N_0\left(1 + \frac{E_{RD}|h_{RD}|^2}{E_{SR}+N_0}\right). \tag{3.6}$$

We can rewrite the received signal normalizing (3.4) with (3.6) as

$$r_{D,2} = \sqrt{\beta_1}\sqrt{E_{RD}}h_{RD}h_{SR}x_1 + \sqrt{\beta_2}\sqrt{E_{SD}}h_{SD}x_2 + n \tag{3.7}$$

where n turns out to be zero-mean complex Gaussian random variable with variance $N_0/2$ per dimension. As earlier noted in Chapter 2, this normalization does not affect the SNR, but simplifies the ensuing presentation. In (3.7), β_1 and β_2 are defined respectively, as

$$\beta_1 = \frac{E_{SR}/N_0}{1+E_{SR}/N_0+|h_{RD}|^2 E_{RD}/N_0}\ , \tag{3.8}$$

$$\beta_2 = \frac{1+E_{SR}/N_0}{1+E_{SR}/N_0+|h_{RD}|^2 E_{RD}/N_0}\ . \tag{3.9}$$

After setting up the basic relay-assisted transmission model given by (3.2) and (3.7), we now introduce space-time coding across the transmitted signals x_1 and x_2. Although different classes of space-time coding proposed originally for co-located antennas can be applied to cooperative diversity schemes in a distributed fashion, we employ orthogonal STBC to exploit its inherent orthogonality; an essential feature for the proposed detection algorithms in the next section. For the considered transmission scenario, we need to use STBC designed for two transmit antennas, i.e., Alamouti's scheme [15]. Considering the broadcasting and relaying phases, we need 4 time slots for the transmission of two Alamouti coded symbols. Assume that the destination terminal makes an observation for a duration length of J (J is an even number). The received signal vector over 4 time slots can be written as

$$\mathbf{r}_m \overset{def}{=} \begin{bmatrix} r_k \\ r_{k+1} \\ r_{k+2} \\ r_{k+3} \end{bmatrix} = \begin{bmatrix} \sqrt{E_{SD}}\,h_{2,k}x_{1,m} + n_k \\ \sqrt{\beta_{1,k+1}}\sqrt{E_{RD}}\,h_{1,k+1}x_{1,m} + \sqrt{\beta_{2,k+1}}\sqrt{E_{SD}}\,h_{2,k+1}x_{2,m} + n_{k+1} \\ -\sqrt{E_{SD}}\,h_{2,k+2}x_{2,m}^* + n_{k+2} \\ -\sqrt{\beta_{1,k+3}}\sqrt{E_{RD}}\,h_{1,k+3}x_{2,m}^* + \sqrt{\beta_{2,k+3}}\sqrt{E_{SD}}\,h_{2,k+3}x_{1,m}^* + n_{k+3} \end{bmatrix}, \tag{3.10}$$

where $m = 1,2,...J/4$, $k = 4(m-1)$, $h_{1,k}$ and $h_{2,k}$ are defined as $h_{1,k} = h_{SR,k-1}h_{RD,k}$ and $h_{2,k} = h_{SD,k}$, respectively. Further introducing $\mathbf{h}_m = [h_{1,k}, h_{2,k}, ..., h_{1,k+3}, h_{2,k+3}]^{\mathrm{T}}$, $\mathbf{n}_m = [n_k, .., n_{k+3}]^{\mathrm{T}}$, and

$$\mathbf{X}_m = \begin{bmatrix} \mathbf{X}_{m_1} & \mathbf{0}_{2\times 4} \\ \mathbf{0}_{2\times 4} & \mathbf{X}_{m_2} \end{bmatrix}, \tag{3.11}$$

with

$$\mathbf{X}_{m_1} = \begin{bmatrix} 0 & \sqrt{E_{SD}}x_{1,m} & 0 & 0 \\ 0 & 0 & \sqrt{\beta_{1,k+1}E_{RD}}x_{1,m} & \sqrt{\beta_{2,k+1}E_{SD}}x_{2,m} \end{bmatrix},$$

$$\mathbf{X}_{m_2} = \begin{bmatrix} 0 & -\sqrt{E_{SD}}x_{2,m}^* & 0 & 0 \\ 0 & 0 & -\sqrt{\beta_{1,k+1}E_{RD}}x_{2,m}^* & \sqrt{\beta_{2,k+1}E_{SD}}x_{1,m}^* \end{bmatrix},$$

the received signal vector over the whole observation period can be obtained as

$$\underbrace{\begin{bmatrix} \mathbf{r}_1 \\ \mathbf{r}_2 \\ \cdots \\ \mathbf{r}_{J/4} \end{bmatrix}}_{\mathbf{r}} = \underbrace{\begin{bmatrix} \mathbf{X}_1 & \mathbf{0} & \cdots & \mathbf{0} \\ \mathbf{0} & \mathbf{X}_2 & \ddots & \vdots \\ \vdots & \ddots & \ddots & \mathbf{0} \\ \mathbf{0} & \cdots & \mathbf{0} & \mathbf{X}_{J/4} \end{bmatrix}}_{\mathbf{X}} \underbrace{\begin{bmatrix} \mathbf{h}_1 \\ \mathbf{h}_2 \\ \cdots \\ \mathbf{h}_{J/4} \end{bmatrix}}_{\mathbf{h}} + \underbrace{\begin{bmatrix} \mathbf{n}_1 \\ \mathbf{n}_2 \\ \cdots \\ \mathbf{n}_{J/4} \end{bmatrix}}_{\mathbf{n}}. \tag{3.12}$$

where $\mathbf{X}$ represents the data matrix with size $J \times 2J$, $\mathbf{h}$ is the channel vector with size $2J \times 1$, and $\mathbf{n}$ denotes the noise vector with size $J \times 1$.

3.2 Non-Coherent Detection for Distributed STBCs

In this section, we investigate non-coherent detection for distributed STBC systems without assuming channel knowledge over both time-varying and quasi-static fading channels.

3.2.1 Non-Coherent Detection over Time-Varying Fading Channels

First, we consider the general case where all underlying links experience time-selectivity. Conditioned on both the data matrix $\mathbf{X}$ and $R \to D$ link fading coefficients, the probability density function of $\mathbf{r}$ can be written as [87]

$$p\left(\mathbf{r}\middle|\mathbf{X}, h_{RD,l}, l = 0,1,\ldots J-1\right) = \left(\pi^J \det\left(\mathbf{R}_\mathbf{r}\right)\right)^{-1} \exp\left(-\mathbf{r}^{\mathrm{H}}\mathbf{R}_\mathbf{r}^{-1}\mathbf{r}\right) \tag{3.13}$$

where $\mathbf{R_r}$ is defined as the autocorrelation matrix of $\mathbf{r}$ (conditioned on $\mathbf{X}$ and $h_{RD,l}$) and is given by

$$\mathbf{R_r} = \mathbf{X}\mathbf{R_h}\mathbf{X}^{\mathrm{H}} + N_0\mathbf{I}_J \tag{3.14}$$

with $\mathbf{R_h}$ denoting the autocorrelation matrix of $\mathbf{h}$ (conditioned on $h_{RD,l}$). Based on (3.14), it can be easily shown that the ML decision metric is obtained as

$$\mu(\mathbf{X}) = \arg\max_{\mathbf{X}} \left\{ \int_0^{\infty} \ldots \int_0^{\infty} \left(\pi^J \det(\mathbf{R}_r)\right)^{-1} \exp\left(-\mathbf{r}^{\mathrm{H}}\mathbf{R}_r^{-1}\mathbf{r}\right) f\left(\left|\mathbf{h}_{RD}\right|\right) d\left|\mathbf{h}_{RD}\right| \right\} \tag{3.15}$$

where $f\left(\left|\mathbf{h}_{RD}\right|\right)$ is the joint density function of the fading coefficients' magnitudes over $R \to D$ link for the observation length of *J*, i.e., $\mathbf{h}_{RD} = [h_{RD,0} \quad \cdots \quad h_{RD,J-1}]$. The direct implementation of (3.15) requires an exhaustive search over all possible sequences and computation of *J*-dimensional integrations, which make the practical decoder design infeasible especially for large sequence lengths

For the special case of non-fading $R \to D$ link, i.e., $\mathbf{h}_{RD} = [1,1,\ldots,1]$, (3.15) can be rewritten as

$$\mu(\mathbf{X}) = \arg\min_{\mathbf{X}} \left\{ \ln\left(\det(\mathbf{R}_r)\right) + \mathbf{r}^{\mathrm{H}}\mathbf{R}_r^{-1}\mathbf{r} \right\}. \tag{3.16}$$

Non-fading assumption can be justified in practical scenarios where the destination and relay terminals have a strong line-of-sight connection [33]. The resulting form of ML metric for such a scenario avoids the integrals due to the non-fading nature of $R \to D$ link, however still requires an exhaustive search over all possible sequences. Since the argument of the determinant term in (3.16) is dependent on data sequence, it is not possible to derive a recursive expression *directly* from this rule. However, an *indirect* approach, similar to [87], is possible to derive for the considered case by first filtering the received sequence to transform the determinant term into a diagonal one, which will then lend itself to the derivation of a recursive

form. This requires computation of prediction filter coefficients for branch metrics at each step bringing additional complexity and will not be pursued here.

3.2.2 Non-Coherent Detection over Quasi-Static Fading Channels

Now we return our attention to the quasi-static fading case where the fading coefficients of all underlying links are assumed to remain constant over the observation period. For this case, $\mathbf{X}_m$ in (3.11) reduces to

$$\mathbf{X}_m = \begin{bmatrix} 0 & \sqrt{\beta_1 E_{RD}}\,x_{1,m} & 0 & -\sqrt{\beta_1 E_{RD}}\,x_{2,m}^* \\ \sqrt{E_{SD}}\,x_{1,m} & \sqrt{\beta_2 E_{SD}}\,x_{2,m} & -\sqrt{E_{SD}}\,x_{2,m}^* & \sqrt{\beta_2 E_{SD}}\,x_{1,m}^* \end{bmatrix}^{\mathrm{T}},\ m = 1,2,...,J/4.$$

The received signal vector can be now written in the matrix form as

$$\underbrace{\begin{bmatrix} \mathbf{r}_1 \\ \mathbf{r}_2 \\ \dots \\ \mathbf{r}_{J/4} \end{bmatrix}}_{\mathbf{r}} = \underbrace{\begin{bmatrix} \mathbf{X}_1 \\ \mathbf{X}_2 \\ \vdots \\ \mathbf{X}_{J/4} \end{bmatrix}}_{\mathbf{X}} \underbrace{\begin{bmatrix} h_1 \\ h_2 \end{bmatrix}}_{\mathbf{h}} + \underbrace{\begin{bmatrix} \mathbf{n}_1 \\ \mathbf{n}_2 \\ \dots \\ \mathbf{n}_{J/4} \end{bmatrix}}_{\mathbf{n}} \tag{3.17}$$

where $h_1 = h_{SR}h_{RD}$, $h_2 = h_{SD}$, $\mathbf{X}$ is the data matrix with size $J \times 2$, and $\mathbf{n}$ denotes a $J \times 1$ noise vector. Here, we have dropped the subscript denoting time in the fading coefficients' representation since they are already assumed to be constant over J intervals. Under the quasi-static channel assumption, the ML decision metric is obtained as

$$\begin{aligned} \mu(\mathbf{X}) &= \arg\max_{\mathbf{X}} \left\{ \mathop{\mathrm{E}}_{|h_{RD}|} \left[\left(\pi^J \det(\mathbf{R}_r) \right)^{-1} \exp\left(-\mathbf{r}^{\mathrm{H}} \mathbf{R}_r^{-1} \mathbf{r} \right) \right] \right\} \\ &= \arg\max_{\mathbf{X}} \left\{ \int_0^{\infty} \left(\pi^J \det(\mathbf{R}_r) \right)^{-1} \exp\left(-\mathbf{r}^{\mathrm{H}} \mathbf{R}_r^{-1} \mathbf{r} \right) f\left(|h_{RD}| \right) d|h_{RD}| \right\} \end{aligned} \tag{3.18}$$

The integral of (3.18) with respect to h_{RD} does not readily yield a closed-form solution. As an alternative solution, we modify the decision metric as

$$\mu(\mathbf{X}) = \mathop{\mathrm{E}}_{|h_{RD}|} \left[\arg\max_{\mathbf{X}} \left\{ \left(\pi^J \det(\mathbf{R}_r) \right)^{-1} \exp\left(-\mathbf{r}^{\mathrm{H}} \mathbf{R}_r^{-1} \mathbf{r} \right) \right\} \right] \tag{3.19}$$

Replacing (3.14) in (3.19), we have

$$\mu(\mathbf{X}) = \underset{|h_{RD}|}{E}\left[\arg\min_{\mathbf{X}}\left\{ J\ln(\pi) + \ln\left(\det\left(\mathbf{X}\mathbf{R}_{\mathbf{h}}\mathbf{X}^{\mathrm{H}} + N_0\mathbf{I}_J\right)\right) + \mathbf{r}^{\mathrm{H}}\left(\mathbf{X}\mathbf{R}_{\mathbf{h}}\mathbf{X}^{\mathrm{H}} + N_0\mathbf{I}_J\right)^{-1}\mathbf{r} \right\}\right] \tag{3.20}$$

Using the matrix identity $(\boldsymbol{A}+\boldsymbol{BCD})^{-1} = \boldsymbol{A}^{-1} - \boldsymbol{A}^{-1}\boldsymbol{B}\left(\boldsymbol{C}^{-1} + \boldsymbol{D}\boldsymbol{A}^{-1}\boldsymbol{B}\right)^{-1}\boldsymbol{D}\boldsymbol{A}^{-1}$ [88], the argument of the determinant term in (3.20) can be rearranged as

$$\left(\mathbf{X}\mathbf{R}_{\mathbf{h}}\mathbf{X}^{\mathrm{H}} + N_0\mathbf{I}_J\right)^{-1} = \frac{\mathbf{I}_J}{N_0} - \frac{1}{N_0^2}\mathbf{X}\left(\mathbf{R}_h^{-1} + \frac{1}{N_0}\mathbf{X}^{\mathrm{H}}\mathbf{X}\right)^{-1}\mathbf{X}^{\mathrm{H}} \ . \tag{3.21}$$

Further replacing $\mathbf{R}_{\mathbf{h}} = \mathrm{diag}\left(|h_{RD}|^2, 1\right)$ in (3.21) and exploiting the embedded orthogonality of data sequence in the resulting expression, i.e.,

$$\mathbf{X}^H\mathbf{X} = \begin{bmatrix} (J/2)\beta_1 E_{RD} & 0 \\ 0 & (J/2)(\beta_2+1)E_{SD} \end{bmatrix},$$

we rewrite (3.21) as

$$\left(\mathbf{X}\mathbf{R}_{\mathbf{h}}\mathbf{X}^{\mathrm{H}} + N_0\mathbf{I}_J\right)^{-1} = \frac{\mathbf{I}_J}{N_0} - \frac{1}{N_0^2}\mathbf{X}\mathbf{A}\,\mathbf{X}^{\mathrm{H}} \tag{3.22}$$

where **A** is defined by

$$\mathbf{A} = \begin{bmatrix} \dfrac{|h_{RD}|^2}{1+\dfrac{J}{2}\beta_1\dfrac{E_{RD}}{N_0}|h_{RD}|^2} & 0 \\ 0 & \dfrac{1}{1+\dfrac{J}{2}(\beta_2+1)\dfrac{E_{SD}}{N_0}} \end{bmatrix}.$$

Using the matrix identity $\det(\mathbf{I}+\mathbf{AB}) = \det(\mathbf{I}+\mathbf{BA})$ [88] and again exploiting the orthogonality structure of the underlying STBC, the determinant term in (3.20) can be shown to be independent of the data sequence. Replacing (3.22) in (3.20) and dropping unnecessary terms which do not affect maximization, we obtain

$$\mu(\mathbf{X}) = \underset{|h_{RD}|}{\mathrm{E}}\left[\arg\min_{\mathbf{X}}\left\{-\frac{1}{N_0^2}\mathbf{r}^{\mathrm{H}}\mathbf{X}\mathbf{A}\mathbf{X}^{\mathrm{H}}\mathbf{r}\right\}\right]. \tag{3.23}$$

The expectation of (3.23) with respect to h_{RD} does not yield a closed-form solution for the general case. In the following, we demonstrate that a closed-form decision metric can be obtained imposing some assumptions on the underlying links.

Case 1 (Power control between $S \to D$ and $R \to D$ links and high SNR in $S \to R$ link): Assume perfect power control where $S \to D$ and $R \to D$ links are balanced, i.e., $E_{RD}/N_0 = E_{SD}/N_0$, and sufficiently large SNR for the $S \to R$ link, i.e., $E_{SR}/N_0 >> E_{SD}/N_0$. Under these assumptions, **A** reduces to the form of

$$\mathbf{A} = \begin{bmatrix} \dfrac{|h_{RD}|^2}{1+\dfrac{JE_{SD}}{2N_0}|h_{RD}|^2} & 0 \\ 0 & \dfrac{1}{1+J\dfrac{E_{SD}}{N_0}} \end{bmatrix}.$$

Replacing **A** in (3.23) and carrying out the expectation with respect h_{RD}, we obtain the decision metric as

$$\mu(\mathbf{X}) = \arg\max_{\mathbf{X}} \left\|\mathbf{\Phi}\mathbf{X}^{H}\mathbf{r}\right\|^2 \tag{3.24}$$

where

$$\mathbf{\Phi} = \begin{bmatrix} \sqrt{\psi\left(1-\beta e^{\psi}\Gamma(0,\psi)\right)} & 0 \\ 0 & \sqrt{\dfrac{1}{1+JE_{SD}/N_0}} \end{bmatrix}. \tag{3.25}$$

with $\psi = 2/(NE_{SD}/N_0)$ and $\Gamma(.,.)$ denotes the incomplete gamma function [71]. Under the assumption of $E_{RD}/N = E_{SD}/N_0 >> 1$, $\mathbf{\Phi}$ further reduces to

$$\mathbf{\Phi} = \begin{bmatrix} \sqrt{\dfrac{2}{JE_{SD}/N_0}} & 0 \\ 0 & \sqrt{\dfrac{1}{JE_{SD}/N_0}} \end{bmatrix}. \tag{3.26}$$

Case 2 (Non-fading $R \to D$ link): Besides the assumptions imposed in Case 1, we also now assume a non-fading $R \to D$ link. It can be easily shown that the decision metric is still given by (3.24) where $\mathbf{\Phi}$ is

$$\mathbf{\Phi} = \begin{bmatrix} \sqrt{\dfrac{1}{1+(J/2)E_{SD}/N_0}} & 0 \\ 0 & \sqrt{\dfrac{1}{1+JE_{SD}/N_0}} \end{bmatrix}. \tag{3.27}$$

One can interestingly note that the derived decoding rule given by (3.24) has a similar form to

$$\mu(\mathbf{X}) = \arg\max_{\mathbf{X}} \left\| \mathbf{X}^H \mathbf{r} \right\|^2 \tag{3.28}$$

which is the quadratic non-coherent receiver derived earlier for conventional (i.e., non-distributed) STBC in [89], [90]. Replacing $\mathbf{\Phi}$ in (3.24) by an identity matrix, one can simply obtain (3.28). In other words, (3.24) is a generalized version of the conventional decoder. In the considered cooperative scenario, the effects of AaF relaying and path loss/shadowing associated with underlying relay links manifest themselves in (3.24) through the scaling matrix $\mathbf{\Phi}$. Through the PEP derivations in the Appendix B.1, we demonstrate that the non-coherent decoding rule is able to collect a diversity order of two which is the full diversity for the considered single-relay scenario. It should be noted that this diversity order is attainable for asymptotically high SNR. In practical range of SNR values, the performance of distributed STBC experiences some degradation in comparison to that of non-distributed STBC.

In the practical implementation of (3.24), one should notice that the quadratic nature of (3.24) results in a phase ambiguity [89]. This ambiguity can be resolved easily by fixing the

first symbol transmitted from each of the links to a specific value, i.e., insertion of a known symbol at the beginning of the frame. Direct implementation of (3.24) is still impractical due to substantial computational complexity. However, this time, unlike (3.15) and (3.16), it is possible to develop a recursive expression from (3.24) which can be easily implemented by a Viterbi-type algorithm. Expanding (3.24), we can readily obtain the desired recursive form as

$$\mu^m(\mathbf{X}) = \mu^{m-1}(\mathbf{X}) + \mathrm{Re}\left\{\mathbf{r}_m^H \mathbf{X}_m \mathbf{\Phi}\left[\sum_{j=\max(1,m-I)}^{m-1} \mathbf{\Phi}\mathbf{X}_i^{\mathrm{H}}\mathbf{r}_i\right]\right\},\ m = 1,\ldots J/4 \tag{3.29}$$

where $\mathbf{X}_m$ is defined earlier in (3.17). The inner term in (3.29) can be interpreted as a channel estimate based on a truncation interval of previous I sub-blocks. Although the derived decoding rule is based on a quasi-static fading assumption, this inherent channel tracking ability makes it a suitable candidate for deployment over time-varying channels.

3.3 Mismatched-Coherent Detection for Distributed STBCs

In this section, we consider a mismatched-coherent receiver, i.e., coherent detection with imperfect channel estimation, as a possible alternative to the non-coherent receiver proposed in the previous section. For channel estimation purposes, we employ pilot symbols (i.e., a set of symbols whose location and values are known to the receiver) multiplexed with the information-bearing data. To the best of our knowledge, pilot-symbol-assisted channel estimation has not been yet fully studied in the context of cooperative communication.

3.3.1 Mismatched-Coherent Detection over Quasi-Static Fading Channels

Let $\mathbf{X}_T$ denote the pilot symbol matrix transmitted by the source terminal followed by a data matrix $\mathbf{X}_D$. Under the assumption that fading coefficients are constant over the entire transmission frame, the received signals during the training and data transmission phases are given, respectively, as

$$\mathbf{r}_T = \mathbf{X}_T\mathbf{h} + \mathbf{n}_T \tag{3.30}$$

$$\mathbf{r}_D = \mathbf{X}_D\mathbf{h} + \mathbf{n}_D \tag{3.31}$$

where $\mathbf{h} = (h_1, h_2)^{\mathrm{T}}$ with $h_1 = h_{SR}h_{RD}$ and $h_2 = h_{SD}$. In (3.30)-(3.31), the entries of $\mathbf{n}_T$ and $\mathbf{n}_D$ are zero-mean complex Gaussian random variables with variance $N_0/2$ per dimension. The channel coefficients are first estimated using $\mathbf{r}_T$ and $\mathbf{X}_T$ to obtain the channel estimate $\hat{\mathbf{h}}$, which can be then used to minimize the following coherent ML metric as if the channel was perfectly known.

$$\mu(\mathbf{X}_D) = \arg\min_{\mathbf{X}_D} \left\| \mathbf{r}_D - \mathbf{X}_D\hat{\mathbf{h}} \right\|^2. \tag{3.32}$$

The performance of the mismatched receiver relies on the choice of the channel estimator. Here, we consider ML and linear-minimum-mean-square-error (LMMSE) estimators.

ML Estimator: Conditioned on $\mathbf{h}$ and $\mathbf{X}_T$, the ML estimate of the channel matrix is amount to minimizing $\|\mathbf{r}_T - \mathbf{X}_T\mathbf{h}\|^2$ with respect to **h**. Therefore, under the same SNR assumptions, (i.e., $E_{RD}/N_0 = E_{SD}/N_0$, $E_{SR}/N_0 >> E_{SD}/N_0$) imposed in the previous section, the ML estimate of **h** is given as [91]

$$\hat{\mathbf{h}}_{ML} = \left(\mathbf{X}_T^{\mathrm{H}}\mathbf{X}_T\right)^{-1}\mathbf{X}_T^{\mathrm{H}}\mathbf{r}_T. \tag{3.33}$$

Replacing (3.30) in (3.33), we obtain

$$\hat{\mathbf{h}}_{ML} = \mathbf{h} + \boldsymbol{\varepsilon}_{ML} \tag{3.34}$$

where we define the channel estimation error vector $\boldsymbol{\varepsilon}_{ML} = \left(\mathbf{X}_T^{\mathrm{H}}\mathbf{X}_T\right)^{-1}\mathbf{X}_T^{\mathrm{H}}\mathbf{n}_T$ with covariance matrix

$$\mathrm{E}\left[\boldsymbol{\varepsilon}_{ML}\boldsymbol{\varepsilon}_{ML}^{\mathrm{H}}\right] = \begin{bmatrix} \dfrac{1}{0.5PE_{SD}/N_0} & 0 \\ 0 & \dfrac{1}{PE_{SD}/N_0} \end{bmatrix}. \tag{3.35}$$

where P denotes the number pilot symbols.

LMMSE estimator: The LMMSE estimate of the channel matrix is obtained by the linear transformation $\mathbf{B}\mathbf{r}_T$, where $\mathbf{B}$ minimizes $E[\|\mathbf{B}\mathbf{r}_T - \mathbf{h}\|^2]$. Hence, the channel estimate $\hat{\mathbf{h}}_{LMMSE}$ is given as [92]

$$\hat{\mathbf{h}}_{LMMSE} = \left(\mathbf{X}_T^{\mathrm{H}}\mathbf{X}_T + N_0\mathbf{R}_{\mathbf{h}}^{-1}\right)^{-1}\mathbf{X}_T^{\mathrm{H}}\mathbf{r}_T \tag{3.36}$$

where $\mathbf{R}_{\mathbf{h}}$ is the autocorrelation matrix of $\mathbf{h}$. Replacing (3.30) in (3.36), we obtain

$$\hat{\mathbf{h}}_{LMMSE} = \left(\mathbf{X}_T^{\mathrm{H}}\mathbf{X}_T + N_0\mathbf{R}_{\mathbf{h}}^{-1}\right)^{-1}\mathbf{X}_T^{\mathrm{H}}\mathbf{X}_T\mathbf{h} + \boldsymbol{\varepsilon}_{LMMSE} \tag{3.37}$$

where channel estimation error vector is defined as $\boldsymbol{\varepsilon}_{LMMSE} = \left(\mathbf{X}_T^{\mathrm{H}}\mathbf{X}_T + N_0\mathbf{R}_{\mathbf{h}}^{-1}\right)^{-1}\mathbf{X}_T^{\mathrm{H}}\mathbf{n}_T$. Under the assumption of $E_{SD}/N_0 \to \infty$, the covariance matrix of $\boldsymbol{\varepsilon}_{LMMSE}$ converges to (3.35) of ML estimator. In Appendix B.2, we demonstrate through PEP derivation that the mismatched-coherent receiver is able to achieve full diversity order over quasi-static channels.

3.3.2 Mismatched-Coherent Detection over Time-Varying Fading Channels

In this subsection, we assume all underlying links experience time-selectivity. In the considered single-relay scenario, Alamouti-coded pilot symbols are sent over four time slots: Specifically, in time slot k, the source terminal simultaneously transmits the pilot symbol p_1 to the destination terminal and the relay terminal. In time slot k+1, the relay terminal transmits the received version of pilot symbol (after energy normalization) to the destination terminal. In the same time slot, the source terminal transmits the other pilot symbol p_2 to the destination terminal. The same procedure is repeated for the transmission of $-p_2^*$ and p_1^*. The destination terminal makes an observation of L frames, each of which consists of J symbols and extracts $4L$ observations of the nearest pilot symbols for channel estimation purpose (see Figure 3.2).

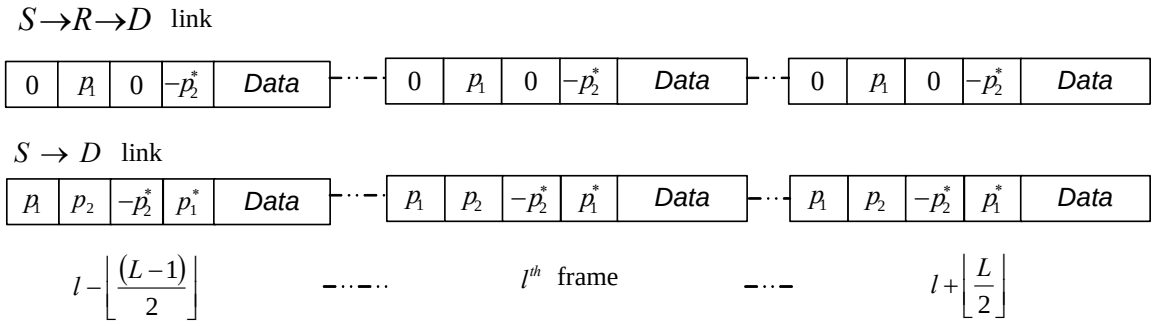

Figure 3.2: Frame structure for pilot-symbol-assisted channel estimation.

The destination terminal interpolates these observations (using MMSE filter) to form an estimate of the channel coefficient at the data symbol to be detected [93]. Assuming that the pilot symbols are located at the first 4 time slots of each frame, and furthermore introducing the received signal vector representing the observed pilot symbols, i.e., $\bar{\mathbf{r}}_l = [\mathbf{r}_{l,-\lfloor (L-1)/2 \rfloor} \quad \cdots \quad \mathbf{r}_{l,\lfloor L/2 \rfloor}]$, $\mathbf{r}_{l,k} = [r_{l+k}^0 \quad r_{l+k}^1 \quad r_{l+k}^2 \quad r_{l+k}^3]$, $k = \lfloor -(L-1)/2 \rfloor, ...0, ..., \lfloor L/2 \rfloor$, the fading estimates for $S \to D$ and $S \to R \to D$ links at the j^{th} symbol period in the l^{th} frame are obtained as

$$\hat{h}_{1,l}^j = \hat{h}_{SD,l}^j = \mathrm{E}[h_{SD,l}^j \bar{\mathbf{r}}_l^{\mathrm{H}}]\mathrm{Cov}(\bar{\mathbf{r}}_l)^{-1}\bar{\mathbf{r}}_l, \tag{3.38}$$

$$\hat{h}_{2.j}^j = \hat{h}_{RD,l}^j \hat{h}_{SR,l}^j = \mathrm{E}[h_{RD,l}^j h_{SR,l}^j \bar{\mathbf{r}}_l^{\mathrm{H}}]\mathrm{Cov}(\bar{\mathbf{r}}_l)^{-1}\bar{\mathbf{r}}_l \ . \tag{3.39}$$

3.4 Numerical Results

In this section, we present an extensive Monte-Carlo simulation study to demonstrate the error rate performance of the non-coherent and mismatched-coherent distributed STBC schemes considered so far. In our simulation study, we consider BPSK modulation and assume $E_{SD} = E_{RD}$, i.e., $S \to D$ and $R \to D$ links are balanced, which can be achieved through power control. As for the $S \to R$ link, we set $E_{SR}/N_0 = 35\mathrm{dB}$. We assume Rayleigh fading for underlying links and assume one receive antenna at the destination termination terminal unless otherwise noted.

In Figure 3.3, we present the bit error rate (BER) performance of the ML-optimum decoding rule given by (3.18) implemented through exhaustive search over all possible sequences, and the derived decoding rule given by (3.24) in conjunction with scaling matrix $\mathbf{\Phi}$ given by (3.25), (3.26), and (3.27). We assume quasi-static fading for all underlying links. It is observed that optimum decoding rule and proposed decoder yield nearly identical performance. This is very promising since the implementation complexity of (3.24) is much lower than the optimum decoder which requires multi-dimensional integral and does not yield a closed-form solution.

It is also interesting to observe that different forms of scaling matrix $\mathbf{\Phi}$, i.e., (3.25) and (3.27) do not result in a significant change in the performance although they have been obtained under the assumption of fading and non-fading $R \to D$ links, respectively. One can also note that (3.26) is the simplified version of (3.25) under high SNR assumption (see the discussion in Section 3.2.2). Considering the nearly identical performance observed for three different scaling matrices, (3.26) and (3.27) are favorable choices since they avoid the use of incomplete gamma function unlike (3.25). As a benchmark, we also investigate the performance of the non-coherent decoder rule given by (3.28) for conventional (non-distributed) STBC within the considered cooperative scenario. It is observed that there is a performance loss of $\approx 1\text{dB}$ at $\text{BER} = 10^{-3}$. This performance degradation further decreases with the increasing number of receive antennas employed at the destination terminal. It should be emphasized (3.28) does not require any kind of information on the underlying links unlike (3.25)-(3.26)-(3.27) which need average SNR estimation for the underlying links. Therefore, (3.28) can be possibly used as an alternative sub-optimal detector for distributed STBC.

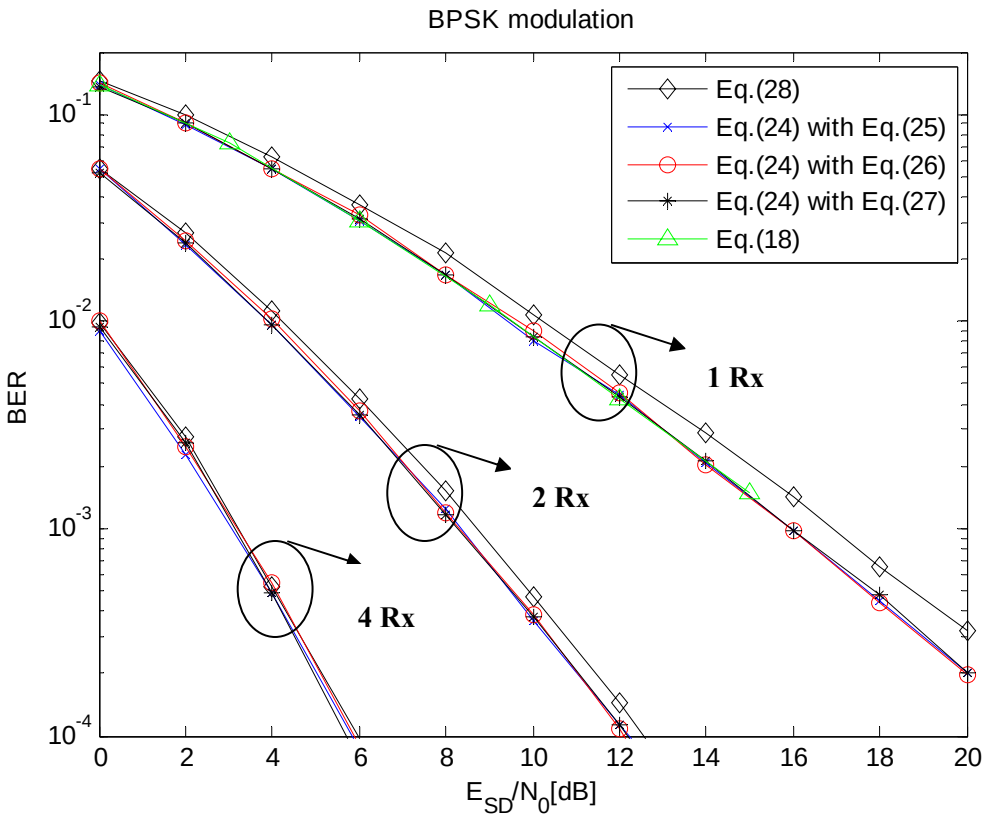

Figure 3.3: BER of the derived non-coherent decoders for distributed STBC over the quasi-static fading S→R, S→D and R→D links.

In Figure 3.4.a, we provide further results on the performance of the proposed decoding rule (3.24) to discuss the effect of fading in the $R \to D$ link. Under the assumption of high E_{SD}/N_0 values, it is observed that a diversity order of two is achieved confirming our diversity gain analysis through PEP derivation in the Appendix B.1. The presence of fading in $R \to D$ link results in some performance degradation, e.g., 1.2 dB at BER=10^{-3}. It should be further emphasized that this performance degradation is essentially a coding gain loss, (i.e., horizontal shift in the performance), but the asymptotical diversity order remains unaffected. This can be more clearly seen in Figure 3.4.b. where we plot the *effective* diversity order gains, i.e., $\log PEP / \log(E_{SD}/N_0)$ [94] relying on the PEP expressions (3.47) and (3.48) obtained for fading and non-fading $R \to D$ links, respectively. It is observed that these curves

converge to two in the asymptotical high SNR attaining the maximum achievable diversity order. However, the convergence of (3.47) is rather slow due to the presence of the term $\log(E_{SD}/N_0)$ reflecting the effect of fading in the $R \to D$ link. In Fig. 3.4., we also include the performance of recursive implementation of (3.24). This requires a Viterbi-type decoding algorithm with the metric given as (3.29). We assume a 4-state trellis, which corresponds to a truncation to the previous sub-block, i.e., I=1. We choose the frame length J=8, resulting in a pilot insertion rate (PIR) of 1/4. The simulation results clearly illustrate that the recursive implementation of the proposed decoder demonstrates a close performance to that of the one given by (3.24). The performance degradation is about 1.3 dB which can be further decreased by increasing the truncation length.

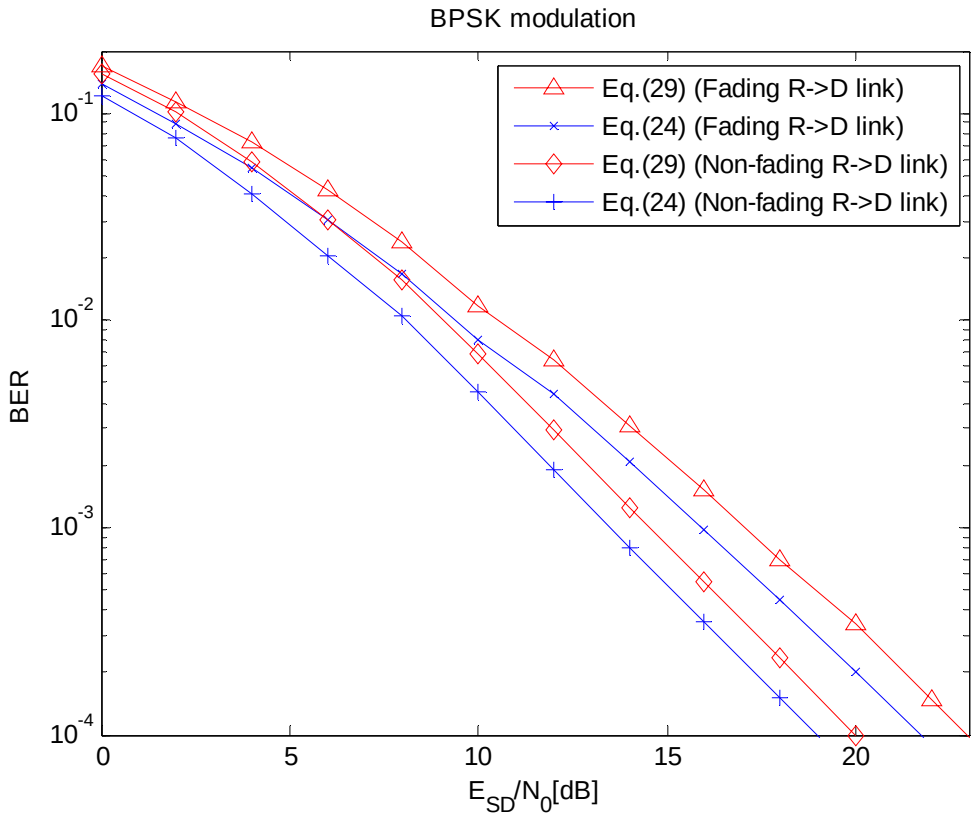

Figure 3.4.a: BER of the proposed non-coherent decoder given by Eq.(3.24) and its recursive implementation given by Eq.(3.29) over the quasi-static fading S→R and S→D links.

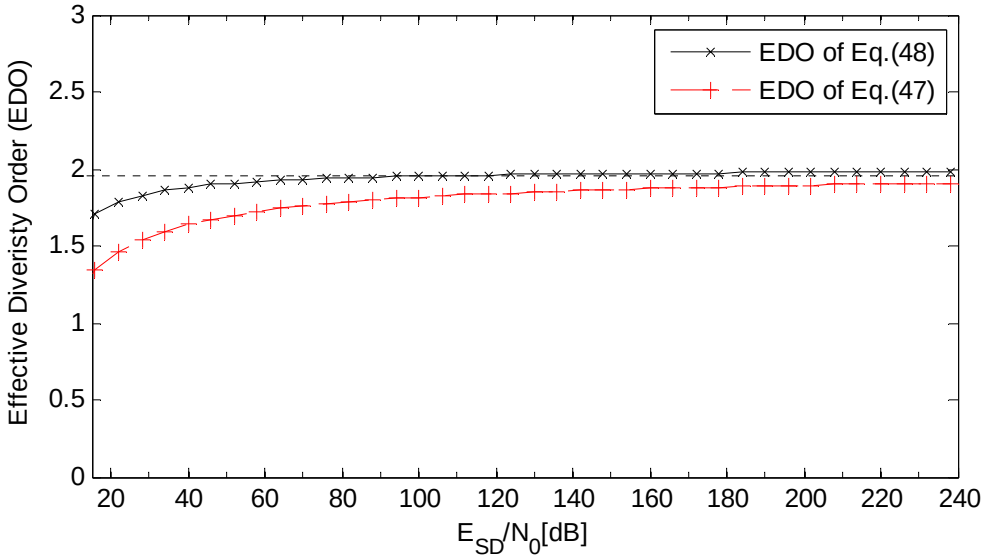

Figure 3.4.b: Effective diversity order of distributed STBC.

In Figure 3.5, we illustrate the performance of mismatched-coherent receiver for distributed STBC over quasi-static fading channels. As a benchmark, we include the performance of "genie" receiver which assumes perfect CSI. For mismatched-coherent receiver, we use the ML channel estimator as given by (3.33). The frame length is chosen as J=64. Our simulation results indicate that the mismatched receiver performance loss with respect to the genie receiver is ~ 3 dB at BER $= 10^{-3}$ with P=1, however diversity order remains unaffected confirming our diversity gain analysis in the Appendix B.2. It can be noticed that the performance degradation in the mismatched-coherent receiver due to channel estimation errors decreases as the number of pilot symbols increases. For example, with P=6, the performance degradation with respect to the genie receiver reduces to ~ 1.2 dB.

In Figure 3.5, we also include the performance of the non-coherent decoder for further comparison with mismatched-coherent receiver. Assuming P=1[1], the proposed non-coherent receiver given by (3.24) outperforms the mismatched-coherent receiver by $\sim 1.8\,\text{dB}$ at $\text{BER} = 10^{-3}$. The recursive implementation of the non-coherent receiver given by (3.29) still outperforms the mismatched-coherent receiver by $\sim 0.5\,\text{dB}$ at $\text{BER} = 10^{-3}$. With the increasing number of pilot symbols (therefore at the cost of decreasing throughput), mismatched-coherent receiver is able to provide a better performance in comparison to its competitor. For example, with P=6, mismatched-coherent receiver outperforms the recursive implementation of the non-coherent receiver by $\sim 2\,\text{dB}$ at $\text{BER} = 10^{-3}$ and is $\sim 1.2\,\text{dB}$ away from the genie receiver performance.

In Figure 3.6, we consider a time-varying channel scenario and present a performance comparison of non-coherent and mismatched-coherent receivers. We assume that $S \to R$ and $S \to D$ fading links experience Bessel-type autocorrelation function, i.e., Jakes Channel model, with normalized Doppler values of $fT_{SR} = fT_{SD} = 0.01$. A non-fading channel is assumed for the $R \to D$ link. We observe that the recursive implementation of the proposed non-coherent receiver, i.e. (3.29), still demonstrates close results in comparison to the optimum decoder given by (3.16) for time-varying channels although it is originally derived under the quasi-static channel assumption. For the mismatched-coherent receiver, pilot-symbol assisted channel estimator with Wiener filter is used as described in Section 3.3.2. The estimated fading coefficients are then used to minimize the metric given by (3.32). For both non-coherent and mismatched-coherent receivers, we use pilot insertion rate (PIR) =1/4, there-

[1] It should be noted that only one pilot symbol is required for the non-coherent decoder to resolve the phase ambiguity.

fore, the loss attributable to pilot symbols in both schemes is the same. Our simulation results illustrate that both receivers provide similar performance in the lower E_{SD}/N_0 region. As E_{SD}/N_0 increases, the non-coherent decoder is able to outperform slightly the mismatched-coherent receiver.

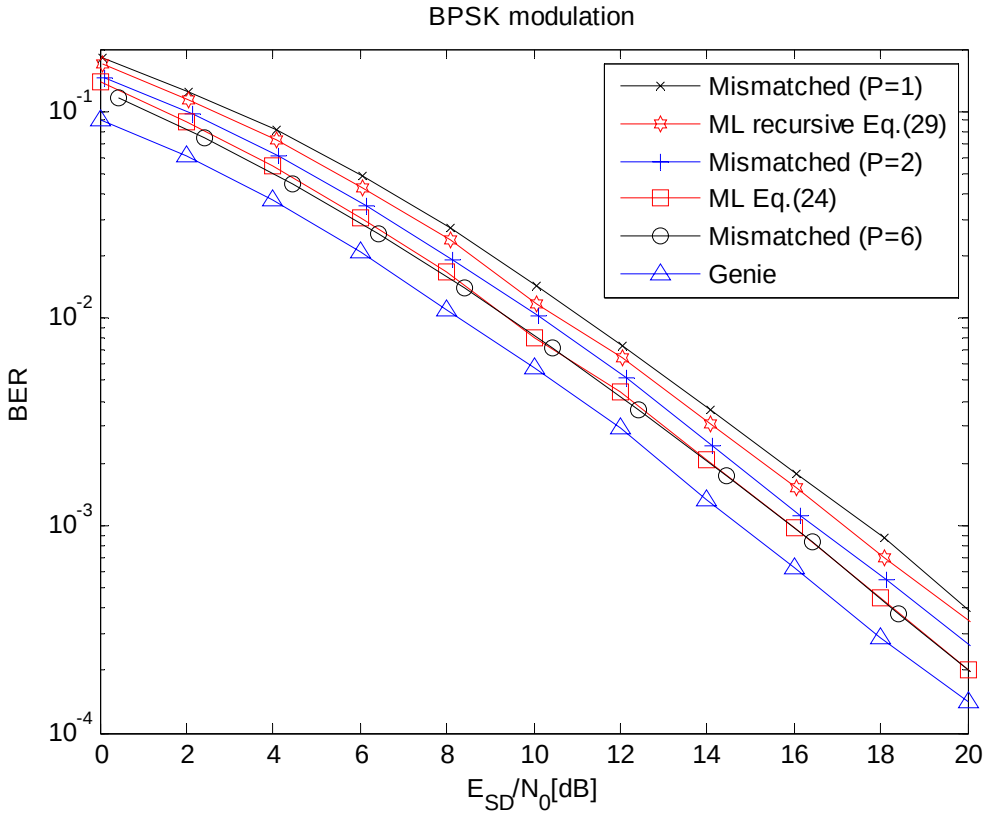

Figure 3.5: Performance comparison of mismatched-coherent and non-coherent decoders for distributed STBC over quasi-static fading links.

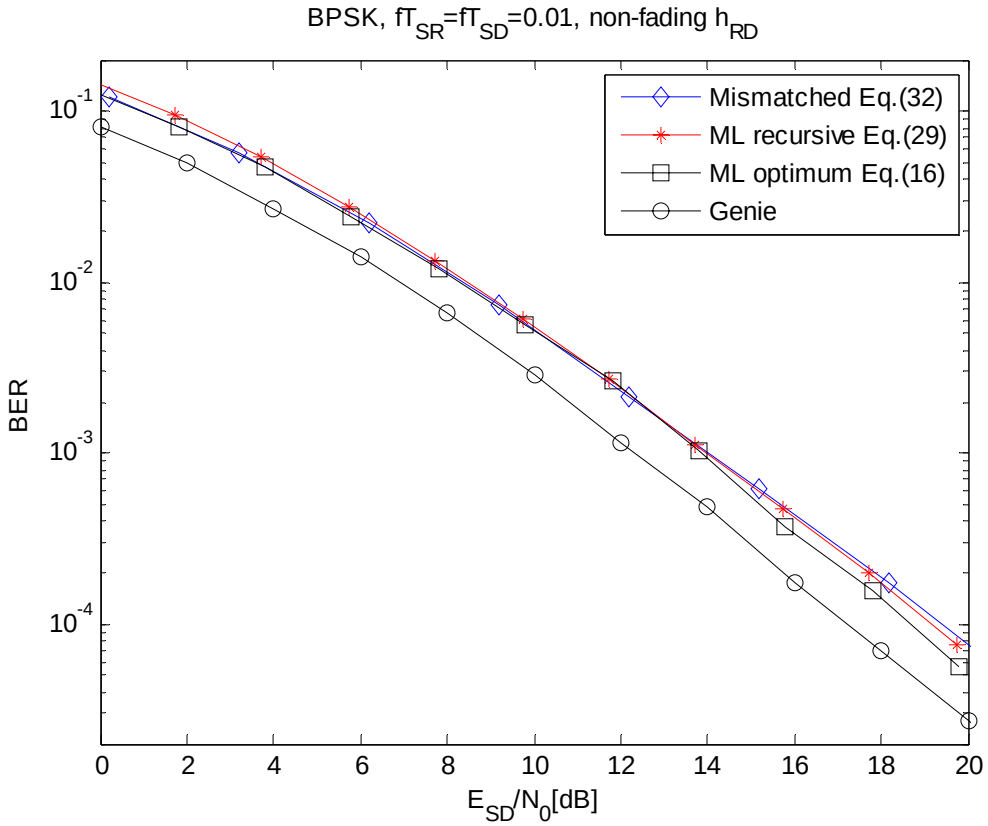

Figure 3.6: BER performance comparison of the non-coherent optimal decoder, non-coherent recursive decoder, and mismatched-coherent decoder for distributed STBC with non-fading $R \rightarrow D$ link. Normalized Doppler values for $S \rightarrow R$ and $S \rightarrow D$ links are $fT_{SR} = fT_{SD} = 0.01$.

In Figure 3.7, we consider a similar scenario as in the above, however, this time we assume a time-varying channel model also for the $R \rightarrow D$ link instead of the non-fading link assumption considered in Figure 3.6. In our simulation study, we assume the normalized Doppler values experienced in $S \rightarrow R$, $S \rightarrow D$ and $R \rightarrow D$ links are identical, i.e., $fT = fT_{SR} = fT_{SD} = fT_{RD}$. Within the considered SNR range, it is observed that the non-coherent decoder outperforms mismatched-coherent decoder for low and medium mobility scenarios. Specifically, we observe that for $fT = 0.01$ and $fT = 0.02$, the non-coherent decoder is able to provide a better performance. For $fT = 0.05$, it is observed that that mis-

matched-coherent receiver performs better although both receivers suffer from an error floor for this specific Doppler value. From the comparison of Figures 3.6 and 3.7, we further observe that the presence of time-selective fading in $R \to D$ link with $fT = 0.01$ results in a performance degradation of ~3 dB at BER=10^{-3} for both decoders.

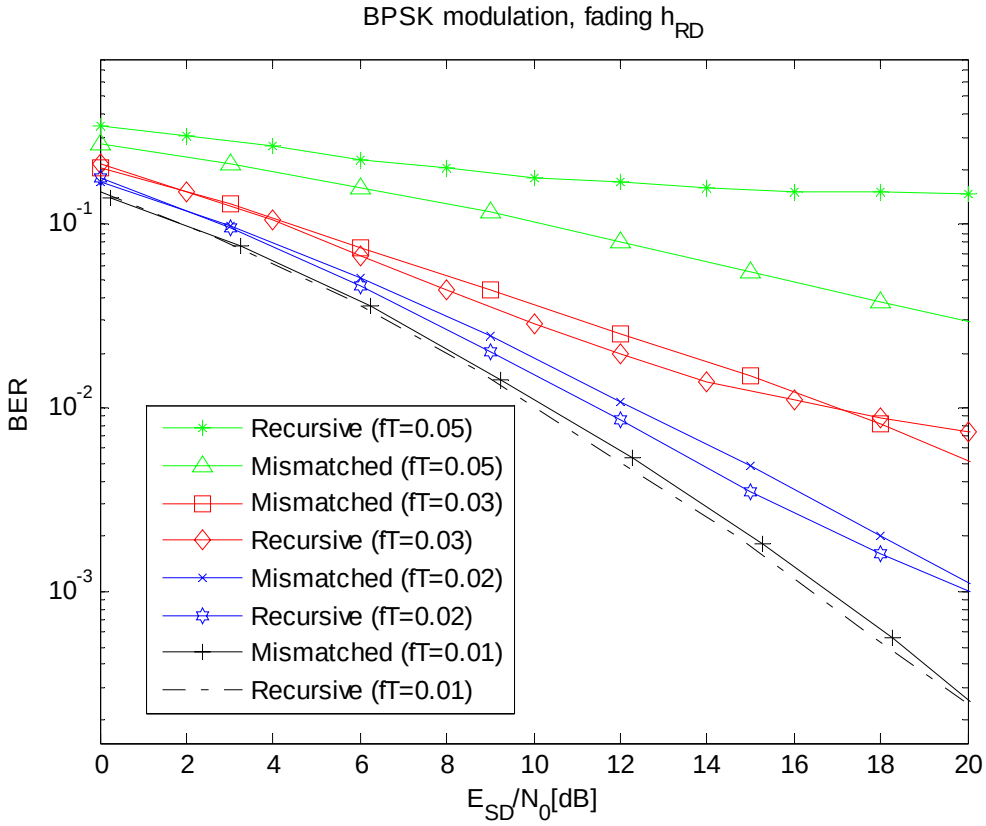

Figure 3.7: BER performance comparison of the non-coherent recursive decoder and mismatched-coherent decoder for distributed STBC with fading $R \rightarrow D$ link. Normalized Doppler values for $S \rightarrow R$, $R \rightarrow D$ and $S \rightarrow D$ links are $fT = fT_{SR} = fT_{RD} = fT_{SD} = 0.01,0.02,0.03,0.05$.

To have further insight into the performance comparison of non-coherent and mismatched-coherent decoders under various mobility scenarios, we plot the BER performance vs. normalized Doppler values in Figure 3.8.a. Here, we fix the E_{SD}/N_0 at 15 dB. It is observed that the non-coherent decoder is able to outperform the mismatched-coherent decoder

for low and intermediate Doppler values. For higher Doppler values, it can be seen that the mismatched-coherent decoder outperforms its competitor. In Figure 3.8.b., we further let the Doppler values in the underlying links be different from each other. Specifically, we assume the following three scenarios:

S.1) $fT_{RD} = fT_{SD} = 0.01$ and $fT_{SR} = fT = [0.01, 0.06]$.

S.2) $fT_{SR} = fT_{SD} = 0.01$ and $fT_{RD} = fT = [0.01, 0.06]$.

S.3) $fT_{SR} = fT_{RD} = 0.01$ and $fT_{SD} = fT = [0.01, 0.06]$.

Our simulation results reveal that the first two scenarios yield identical performance. This is due the symmetrical structure of $S \rightarrow R$ and $R \rightarrow D$ links in the cascaded relay channel. Thus, for the sake of presentation simplicity, we only include the performance of the first scenario in the figure. For scenarios in S.1) and S.3), we observe that the non-coherent decoder is able to outperform mismatched-coherent decoder for normalized Doppler values less than 0.045 and 0.015, respectively.

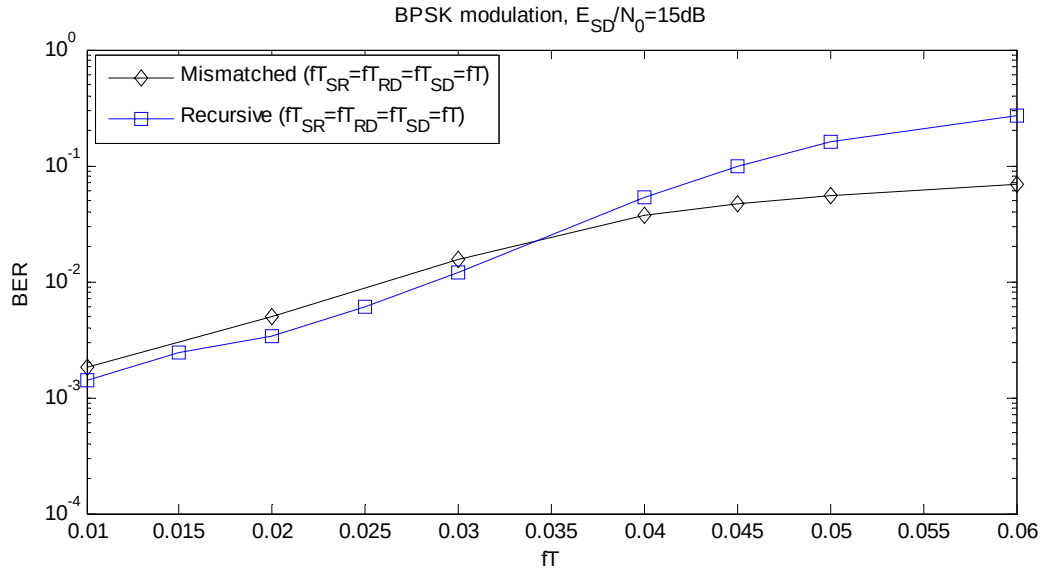

(a)

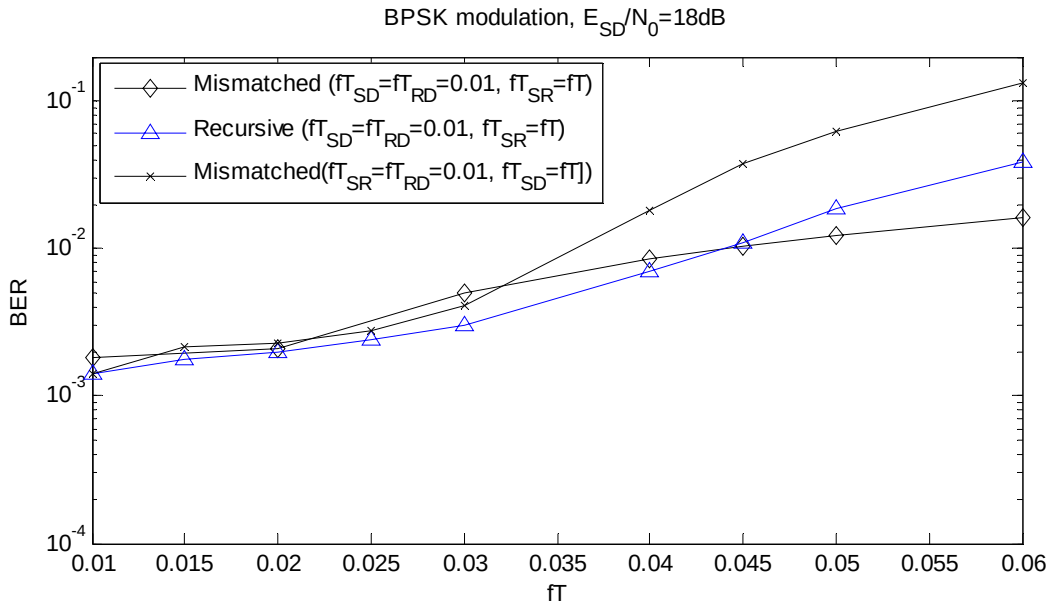

(b)

Figure 3.8: BER vs. Doppler spread for distributed STBC with non-coherent recursive decoder and mismatched-coherent decoder.

Appendix B

In this section, we present a diversity gain analysis for the non-coherent and coherent mismatched detectors through the derivation of PEP.

B.1 PEP Derivation for Non-coherent Detector

Let the transmitted codeword be $\mathbf{X}_c = \left[\mathbf{X}_1, \mathbf{X}_2, ..., \mathbf{X}_{J/4}\right]^{\mathrm{T}}$. Conditioned on h_{RD}, the asymptotic PEP for non-coherent receivers is readily found as [95-Eq.28]

$$P(\mathbf{X}_c \to \mathbf{X}_e \mid h_{RD}) = \left(\prod_{m=1}^{2} \lambda_m\right)^{-1} \sum_{k=0}^{2} \binom{4-k}{2} \frac{1}{k!} \left(\ln\left(\frac{|\mathbf{R}_{cc}|}{|\mathbf{R}_{ee}|}\right)\right)^k \tag{3.40}$$

where $\mathbf{R}_{cc} = \mathbf{X}_c^{\mathrm{H}} \mathbf{X}_c$ and $\mathbf{R}_{ee} = \mathbf{X}_e^{\mathrm{H}} \mathbf{X}_e$ denote the autocorrelation matrices of $\mathbf{X}_e$ and $\mathbf{X}_c$, respectively. In (3.40), λ_m, $m = 1,2$ are the positive eigenvalues of the matrix $\mathbf{\Psi}_{ce} = (\mathbf{R}_{\mathbf{r}} / \mathbf{X}_c)(\boldsymbol{\kappa}_e - \boldsymbol{\kappa}_c)$ where $\mathbf{R}_r / \mathbf{X}_c = \mathbf{X}_c \mathbf{\Sigma} \mathbf{X}_c^{\mathrm{H}} + \mathbf{I}_N$, $\boldsymbol{\kappa}_c = -\mathbf{X}_c \left(\mathbf{R}_{cc} + \mathbf{\Sigma}^{-1}\right)^{-1} \mathbf{X}_c^{\mathrm{H}}$, and $\boldsymbol{\kappa}_e = -\mathbf{X}_e \left(\mathbf{R}_{ee} + \mathbf{\Sigma}^{-1}\right)^{-1} \mathbf{X}_e^{\mathrm{H}}$. Here, $\mathbf{\Sigma}$ is defined as

$$\mathbf{\Sigma} = \begin{bmatrix} \beta_1 (E_{RD}/N_0) |h_{RD}|^2 & 0 \\ 0 & \beta_2 (E_{SD}/N_0) \end{bmatrix}. \tag{3.41}$$

Using the definitions of $\boldsymbol{\kappa}_e$ and $\boldsymbol{\kappa}_c$, we can write $\mathbf{\Psi}_{ce}$ in the following form

$$\mathbf{\Psi}_{ce} = \left(\mathbf{X}_c \mathbf{\Sigma} \mathbf{X}_c^{\mathrm{H}} + \mathbf{I}_N\right)\left(\mathbf{X}_c \left(\mathbf{R}_{cc} + \mathbf{\Sigma}^{-1}\right)^{-1} \mathbf{X}_c^{\mathrm{H}} - \mathbf{X}_e \left(\mathbf{R}_{ee} + \mathbf{\Sigma}^{-1}\right)^{-1} \mathbf{X}_e^{\mathrm{H}}\right). \tag{3.42}$$

where we define the cross-correlation matrices of $\mathbf{X}_e$ and $\mathbf{X}_c$ as $\mathbf{R}_{ce} = \mathbf{X}_c^{\mathrm{H}} \mathbf{X}_e$ and $\mathbf{R}_{ec} = \mathbf{X}_e^{\mathrm{H}} \mathbf{X}_c$. After some algebra and using the fact that the non-zero eigenvalues of **AB** and **BA** are equal [88], we can rewrite (3.42) as

$$\mathbf{\Psi}_{ce} = \mathbf{\Sigma}\mathbf{R}_{cc}\left(\mathbf{\Sigma}^{-1} + \mathbf{R}_{cc}\right)^{-1}\mathbf{R}_{cc} - \mathbf{\Sigma}\mathbf{R}_{ce}\left(\mathbf{\Sigma}^{-1} + \mathbf{R}_{ee}\right)^{-1}\mathbf{R}_{ec} + \left(\mathbf{\Sigma}^{-1} + \mathbf{R}_{cc}\right)^{-1}\mathbf{R}_{cc} - \left(\mathbf{\Sigma}^{-1} + \mathbf{R}_{ee}\right)^{-1}\mathbf{R}_{ee} \tag{3.43}$$

Under the high SNR assumption, i.e., $E_{SR}/N_0 >> E_{SD}/N_0 >> 1$ and $E_{SR}/N_0 >> E_{RD}/N_0 >> 1$, the $\mathbf{\Sigma}^{-1}$ term can be ignored and (3.43) reduces to

$$\mathbf{\Psi}_{ce} = \mathbf{\Sigma}\left(\mathbf{R}_{cc} - \mathbf{R}_{ce}\left(\mathbf{R}_{ee}\right)^{-1}\mathbf{R}_{ec}\right). \tag{3.44}$$

The eigenvalues of $\mathbf{\Psi}_{ce}$ are then obtained as $\lambda_1 = (E_{RD}/N_0)|h_{RD}|^2 \chi_1$ and $\lambda_2 = (E_{SD}/N_0)\chi_2$ where χ_i, $i = 1,2$ denote the eigenvalues of $\left(\mathbf{R}_{cc} - \mathbf{R}_{ce}(\mathbf{R}_{ee})^{-1}\mathbf{R}_{ec}\right)$. Replacing the eigenvalues of (3.44) in (3.40) and noting $\mathbf{R}_{cc} = \mathbf{R}_{ee}$ (due to the orthogonal structure), (3.40) simplifies to[2]

$$P(\mathbf{X}_{cc} \to \mathbf{X}_{ee}) \approx 6 \underset{\substack{|h_{RD}| \\ \delta \to 0}}{E} \left(\left(\frac{E_{RD}}{N_0} \chi_1 |h_{RD}|^2 + \delta \right)^{-1} \right) \left(\frac{E_{SD}}{N_0} \chi_2 \right)^{-1}. \tag{3.45}$$

Under the assumption of perfect power control, i.e., $E_{SD} = E_{RD}$, the unconditional PEP for the non-coherent receiver is found as

$$P(\mathbf{X}_{cc} \to \mathbf{X}_{ee}) \approx 6 \left(\frac{E_{SD}}{N_0} \right)^{-2} \left(\prod_{i=1}^{2} \chi_i \right)^{-1} e^{\delta \left(\frac{E_{SD}}{N_0} \chi_1 \right)^{-1}} \Gamma\left(0, \delta \Big/ \frac{E_{SD}}{N_0} \chi_1 \right). \tag{3.46}$$

where $\Gamma(.,.)$ denotes the incomplete gamma function [71]. Using the limiting expression $\Gamma(0,z) \approx -\log(z)$ for $z \to 0$ [71] and noting that $e^{\delta(\chi_1 E_{SD}/N_0)^{-1}} \approx 1$, we can write (3.46) as

$$P(\mathbf{X}_{cc} \to \mathbf{X}_{ee}) \approx 6 \left(\frac{E_{SD}}{N_0} \right)^{-2} \log\left(\frac{E_{SD}}{N_0} \right) \left(\prod_{i=1}^{2} \chi_i \right). \tag{3.47}$$

For sufficiently high E_{SD}/N_0, the term $\log(E_{SD}/N_0)$ can be ignored with respect to the dominating term of $(E_{SD}/N_0)^{-2}$. Thus, asymptotically, the second order diversity is achieved, realizing the maximum achievable diversity for the considered scenario with single relay. It should be pointed out that for a non-fading $R \to D$ link assumption, i.e., $h_{RD} = 1$, (3.45) simply reduces to

$$P(\mathbf{X}_{cc} \to \mathbf{X}_{ee}) \approx 6 \left(\frac{E_{SD}}{N_0} \right)^{-2} \left(\prod_{i=1}^{2} \chi_i \right)^{-1}. \tag{3.48}$$

[2] Due to the underlying assumptions in the derivation, PEP expression is an approximation, rather than the exact expression given by (3.40).

which has a similar form to the PEP expression derived for conventional STBC with 2 transmit and one receive antenna, c.f., [95-Eq.28]. Comparison of (3.47) and (3.48) further reveals that, asymptotically, the factor $\log(E_{SD}/N_0)$ incurs a coding gain loss only.

B.2 PEP Derivation for Mismatched-Coherent Detector

In this section, we present a diversity gain analysis for the mismatched-coherent detector with LMMSE channel estimator considered in Section 3.3.1. We assume perfect power control where $S \to D$ and $R \to D$ links are balanced, i.e., $E_{RD}/N_0 = E_{SD}/N_0 >> 1$, and sufficiently large SNR for the $S \to R$ link, i.e., $E_{SR}/N_0 >> E_{SD}/N_0$. Noting that the channel estimate $\hat{\mathbf{h}}_{LMMSE}$ and the channel estimation error $\boldsymbol{\varepsilon}_{LMMSE}$ are uncorrelated and omitting the subscript LMMSE in (3.37), we can rewrite (3.31) in scalar form as

$$r_{D_j} = \sum_{i=1}^{2} x_{ji}\hat{h}_i + \eta_{D\,j},\ j = 0,...,J-1 \tag{3.49}$$

where we define $\eta_{D_j} = -\sum_{i=1}^{2} x_{ji}\varepsilon_i + n_{D\,j}$ which is complex Gaussian with variance of $\sigma_{\eta_j}^2 = E_{SD}\sum_{i=1}^{2}\sigma_{\varepsilon_i}^2 + N_0$. In (3.49), x_{ji} denotes the data symbol transmitted over the i^{th} link at time j. Notice that $x_{j1} = 0$ for $j = 0,2,...,J-2$. Noting that the decoder metric is given by $\sum_{j=1}^{J}\left\| r_{D_j} - x_{ji}\hat{h}_i \right\|^2$, the Chernoff bound on the conditional PEP is then given as

$$P\left(\mathbf{X}_D \to \hat{\mathbf{X}}_D \mid \hat{\mathbf{h}}\right) \le \exp\left(-\frac{d^2\left(\mathbf{X}_D, \hat{\mathbf{X}}_D\right)}{4\Omega}\right) \tag{3.50}$$

with

$$d^2\left(\mathbf{X}_D, \hat{\mathbf{X}}_D\right) = \sum_{j=1}^{J}\left\|\sum_{i=1}^{2}\left(x_{ji} - \hat{x}_{ji}\right)\hat{h}_i\right\|^2 = \tilde{\lambda}_1\left|\hat{h}_1\right|^2 E_{SD} + \tilde{\lambda}_2\left|\hat{h}_2\right|^2 E_{SD} \tag{3.51}$$

where $\tilde{\lambda}_i$, $i = 1,2$ denote the eigenvalues of $\left(\mathbf{X}_D - \hat{\mathbf{X}}_D\right)^{\mathrm{H}}\left(\mathbf{X}_D - \hat{\mathbf{X}}_D\right)$ and $\Omega = N_0 + E_{SD}\sum_{i=1}^{2}\sigma_{\varepsilon_i}^2 \ge \sigma_{\eta_j}^2$. Defining the covariance matrix $\mathrm{cov}(\hat{\mathbf{h}}) = \mathrm{diag}\left(\left|h_{RD}\right|^2 + \sigma_{\varepsilon_1}^2,\ 1 + \sigma_{\varepsilon_2}^2\right)$ for the estimated channel coefficients $\hat{\mathbf{h}} = [\hat{h}_1 \quad \hat{h}_2]^{\mathrm{T}}$, we can obtain the unconditional PEP as

$$P(\mathbf{X}_D, \hat{\mathbf{X}}_D) \le \left(\frac{E_{SD}}{4\Omega}\right)^{-2} \frac{1}{\tilde{\lambda}_1 \tilde{\lambda}_2 \left(1+\sigma_{\varepsilon_2}^2\right)} \exp\left(\frac{4\Omega}{\tilde{\lambda}_1 E_{SD}} + \sigma_{\varepsilon_1}^2\right) \Gamma\left(0, \frac{4\Omega}{\tilde{\lambda}_1 E_{SD}} + \sigma_{\varepsilon_1}^2\right). \tag{3.52}$$

Using the limiting expression $\lim_{z\to 0} \Gamma(0,z) \approx -\log(z)$ [71], we can write (3.52) as

$$P(\mathbf{X}_D, \hat{\mathbf{X}}_D) \le \left(\frac{E_{SD}}{4\Omega}\right)^{-2} \log\left(\frac{E_{SD}}{\Omega}\right) \frac{1}{\tilde{\lambda}_1 \tilde{\lambda}_2 \left(1+\sigma_{\varepsilon_2}^2\right)}. \tag{3.53}$$

For large E_{SD}/Ω values, the term $\log(E_{SD}/\Omega)$ can be ignored with respect to the dominating term of $(E_{SD}/\Omega)^{-2}$. Thus, asymptotically, the second order diversity is achieved, realizing the maximum achievable diversity for the considered scenario with single relay. Furthermore, we observe that the presence of channel estimation errors does not affect the diversity order. Similar observations have been earlier reported for conventional space time coding in [96]-[98]. It should noted that as $P \to \infty$, we have $\sigma_{\varepsilon_1}^2 = \sigma_{\varepsilon_2}^2 = 0$, thus reducing (3.52) to

$$P(\mathbf{X}_D, \hat{\mathbf{X}}_D) \le \frac{1}{\tilde{\lambda}_1 \tilde{\lambda}_2} \left(\frac{E_{SD}}{4N_0}\right)^{-2} \exp\left(\frac{4N_0}{\tilde{\lambda}_1 E_{SD}}\right) \Gamma\left(0, \frac{4N_0}{\tilde{\lambda}_1 E_{SD}}\right) \tag{3.54}$$

which was earlier reported in [33] for perfect CSI.

Chapter 4

Cooperative Communication with Multiple-Antenna Nodes

Introduction

So far, we have focused on cooperative communication scenarios where each node is equipped with single transmit and receive antennas. In this chapter, we investigate the effect of multiple antenna deployment assuming different relaying techniques. Specifically, we consider Protocol II with blind AaF, CSI-assisted AaF, DaF relaying and quantify analytically the impact of multiple antenna deployment at the source, relay and/or destination terminals on the diversity order for each of the relaying methods under consideration.

4.1 Transmission Model

We consider a wireless communication scenario where the source terminal S transmits information to the destination terminal D with the assistance of a single relay terminal R (c.f. Fig. 4.1). The source and destination are equipped with M_S and N antennas, respectively. The relay terminal is equipped with M_R receive and M_T transmit antennas. We further as-

sume $M_S = M_R = M_T = M$ [1]. We assume perfect knowledge of CSI at the destination. Whether or not CSI is available at the relay terminal depends on the relaying technique. In blind AaF relaying, no CSI is available at the relay while CSI-assisted AaF and DaF assume perfect CSI.

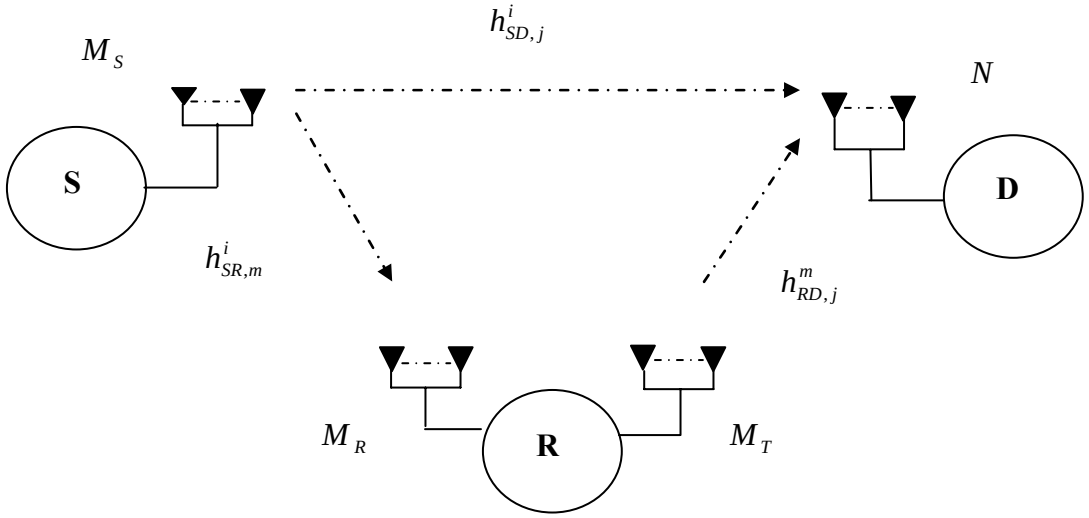

Figure 4.1: Schematic representation of relay-assisted transmission with multi-antenna nodes.

Our transmission model is built upon Protocol II [33], [28]: In the first W time slots (i.e., broadcasting phase), the source terminal communicates with the relay and destination terminals relying on an orthogonal STBC [13], [15] with a rate of G/W designed for M transmit antennas[2]. In the consecutive W time slots (i.e., relaying phase), only the relay terminal communicates with the destination relying on the same orthogonal STBC[3]. The destination per-

[1] In practical scenarios, the same antenna elements can be used for transmission and reception, therefore, it is reasonable to assume M_R=M_T . Since source and relay terminals are cooperating nodes and designed for a given application, they typically share the same physical features. It, therefore, makes practical sense to further assume M_R=M_T=M_S. The sole purpose of assigning different variables for antenna numbers is to distinguish each of their effects on the diversity order.

[2] G symbols are sent over W time slots using M transmit antennas.

[3] For blind AaF relaying, STBC is employed only in broadcasting phase due to the nature of this technique.

forms maximum likelihood decoding on the signals received from the source and relay over $2W$ time slots.

Let E_{SD}, E_{SR}, and E_{RD} represent the average energies available at the destination and relay terminals taking into account for possibly different path loss and shadowing effects in $S \to D$ link, $S \to R$ and relay-to-destination $R \to D$ links, respectively. Let $h^i_{SD,j}$, $h^i_{SR,m}$, and $h^m_{RD,j}$ denote the complex fading coefficients over $S \to D$ link from the i^{th} transmit antenna to the j^{th} receive antenna, $S \to R$ link from the i^{th} transmit antenna to the m^{th} receive antenna, and $R \to D$ link from the m^{th} transmit antenna to the j^{th} receive antenna. These coefficients are modeled as zero-mean complex Gaussian with variance 0.5 per dimension leading to the well-known Rayleigh fading channel model. Unless otherwise indicated, the variables n (regardless of index) are i.i.d. zero mean complex Gaussian samples with $N_0/2$ per dimension and model the additive noise. The received signals at the j^{th} receive antenna of the destination terminal are given by

$$r^w_{D,j} = \sqrt{\frac{E_{SD}}{M_S}} \sum_{i=1}^{M_S} h^i_{SD,j} x_{i,w} + n^w_{D,j}, \quad w = 1,2,...,W, \ j = 1,2,...,N \tag{4.1}$$

where $x_{i,w}$ is the encoded modulation symbol sent from the i^{th} transmit antenna in time interval w. Similarly, the received signals at the m^{th} receive antenna of the relay terminal are given by

$$r^w_{R,m} = \sqrt{\frac{E_{SR}}{M_S}} \sum_{i=1}^{M_S} h^i_{SR,m} x_{i,w} + n^w_{R,m}, \quad w = 1,2,...,W, \ m = 1,2,...,M_R \tag{4.2}$$

In matrix notation, we can rewrite (4.2) as

$$\mathbf{r}_{R,m} = \sqrt{\frac{E_{SR}}{M_S}} \mathbf{H}_{SR,m} \mathbf{x} + \mathbf{n}_{R,m}, \quad m = 1,...,M_R \tag{4.3}$$

where $\mathbf{H}_{SR,m}$ is the channel matrix with size $W \times G$, $\mathbf{x} = [x_1 \ \cdots \ x_G]^{\mathrm{T}}$ denotes the data vector, and $\mathbf{n}_{R,m} = [n^1_{R,m} \ \ ... \ \ n^W_{R,m}]^{\mathrm{T}}$ represents the noise vector. The received signal at the

relay terminal is then processed and forwarded to the destination terminal. The type of processing depends on the deployed relaying technique. In the following, we present the signal models for blind AaF, CSI-assisted AaF, and DaF relaying techniques.

4.1.1 Blind AaF relaying

In blind AaF relaying, the relay terminal does not have CSI. To allow fair comparison between the competing schemes, we assume that the relay terminal simply combines the received signals to yield $\xi^w = \sum_{m=1}^{M_R} r_{R,m}^w$ and then normalizes the resulting signal by a factor of $\sqrt{E[\,|\xi^w\,|^2]} = \sqrt{M_R(E_{SR}+N_0)}$ to ensure the unity of average energy. Normalized signals are transmitted through M_T antennas. The received signals at the destination terminal are given as

$$r_{D,j}^l = \sqrt{\frac{E_{RD}}{M_T}} \sum_{t=1}^{M_T} h_{RD,j}^t \frac{\xi^w}{\sqrt{M_R(E_{SR}+N_0)}} + n_{D,j}^l, \tag{4.4}$$

for $l = W+1, W+2, ..., 2W$, $w = l - W$, $j = 1,2,..., N$. Replacing (4.2) in (4.4), we obtain

$$r_{D,j}^l = \sqrt{\frac{E_{SR}E_{RD}}{M_T M_S M_R(E_{SR}+N_0)}} \sum_{t=1}^{M_T} h_{RD,j}^t \sum_{m=1}^{M_R}\sum_{i=1}^{M_S} h_{SR,m}^i x_{i,w} + \hat{n}_{D,j}^l, \tag{4.5}$$

where the effective noise term is

$$\hat{n}_{D,j}^l = \sqrt{\frac{E_{RD}}{M_T M_R(E_{SR}+N_0)}} \sum_{t=1}^{M_T} h_{RD,j}^t \sum_{m=1}^{M_R} n_{R,m}^w + n_{D,j}^l \tag{4.6}$$

which is complex Gaussian (conditioned on $h_{RD,j}^t$) with zero mean and variance of

$$E\left[\left|\hat{n}_{D,j}^l\right|^2 \mid h_{RD,j}^t\right] = N_0\left(1 + \frac{E_{RD}}{M_T(E_{SR}+N_0)}\left(\sum_{t=1}^{M_T} h_{RD,j}^t\right)^2\right). \tag{4.7}$$

The destination terminal normalizes the received signal given by (4.5) with

$$\left(1+\frac{E_{RD}}{M_T\left(E_{SR}+N_0\right)}\left(\sum_{t=1}^{M_T}h_{RD,j}^{t}\right)^2\right)^{1/2},$$

resulting in

$$r_{D,j}^{l}=\sqrt{\omega_j}\sqrt{E_{RD}}\sum_{t=1}^{M_T}h_{RD,j}^{t}\sum_{m=1}^{M_R}\sum_{i=1}^{M_S}h_{SR,m}^{i}x_{i,w}+\tilde{n}_{D,j}^{l}, \tag{4.8}$$

where $\tilde{n}_{D,j}^{l}$ turns out to be zero-mean complex Gaussian with variance $N_0/2$ per dimension and the scaling factor ω_j is defined as

$$\omega_j=\frac{1}{M_S M_R}\frac{E_{SR}}{N_0}\frac{1}{\left(M_T\left(1+\frac{E_{SR}}{N_0}\right)+\left(\sum_{t=1}^{M_T}h_{RD,j}^{t}\right)^2\frac{E_{RD}}{N_0}\right)}. \tag{4.9}$$

Let $\bar{h}_{RD,j}=\left(1/\sqrt{M_T}\right)\sum_{t=1}^{M_T}h_{RD,j}^{t}$ and $\bar{h}_{SR}^{i}=\left(1/\sqrt{M_R}\right)\sum_{m=1}^{M_R}h_{SR,m}^{i}$. It can be then easily shown that $\bar{h}_{RD,j}$ and $\bar{h}_{SR,j}^{i}$ are i.i.d. zero mean complex Gaussian random variables with variance 0.5 per dimension. Therefore, (4.8) can be rewritten as

$$r_{D,j}^{l}=\sqrt{M_T M_R\omega_j}\sqrt{E_{RD}}\bar{h}_{RD,j}\sum_{i=1}^{M_S}\bar{h}_{SR}^{i}x_{i,l}+\tilde{n}_{D,j}^{l}\quad,\ j=1,2,...N \tag{4.10}$$

The received signals at N receive antennas of the destination terminal, i.e., $r_{D,j}^{l}$, $j=1,2,...N$ are then fed to the ML decoder.

4.1.2 CSI-assisted AaF relaying

In CSI-assisted AaF relaying, the relay terminal is assumed to have CSI of the $S\rightarrow R$ link. The relay terminal first performs spatio-temporal filtering and then adds the resulting signals to yield

$$y_g^{'}=\sum_{m=1}^{M_R}\frac{1}{\beta_{SR,m}}\mathbf{H}_{SR,m}\mathbf{r}_{R,m}=\sqrt{\frac{E_{SR}}{M_S}}\sum_{m=1}^{M_R}\beta_{SR,m}x_g+\sum_{m=1}^{M_R}\eta_m^g,\quad g=1,2,...G \tag{4.11}$$

where $\beta_{SR,m} = \nu^{1/2}(|h_{SR,m}^1|^2 + |h_{SR,m}^2|^2,....+|h_{SR,m}^{M_S}|^2)^{1/2}$ with ν as a constant which depends on the choice of the orthogonal code[4]. In (4.11), x_g denotes the g^{th} entry of the data vector $\mathbf{x} = [x_1 \quad \cdots \quad x_G]^{\mathrm{T}}$ and η_m^g is the g^{th} entry of the filtered noise vector $\boldsymbol{\eta}_m = [\eta_m^1,...,\eta_m^G]$[5] which is still complex Gaussian with zero-mean and variance $N_0/2$ per dimension. After scaling (4.11) by $\left((\sum_{m=1}^{M_R}\beta_{SR,m})^2 E_{SR}/M_S + M_R N_0\right)^{1/2}$ to ensure the unity of average energy at the relay output, we obtain

$$y_g'' = \sqrt{\frac{E_{SR}/M_S}{\left(\sum_{m=1}^{M_R}\beta_{SR,m}\right)^2 E_{SR}/M_S + M_R N_0}}\sum_{m=1}^{M_R}\beta_{SR,m}x_g + \sqrt{\frac{M_R}{\left(\sum_{m=1}^{M_R}\beta_{SR,m}\right)^2 E_{SR}/M_S + M_R N_0}}\eta_g \tag{4.12}$$

The resulting signals $y_1'', \quad y_2'', \quad \cdots \quad , y_G''$ are encoded by a STBC with rate of G/W and then sent to the destination terminal. Let $y_{m,l}$ denote the STBC-encoded modulation symbols transmitted from the m^{th} antenna at the time l. The received signals at the destination terminal are given by

$$r_{D,j}^l = \sqrt{\frac{E_{RD}}{M_T}}\sum_{m=1}^{M_T} h_{RD,j}^m y_{m,l} + n_{D,j}^l, \quad l = W+1, W+2,...,2W,\ j = 1,2,...,N \tag{4.13}$$

where $n_{D,j}^l$ is the additive noise at the destination terminal. The destination terminal applies spatio-temporal matched filtering to the received signal vector i.e., multiplying $\mathbf{r}_{D,j} = [r_{D,j}^{W+1} \quad ... \quad r_{D,j}^{2W}]$ with $(1/\beta_{RD,j})\mathbf{H}_{RD,j}^{\mathrm{H}}$ where $\mathbf{H}_{RD,j}$ is the channel matrix of size $W \times G$ and $\beta_{RD,j} = \sqrt{\upsilon\left(\left|h_{RD,j}^1\right|^2 + \left|h_{RD,j}^2\right|^2,.... + \left|h_{RD,j}^{M_T}\right|^2\right)}$. This yields

$$r_{D,j}^g = \sqrt{\frac{E_{RD}}{M_T}}\beta_{RD,j}y_g'' + \tilde{\eta}_j^g, \quad g = 1,...,G,\ j = 1,2,...,N \tag{4.14}$$

[4] For Alamouti scheme, ν =1. For G3 and G4 codes of [13], ν =2.

[5] Here, $\boldsymbol{\eta}_m = [\eta_m^1,...,\eta_m^G]^{\mathrm{T}} = (1/\beta_{SR,m})\mathbf{H}_{SR,m}^{\mathrm{H}}\mathbf{n}_{R,m}$. Thus, due to the orthogonality of the channel matrix $\mathbf{H}_{SR}$, the entries of $\boldsymbol{\eta}_m$ are still white, i.e., $E[\boldsymbol{\eta}_m\boldsymbol{\eta}_m^{\mathrm{H}}] = N_0\mathbf{I}_G$.

where the filtered noise $\tilde{\eta}_j^g$ is still zero-mean complex Gaussian. Replacing (4.12) in (4.14), we obtain

$$r_{D,j}^g = \sqrt{\frac{E_{SR}E_{RD}}{M_T M_S\left(\left(\sum_{m=1}^{M_R}\beta_{SR,m}\right)^2 E_{SR}/M_S + M_R N_0\right)}}\beta_{RD,j}\sum_{m=1}^{M_R}\beta_{SR,m}x_g + \hat{n}_{D,j}^g, \tag{4.15}$$

where the effective noise term is defined as

$$\hat{n}_{D,j}^g = \sqrt{\frac{M_R E_{RD}}{M_T\left(\left(\sum_{m=1}^{M_R}\beta_{SR,m}\right)^2 E_{SR}/M_S + M_R N_0\right)}}\beta_{RD,j}\eta_g + \tilde{\eta}_j^g \tag{4.16}$$

which is complex Gaussian (conditioned on $\beta_{SR,m}$ and $\beta_{RD,j}$) with zero mean and variance of

$$E\left[\left|\hat{n}_{D,j}^g\right|^2 \mid \beta_{RD,j},\beta_{SR,m}\right] = N_0\left(1+\frac{M_R E_{RD}\beta_{RD,j}^2}{M_T\left(\left(\sum_{m=1}^{M_R}\beta_{SR,m}\right)^2 E_{SR}/M_S + M_R N_0\right)}\right). \tag{4.17}$$

The destination terminal normalizes the received signal given by (4.15) with

$$\left(1+\frac{M_R\beta_{RD,j}^2 E_{RD}}{M_T\left(\left(\sum_{m=1}^{M_R}\beta_{SR,m}\right)^2 E_{SR}/M_S + M_R N_0\right)}\right)^{1/2},$$

resulting in

$$\tilde{r}_{D,j}^g = \sqrt{\alpha_j}\,\beta_{RD,j}\sum_{m=1}^{M_R}\beta_{SR,m}x_g + \tilde{n}_{D,j}^g, \quad j = 1,2,\ldots N \tag{4.18}$$

where

$$\alpha_j = \frac{(E_{SR}/N_0)E_{RD}}{\left(M_T\left(\sum_{m=1}^{M_R}\beta_{SR,m}\right)^2(E_{SR}/N_0) + M_S M_T M_R\right) + M_S M_R\beta_{RD,j}^2(E_{RD}/N_0)}. \tag{4.19}$$

The received signals at N receive antennas of the destination terminal, i.e., $\tilde{r}_{D,j}^{g}$, $j = 1,2,...N$ are then fed to the ML decoder.

4.1.3 DaF relaying

We consider adaptive DaF relaying [26] where the relay terminal decodes the received signals received if $\gamma_{SR} \geq \gamma_{th}$, where γ_{SR} is the received instantaneous SNR at the relay terminal and γ_{th} is a threshold value required to initiate the DaF operation. Once this condition is satisfied, the relay makes a ML estimate of the data from the received signal and then feeds the decoded data into a space-time block encoder for transmission to the destination terminal. The received signals at the destination terminal can be written as

$$r_{D,j}^{l} = \sqrt{\frac{E_{RD}}{M_R}} \sum_{m=1}^{M_T} h_{RD,j}^{m} y_{m,l} + n_D^l, \quad l = W+1,...,2W, \; j = 1,2,..., N \tag{4.20}$$

where $y_{m,l}$ denote the STBC-encoded modulation symbols transmitted from the relay's m^{th} transmit antenna in time interval l. The received signals at N receive antennas of the destination terminal , i.e., $r_{D,j}^{l}$, $j = 1,2,...N$ are then fed to the ML decoder.

4.2 Diversity Gain Analysis

In this section, we investigate the achievable diversity gains for each of the considered relaying techniques through the derivation of PEP expressions. Defining the transmitted codeword vector from the source and the erroneously-decoded codeword vector at the destination terminal, respectively, as $\mathbf{x} = [x_1 \quad \cdots \quad x_G]^{\mathrm{T}}$ and $\hat{\mathbf{x}} = [\hat{x}_1 \quad \cdots \quad \hat{x}_G]^{\mathrm{T}}$, the conditional PEP is given as

$$P(\mathbf{x}, \hat{\mathbf{x}} \mid h_{SR,m}^{i}, h_{RD,j}^{m}, h_{SD,j}^{i}, i = 1,...,M_S, m = 1,...,M_T, j = 1,...,N) = Q\left(\sqrt{\frac{d^2(\mathbf{x},\hat{\mathbf{x}})}{2N_0}}\right), \tag{4.21}$$

assuming ML decoding with perfect knowledge of the channel CSI at the destination terminal. Here, $Q(.)$ is the Gaussian-Q function and $d^2(\mathbf{x},\hat{\mathbf{x}})$ denotes the Euclidean distance between $\mathbf{x}$ and $\hat{\mathbf{x}}$. Applying the standard Chernoff bound to (4.21), we obtain

$$P(\mathbf{x},\hat{\mathbf{x}} \mid h^i_{SR,m}, h^m_{RD,j}, h^i_{SD,j}, i=1,...,M_S, m=1,...,M_T, j=1,...,N) \le \exp\left(-\frac{d^2(\mathbf{x},\hat{\mathbf{x}})}{4N_0}\right). \quad (4.22)$$

4.2.1 PEP for blind AaF relaying

The Euclidean distance $d^2(\mathbf{x},\hat{\mathbf{x}})$ for blind AaF relaying can be written as

$$\begin{aligned} d^2(\mathbf{x},\hat{\mathbf{x}}) &= d^2_{S\to R\to D}(\mathbf{x},\hat{\mathbf{x}}) + d^2_{S\to D}(\mathbf{x},\hat{\mathbf{x}}) \\ &= M_R M_T \lambda \sum_{j=1}^{N} \omega_j \left|\bar{h}_{RD,j}\right|^2 \sum_{i=1}^{M_S} \left|\bar{h}^i_{SR}\right|^2 + \frac{\lambda E_{SD}}{M_S} \sum_{j=1}^{N}\sum_{i=1}^{M_S} \left|h^i_{SD,j}\right|^2 . \end{aligned} \quad (4.23)$$

Maximum Achievable Diversity: Since ω_j is a function of $\sum_{t=1}^{M_T} h^t_{RD,j}$ term, c.f., (4.9), the derivation of PEP becomes analytically difficult without any assumptions imposed on the SNR in the underlying links. However, for the asymptotic case of $E_{SD}/N_0 = E_{RD}/N_0 >> 1$ with perfect power control and sufficiently large $E_{SR}/N_0 >> E_{SD}/N_0$ values, ω_j can be approximated as $\omega_j \approx 1/M_S M_R M_T$. Given (4.1) and (4.10), $d^2(\mathbf{x},\hat{\mathbf{x}})$ can be written as

$$d^2(\mathbf{x},\hat{\mathbf{x}}) = \frac{\lambda E_{SD}}{M_S} \sum_{j=1}^{N} \left|\bar{h}_{RD,j}\right|^2 \sum_{i=1}^{M_S} \left|\bar{h}^i_{SR}\right|^2 + \frac{\lambda E_{SD}}{M_S} \sum_{j=1}^{N}\sum_{i=1}^{M_S} \left|h^i_{SD,j}\right|^2 \quad (4.24)$$

where $\lambda = v\left|x_1 - \hat{x}_1\right|^2 + ... + v\left|x_G - \hat{x}_G\right|^2$ denotes the eigenvalue of the codeword difference matrix. Following steps detailed in Appendix C.1, we obtain the PEP expressions

$$P(\mathbf{x},\hat{\mathbf{x}}) \le \frac{\Gamma(N - M_S)\lambda^{-M_S(N+1)}}{\Gamma(N)} \left(\frac{E_{SD}}{4M_S N_0}\right)^{-M_S(N+1)} \quad \text{for } N > M_S \quad (4.25)$$

$$P(\mathbf{x},\hat{\mathbf{x}}) \le \frac{\Gamma(M_S - N)\lambda^{-N(M_S+1)}}{\Gamma(M_S)} \left(\frac{E_{SD}}{4M_S N_0}\right)^{-N(M_S+1)} \quad \text{for } M_S > N \quad (4.26)$$

$$P(\mathbf{x},\hat{\mathbf{x}}) \le \frac{\lambda^{-M_S(N+1)}}{\Gamma(N)} \log\left(\frac{E_{SD}}{N_0}\right)\left(\frac{E_{SD}}{4M_S N_0}\right)^{-M_S(N+1)} \quad \text{for } M_S = N \tag{4.27}$$

It can be observed from (4.25)-(4.27) that the maximum achievable diversity order for the considered scenario is given by $\min(M_S, N) + M_S N$. This illustrates that the smaller of diversity orders experienced in $S \to R$ and $R \to D$ links becomes the performance bottleneck for the relaying path.

Effect of poor inter-user channel: In the above investigation of the maximum achievable diversity order, we have assumed that SNR in $S \to R$ link is sufficiently large, i.e., $E_{SR}/N_0 >> E_{SD}/N_0$. Now we consider the limiting case of $E_{SR}/N_0 \to 0$ (We still assume $E_{SD}/N_0 >> 1$). Under these assumptions, the scaling factor defined as in (4.9) reduces to

$$\omega_j \cong \frac{(E_{SR}/N_0)}{M_S M_R M_T \left|\bar{h}_{RD,j}\right|^2 (E_{SD}/N_0)}. \tag{4.28}$$

Conditioned on $\bar{h}_{RD,j}$, the noise terms at different antennas at the destination terminal are still Gaussian, but no longer white, i.e., spatially correlated (See (4.6)). In the following, to simplify performance analysis, we assume that the number of receive antennas at the destination terminal seen by the $S \to R \to D$ link is equal to unity[6]. The Euclidean distance can be then written as

$$d^2(\mathbf{x},\hat{\mathbf{x}}) = \frac{\lambda E_{SR}}{M_S} \sum_{i=1}^{M_S} \left|\bar{h}_{SR}^{i}\right|^2 + \frac{\lambda E_{SD}}{M_S} \sum_{j=1}^{N} \sum_{i=1}^{M_S} \left|h_{SD,j}^{i}\right|^2 \quad . \tag{4.29}$$

Following detailed steps in the Appendix C.2, we obtain the final PEP expression given as

[6] It has been observed through a Monte-Carlo simulation experiment that this assumption does not change the error rate performance, since the number of antennas seen by $S \to D$ becomes the determining factor in the performance for low E_{SR}/N_0 values.

$$P(\mathbf{x},\hat{\mathbf{x}}) \le \left(\frac{E_{SD}}{4M_S N_0}\lambda\right)^{-NM_S}\left(1+\frac{E_{SR}}{4M_S N_0}\lambda\right)^{-M_S}. \quad (4.30)$$

Since $E_{SR}/N_0 \to 0$ is assumed, the first term becomes dominant. Therefore, it can be easily concluded that the diversity order in (4.30) is limited to NM_S. This indicates that for poor inter-user channel, the diversity of the relay-assisted transmission is limited to the diversity of the non–cooperative case, i.e., direct transmission

Non-Fading $R \to D$ ***Link:*** Now, we focus on the case where the channel between the relay and the destination terminals is AWGN, i.e., $h_{RD} = 1$. Under the assumptions of $E_{SD}/N_0 = E_{RD}/N_0 >> 1$ and $E_{SR}/N_0 >> E_{SD}/N_0$, ω_j can be approximated as $\omega_j \approx 1/M_S M_R M_T$. $d^2(\mathbf{x},\hat{\mathbf{x}})$ can be then written as

$$d^2(\mathbf{x},\hat{\mathbf{x}}) = \frac{E_{SD}}{M_S}\sum_{j=1}^{N}\sum_{i=1}^{M_S}\left|h_{SD,j}^{i}\right|^2\lambda + N\frac{E_{SD}}{M_S}\sum_{i=1}^{M_S}\left|\bar{h}_{SR}^{i}\right|^2\lambda . \quad (4.31)$$

Following similar steps detailed in Appendix C.2, we obtain the final PEP expression as

$$P(\mathbf{x},\hat{\mathbf{x}}) \le N^{-M_S}\left(\frac{\lambda E_{SD}}{4M_S N_0}\right)^{-M_S(1+N)}. \quad (4.32)$$

Therefore, it can be easily seen the diversity order for a non-fading $R \to D$ link is $M_S(1+N)$ which is obviously either equal or larger than the diversity order observed for the previous scenario with fading $R \to D$ link, i.e., $\min(M_S, N) + M_S N$.

4.2.2 PEP for CSI-assisted AaF relaying

The conditional PEP expression is given by (4.22) where the Euclidean distance now has the form of

$$d^2(\mathbf{x},\hat{\mathbf{x}}) = \frac{\lambda E_{SD}}{M_S}\sum_{j=1}^{N}\sum_{i=1}^{M_S}\left|h_{SD,j}^{i}\right|^2 + \lambda\sum_{j=1}^{N}\alpha_j\sum_{m=1}^{M_T}\left|h_{RD,j}^{m}\right|^2\left(\sum_{m=1}^{M_R}\beta_{SR,m}\right)^2 \quad (4.33)$$

where α_j is earlier defined by (4.19).

Maximum Achievable Diversity: Under the assumptions of perfect power control where $S \to D$ and $R \to D$ links are balanced and high SNRs for all underlying links, i.e., $E_{SD}/N_0 = E_{RD}/N_0 >> 1$ and $E_{SR}/N_0 >> E_{SD}/N_0$, we obtain the PEP expression as (see Appendix C.3)

$$P(\mathbf{x}, \hat{\mathbf{x}}) \le \left(\frac{E_{SD}}{4M_S N_0} \right)^{-N(M_S+M_T)} \lambda^{-N(M_S+M_T)} \tag{4.34}$$

This demonstrates that the diversity order achieved through CSI-assisted AaF is $N(M_S + M_T) = 2NM$. This indicates that CSI-assisted AaF is able to perform better than blind AaF relaying which achieves a diversity order of $\min(M, N) + MN$.

Effect of poor inter-user channel: Now we consider the limiting case of $E_{SR}/N_0 \to 0$. The Euclidean distance takes the form of

$$d^2(\mathbf{x}, \hat{\mathbf{x}}) = \frac{\lambda E_{SD}}{M_S} \sum_{j=1}^{N} \sum_{i=1}^{M_S} \left| h_{SD,j}^{i} \right|^2 + \frac{1}{\nu} \frac{\lambda N E_{SR}}{M_R M_S} \left(\sum_{m=1}^{M_R} \beta_{SR,m} \right)^2. \tag{4.35}$$

Similar to blind AaF scenario, we assume the number of receive antennas seen by the $S \to R \to D$ link is equal to 1 to simplify the performance analysis. Following steps detailed in Appendix C.4, we obtain the PEP expression as

$$P(\mathbf{x}, \hat{\mathbf{x}}) \le \left(\frac{\lambda E_{SD}}{4M_S N_0} \right)^{-NM_S} \tag{4.36}$$

It is observed from (4.36) that for poor inter-user channel, similar to blind AaF, the diversity of CSI-assisted relaying is limited to the diversity of the non–cooperative case, i.e., NM_S.

Non-Fading $R \to D$ Link: Under the assumption of a non-fading $R \to D$ link, the Euclidean distance can be written as

$$d^2(\mathbf{x}, \hat{\mathbf{x}}) = \frac{\lambda E_{SD}}{M_S} \sum_{j=1}^{N} \sum_{i=1}^{M_S} \left| h_{SD,j}^{i} \right|^2 + \lambda N E_{SD}. \tag{4.37}$$

Following detailed steps in Appendix C.5, we obtain the PEP expression as

$$P(\mathbf{x},\hat{\mathbf{x}}) \le \left(\frac{E_{SD}}{4M_S N_0}\right)^{-NM_S} \lambda^{-NM_S} \exp\left(-N\lambda\frac{E_{SD}}{4N_0}\right) \tag{4.38}$$

In (4.38), the exponential term is dominant and, therefore, the diversity order is large and can not be determined by an integer value anymore, i.e., an AWGN-like performance is observed.

4.2.3 PEP for DaF relaying

For DaF relaying, end-to-end PEP can be written as

$$P(\mathbf{x},\hat{\mathbf{x}})_{End-to-End} = \begin{cases} P_{S\to R}(\mathbf{x}, f(\mathbf{x}))P(f(\mathbf{x}),\hat{\mathbf{x}}) + (1-P_{S\to R}(\mathbf{x}, f(\mathbf{x})))P(\mathbf{x},\hat{\mathbf{x}}) & \text{for } \gamma_{SR} \ge \gamma_{th} \\ P_{S\to D}(\mathbf{x},\hat{\mathbf{x}}) & \text{for } \gamma_{SR} < \gamma_{th} \end{cases} \tag{4.39}$$

where $f(\mathbf{x})$ denotes the relay decoded output, $P(f(\mathbf{x}),\mathbf{x})$ is the PEP when cooperation is employed given that the codeword is decoded incorrectly at the relay terminal, $P(\mathbf{x},\hat{\mathbf{x}})$ denotes the PEP when cooperation is employed given that the codeword is decoded correctly at the relay terminal, and $P_{S\to R}(\mathbf{x}, f(\mathbf{x}))$ is the PEP over the $S \to R$ link. For $\gamma_{SR} < \gamma_{th}$, end-to-end PEP is simply restricted to $P_{S\to D}(\mathbf{x},\hat{\mathbf{x}})$ which represents the PEP of the direct transmission. To simplify the performance analysis, we can upper bound $P(\mathbf{x},\hat{\mathbf{x}})_{End-to-End}$ as

$$P(\mathbf{x},\hat{\mathbf{x}})_{End-to-End} \le P_{S\to R}(\mathbf{x}, f(\mathbf{x})) + (1-P_{S\to R}(\mathbf{x}, f(\mathbf{x})))P(\mathbf{x},\hat{\mathbf{x}}) \tag{4.40}$$

where we have used the fact $P(f(\mathbf{x}),\hat{\mathbf{x}}) \le 1$.

Maximum Achievable Diversity: Under the assumptions of perfect power control where $S \to D$ and $R \to D$ links are balanced and high SNRs for all underlying links, i.e., $E_{SD}/N_0 = E_{RD}/N_0 >> 1$ and $E_{SR}/N_0 >> E_{SD}/N_0$, we have $P_{S\to R}(\mathbf{x}, f(\mathbf{x})) \to 0$. Therefore, (4.40) can be approximated as $P(\mathbf{x},\hat{\mathbf{x}})_{End-to-End} \le P(\mathbf{x},\hat{\mathbf{x}})$. The Euclidian distance in this case is given as

$$d^2(\mathbf{x},\hat{\mathbf{x}}) = \frac{E_{SD}}{M_S}\sum_{j=1}^{N}\sum_{i=1}^{M_S}\left|h_{SD,j}^{i}\right|^2\lambda + \frac{E_{SD}}{M_T}\sum_{j=1}^{N}\sum_{t=1}^{M_T}\left|h_{RD,j}^{t}\right|^2\lambda . \tag{4.41}$$

Following similar steps detailed in Appendix C.3, we obtain the PEP expression as

$$P(\mathbf{x},\hat{\mathbf{x}})_{End-to-End} \le \left(\frac{E_{SD}}{4M_S N_0}\right)^{-N(M_S+M_T)} \lambda^{-N(M_S+M_T)} \quad . \tag{4.42}$$

We observe that DaF relaying is able to achieve a diversity order of $N(M_S + M_T)$ which is the same as that of CSI-assisted AaF relaying.

Effect of poor inter-user channel: When the inter-user channel has a very poor quality, we have $P(\gamma_{SR} < \gamma_{th}) \approx 1$. Thus, we obtain the final PEP as

$$P(\mathbf{x},\hat{\mathbf{x}})_{End-toEnd} = P_{S\to D}(\mathbf{x},\hat{\mathbf{x}}) \le \left(\frac{E_{SD}}{4M_S N_0}\right)^{-NM_S} \lambda^{-NM_S} \ . \tag{4.43}$$

Consequently, for poor inter-user channel, similar to the other two relaying protocols, the diversity is limited to the diversity of the non-cooperative scenario.

Non-Fading $R \to D$ ***Link:*** Under the assumption of $E_{SR}/N_0 >> E_{SD}/N_0$ and $E_{SD}/N_0 = E_{RD}/N_0 >> 1$, we observe that $P(\gamma_{SR} \ge \gamma_{th}) \approx 1$, hence, we can safely assume that $P_{S\to R}(\mathbf{x},\, f(\mathbf{x})) \approx 0$ which yields $P(\mathbf{x},\hat{\mathbf{x}})_{End-to-End} \le P(\mathbf{x},\hat{\mathbf{x}})$. Assuming a non-fading $R \to D$ link, the Euclidean distance can be given as

$$d^2(\mathbf{x},\hat{\mathbf{x}}) = \frac{E_{SD}}{M_S}\sum_{j=1}^{N}\sum_{i=1}^{M_S}\left|h_{SD,j}^{i}\right|^2\lambda + N\lambda E_{SD} \tag{4.44}$$

It can be easily seen that (4.44) as a similar form to (4.37). Therefore, following similar steps detailed in Appendix C.5, we obtain the PEP expression as

$$P(\mathbf{x},\hat{\mathbf{x}})_{End-to-End} \le \left(\frac{E_{SD}}{4M_S N_0}\right)^{-NM_S} \lambda^{-NM_S} \exp\left(-N\lambda\frac{E_{SD}}{4N_0}\right) \tag{4.45}$$

We observe from (4.45) that, similar to CSI-assisted AaF relaying, the exponential term dominates and provides an AWGN-like performance.

For the convenience of the reader, Tables 4.1 and 4.2 tabulate the achievable diversity orders of all aforementioned schemes for various scenarios.

Table 4.1: Diversity Orders of AaF, CSI-assisted AaF, and DaF relaying.
(a) Non-fading $R \to D$ Link.

Relaying Protocol	**High** E_{SR}/N_0 **Values**	**Low** E_{SR}/N_0 **Values**
Blind AaF	$M_S(N+1)$	$M_S N$
CSI-assisted AaF	Large	$M_S N$
DaF	Large	$M_S N$

(b) Fading $R \to D$ Link

Relaying Protocol	**High** E_{SR}/N_0 **Values**	**Low** E_{SR}/N_0 **Values**
Blind AaF	$\min(M_S, N) + M_S N$	$M_S N$
CSI-assisted AaF	$N(M_S + M_T)$	$M_S N$
DaF	$N(M_S + M_T)$	$M_S N$

4.3 Numerical Results

In this section, we present Monte-Carlo simulation results for cooperative transmission systems which have been described and analyzed in this paper. We assume a quasi-static Rayleigh fading channel and employ 4-PSK modulation. We further assume $E_{SD} = E_{RD}$, i.e.,

$S \to D$ and $R \to D$ links are balanced, which can be achieved through power control. We assume $E_{SR} / N_0 = 35\,\text{dB}$ unless otherwise noted

In Figure 4.2, we illustrate the SER performance of the blind AaF scheme assuming $M_S = M_T = M_R = M = 2$ and $M_S = M_T = M_R = M = 3$ with N=1. For $M = 2$ and 3, we consider Alamouti scheme and G3-STBC (37) of [13], respectively, as the underlying codes. It is observed that the diversity orders for scenarios of (M=2, N=1) and (M=3, N=1) are 3 and 4, respectively, confirming the diversity order of $\min(M_S, N) + M_S N$ observed through our PEP analysis. In Figure 4.2, we also include the performance of blind AaF scheme in the presence of non-fading $R \to D$ link assuming M=2 and N=1. It is observed that the diversity order is 4 confirming our observation in (4.32).

To demonstrate that M_T and M_R do not affect the diversity order in blind AaF scheme, we include the performance of a scenario with $M_T = M_R = 1$ while keeping $M_S = 2$. It is clearly seen that the performance remains identical to that of previous considered scenario of ($M_S = M_T = M_R = M = 2$, N=1).

To further investigate the effect of poor inter-user quality, we investigate the performance for $E_{SR} / N_0 = 0\,\text{dB}$. It is observed that the diversity order of blind AaF scheme for is limited to the diversity order of non-cooperative transmission, i.e. , $M_S N = 2$, confirming our observation in (4.30).

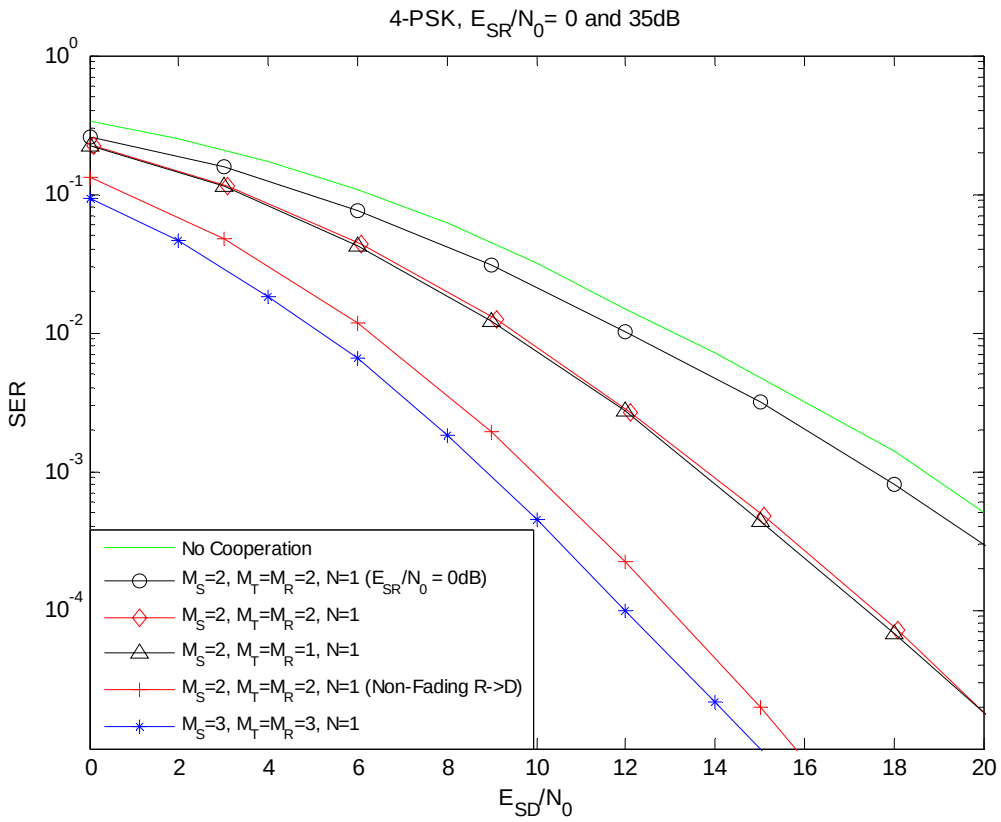

Figure 4.2: SER performances of blind AaF scheme with multi-antenna nodes.

In Figure 4.3, we demonstrate the SER performance of the CSI-assisted AaF relaying scheme. For the scenarios of (M=2, N=1) and (M=3, N=1), we observe diversity orders of 4 and 6, respectively, confirming the diversity order of $N(M_T + M_S)$ observed through our PEP analysis. For the non-fading $R \to D$ link performance, we observe a rapid steep which can be justified by the presence of the exponential term in (4.38). We also consider the scenario of (M=2, N=1) with low and moderate SNRs in the $S \to R$ link, e.g., $E_{SR}/N_0 = 0, 10$ dB. For $E_{SR}/N_0 = 10$ dB, we observe some performance degradation in comparison to high $E_{SR}/N_0 = 35$ dB, and the maximum diversity order can not be achieved anymore. For $E_{SR}/N_0 = 0$ dB, the performance degradation further increases and the

achieved diversity order remains limited to the diversity order of non-cooperative transmission, confirming our observation in (4.36).

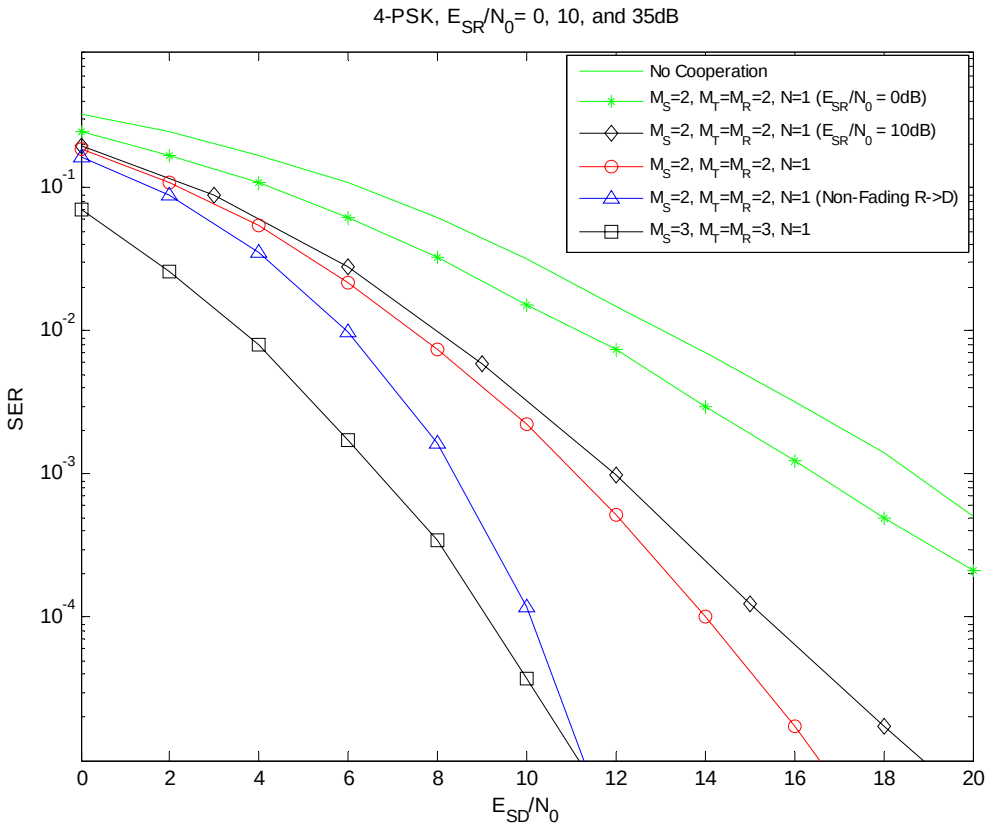

Figure 4.3: SER performances of CSI-assisted AaF scheme with multi-antenna nodes.

In Figure 4.4, we demonstrate the SER performance of the DaF relaying scheme assuming the same scenarios considered for Figure 4.3. Comparison of Figures 4.3 and 4.4 reveals that, for high E_{SR}/N_0 values, both CSI-assisted AaF yield identical performance, confirming our observations in (4.34), (4.38), (4.42), and (4.45). For $E_{SR}/N_0 = 10$ dB, we observe that performance of DaF and CSI-assisted AaF are no longer the same. DaF scheme suffers from

error propagation due to relatively low SNR in $S \to R$ link and is outperformed by CSI-assisted AaF. This indicates that for such moderate E_{SR}/N_0 values, CSI-assisted AaF becomes favorable choice. It is also observed for $E_{SR}/N_0 = 0\,\text{dB}$, similar to other two relaying schemes, that the diversity order of DaF relaying is the same as non-cooperative scenario, confirming our observation in (4.43).

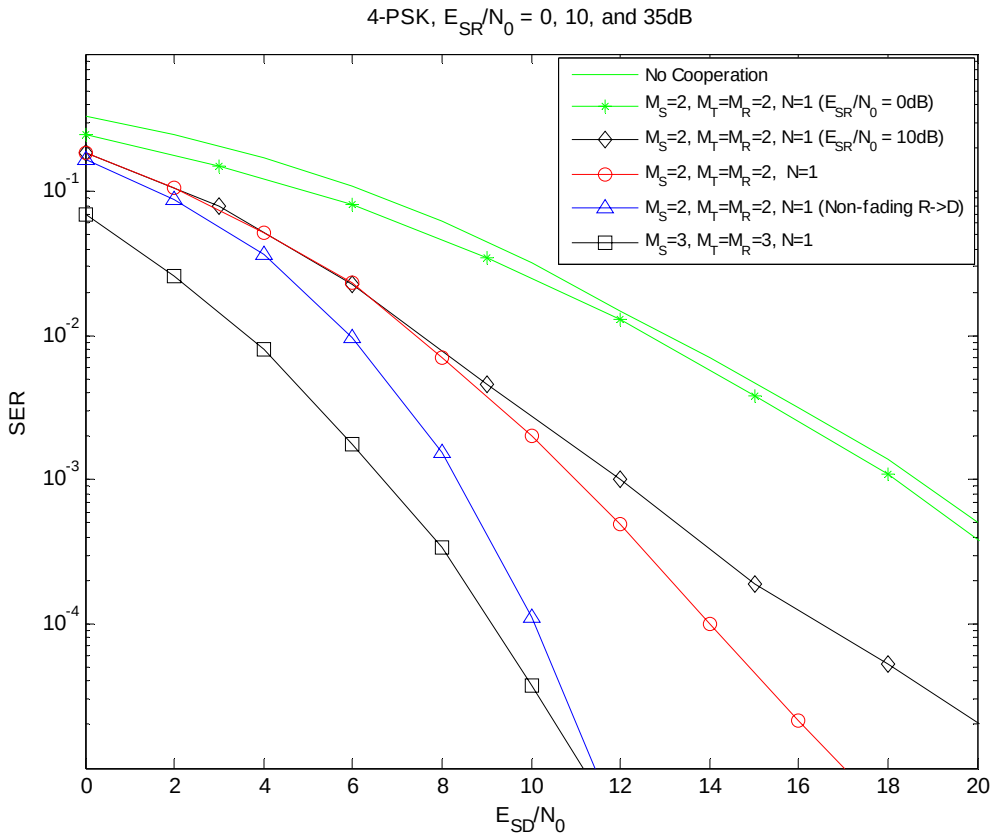

Figure 4.4: SER performances of DaF scheme with multi-antenna nodes.

Appendix C

C.1 Derivation of Eqs. (4.25)-(4.26)-(4.27)

In this Appendix, we derive the PEP expression for blind AaF scheme assuming fading $R \to D$ link. The Euclidean distance $d^2(\mathbf{x}, \hat{\mathbf{x}})$ is given by (4.23) and repeated here for convenience

$$d^2(\mathbf{x}, \hat{\mathbf{x}}) = d^2_{S\to R\to D}(\mathbf{x}, \hat{\mathbf{x}}) + d^2_{S\to D}(\mathbf{x}, \hat{\mathbf{x}})$$
$$= M_R M_T \lambda \sum_{j=1}^{N} \omega_j \left|\bar{h}_{RD,j}\right|^2 \sum_{i=1}^{M_S} \left|\bar{h}^i_{SR}\right|^2 + \frac{\lambda E_{SD}}{M_S} \sum_{j=1}^{N}\sum_{i=1}^{M_S} \left|h^i_{SD,j}\right|^2 . \quad (4.46)$$

For the asymptotic case of $E_{SD}/N_0 = E_{RD}/N_0 >> 1$ with perfect power control and sufficiently large $E_{SR}/N_0 >> E_{SD}/N_0$ values, ω_j can be approximated as $\omega_j \approx 1/M_S M_R M_T$. Therefore, (4.46) reduces to

$$d^2(\mathbf{x}, \hat{\mathbf{x}}) = \frac{\lambda E_{SD}}{M_S} \sum_{j=1}^{N}\sum_{i=1}^{M_S} \left|h^i_{SD,j}\right|^2 + \frac{\lambda E_{SD}}{M_S} \sum_{j=1}^{N} \left|\bar{h}_{RD,j}\right|^2 \sum_{i=1}^{M_S} \left|\bar{h}^i_{SR}\right|^2 . \quad (4.47)$$

Introducing $Y_1 = \sum_{j=1}^{N}\sum_{i=1}^{M_S} \left|h^i_{SD,j}\right|^2$ and $Y_2 = Z_1 Z_2$ with $Z_1 = \sum_{j=1}^{N} \left|\bar{h}_{RD,j}\right|^2$ and $Z_2 = \sum_{i=1}^{M_S} \left|\bar{h}^i_{SR}\right|^2$, we can rewrite (4.47) as

$$d^2(\mathbf{x}, \hat{\mathbf{x}}) = \frac{\lambda E_{SD}}{M_S} Y_1 + \frac{\lambda E_{SD}}{M_S} Y_2 . \quad (4.48)$$

After substituting (4.48) in (4.22), we have the PEP expression as

$$P(\mathbf{x}, \hat{\mathbf{x}} \mid Y_1, Y_2) \le \exp\left(-\frac{\lambda E_{SD}}{4N_0 M_S} Y_1\right) \exp\left(-\frac{\lambda E_{SD}}{4N_0 M_S} Y_2\right) \quad (4.49)$$

The unconditional PEP can be obtained as [84]

$$P(\mathbf{x}, \hat{\mathbf{x}}) \le \Phi_{Y_1}(\omega)\Big|_{j\omega = -\frac{\lambda E_{SD}}{4M_S N_0}} \times \Phi_{Y_2}(\omega)\Big|_{j\omega = -\frac{\lambda E_{SD}}{4M_S N_0}} \quad (4.50)$$

where $\Phi_{Y_1}(\omega)$ and $\Phi_{Y_2}(\omega)$ are the characteristic functions of Y_1 and Y_2, respectively. Since $\left|h^i_{SD,j}\right|$ is Rayleigh distributed, the characteristic function of Y_1 can be readily found as [84]

$$\Phi_{Y_1}(\omega)\Big|_{j\omega=-\frac{\lambda \mathrm{E_{SD}}}{4M_S \mathrm{N_0}}} = \left(1+\frac{E_{SD}}{4M_S N_0}\lambda\right)^{-M_S N} . \tag{4.51}$$

where the first term can be further ignored under high SNR assumption. In the following, we will derive the PEP expression under three different scenarios:

Case 1 ($N > M_S$): The characteristic function of Y_2 can evaluated as [85]

$$\Phi_{Y_2}(\omega) = \int_0^\infty f_{Z_1}(z_1)\Phi_{Z_2}(\omega z_1)dz_1 , \tag{4.52}$$

where $f_{Z_1}(z_1)$ is the pdf of Z_1 and $\Phi_{Z_2}(\omega z_1)$ has the similar form as in (4.51). Here, z_1 is a chi-squared random variable with $2N$ degrees of freedom with the pdf $f_{Z_1}(z_1) = z_1^{N-1}e^{-z_1}/\Gamma(N),\ z_1 \geq 0$ [86] where $\Gamma(.)$ denotes the gamma function [71]. This leads to

$$\Phi_{Y_2}(\omega)\Big|_{j\omega=-\frac{\lambda \mathrm{E_{SD}}}{4M_S N_0}} = \frac{1}{\Gamma(N)}\left(\frac{E_{SD}}{4M_S N_0}\right)^{-M_S}\lambda^{-M_S}\int_0^\infty\left(\frac{4M_S N_0}{\lambda E_{SD}}+z_1\right)^{-M_S} z_1^{N-1}e^{-z_1}dz_1 , \tag{4.53}$$

Assuming high SNR, i.e., $E_{SD}/4N_0 >> 1$ and using the integral form given by [71, p.382, 3.351.3], we obtain

$$\Phi_{Y_2}(\omega)\Big|_{j\omega=-\frac{\lambda \mathrm{E_{SD}}}{4M_S N_0}} = \frac{\Gamma(N-M_S)}{\Gamma(N)}\left(\frac{E_{SD}}{4M_S N_0}\right)^{-M_S}\lambda^{-M_S} \tag{4.54}$$

Substituting (4.54) and (4.51) in (4.50), we find the final PEP expression as

$$P(\mathbf{x},\hat{\mathbf{x}}) \leq \frac{\Gamma(N-M_S)\lambda^{-M_S(N+1)}}{\Gamma(N)}\left(\frac{E_{SD}}{4M_S N_0}\right)^{-M_S(N+1)} \tag{4.55}$$

Case 2 ($M_S > N$): Noting that this case is similar to the previous case with N and M_S now interchanged, we follow similar steps and find the PEP expression as

$$P(\mathbf{x},\hat{\mathbf{x}}) \leq \frac{\Gamma(M_S-N)\lambda^{-N(M_S+1)}}{\Gamma(M_S)}\left(\frac{E_{SD}}{4M_S N_0}\right)^{-N(M_S+1)} \tag{4.56}$$

Case 3 ($M_S = N$): Following the same argument in Case 1 and further defining $u = \upsilon + z_1$, where $\upsilon = 4M_S N_0 / (\lambda E_{SD})$, we write (4.53) as

$$\Phi_{Y_2}(\omega)\Big|_{j\omega=-\frac{\lambda E_{SD}}{4M_S N_0}} = \frac{1}{\Gamma(N)}\left(\frac{E_{SD}}{4M_S N_0}\right)^{-M_S} \lambda^{-M_S} \exp(\upsilon)\int_{\upsilon}^{\infty} u^{-1}(1-\upsilon/u)^{N-1} e^{-u} du \tag{4.57}$$

Under $E_{SD}/4N_0 >> 1$ assumption, $1-\upsilon/u \approx 1$, we can rewrite (4.57) as

$$\Phi_{Y_2}(\omega)\Big|_{j\omega=-\frac{\lambda E_{SD}}{4M_S N_0}} = \frac{1}{\Gamma(N)}\left(\frac{E_{SD}}{4M_S N_0}\right)^{-M_S} \lambda^{-M_S} \exp(\upsilon)\Gamma(0,\upsilon) \tag{4.58}$$

Using the limiting approximation $\Gamma(0,\upsilon) \approx -\log(\upsilon)$ for $\upsilon \to 0$ [71], (4.58) further reduces to

$$\Phi_{Y_2}(\omega)\Big|_{j\omega=-\frac{\lambda E_{SD}}{4M_S N_0}} = \frac{1}{\Gamma(N)}\left(\frac{E_{SD}}{4M_S N_0}\right)^{-M_S} \lambda^{-M_S} \log\left(\frac{E_{SD}}{N_0}\right) \tag{4.59}$$

Substituting (4.59) and (4.51) in (4.50), we find the final PEP expression as

$$P(\mathbf{x},\hat{\mathbf{x}}) \le \frac{\lambda^{-M_S(N+1)}}{\Gamma(N)} \log\left(\frac{E_{SD}}{N_0}\right)\left(\frac{E_{SD}}{4M_S N_0}\right)^{-M_S(N+1)} \tag{4.60}$$

C.2 Derivation of Eq. (4.30)

In this Appendix, we derive the PEP expression for blind AaF relaying scheme assuming the limiting case of $E_{SR}/N_0 \to 0$. Under this scenario, $d^2(\mathbf{x},\hat{\mathbf{x}})$ is given as (4.29) where Y_1 and Y_2 are now defined by $Y_1 = \sum_{j=1}^{N}\sum_{i=1}^{M_S}\left|h_{SD,j}^{i}\right|^2$ and $Y_2 = \sum_{i=1}^{M_S}\left|\bar{h}_{SR}^{i}\right|^2$. Since $\left|h_{SD,j}^{i}\right|$ and $\left|\bar{h}_{SR}^{i}\right|$ are Rayleigh distributed, their characteristic functions are readily available (See Eq. (4.51)). Replacing those in (4.50), we find the PEP as

$$P(\mathbf{x},\hat{\mathbf{x}}) \le \left(\frac{E_{SD}}{4M_S N_0}\lambda\right)^{-NM_S}\left(1+\frac{E_{SR}}{4M_S N_0}\lambda\right)^{-M_S} \tag{4.61}$$

C.3 Derivation of Eq. (4.34)

In this Appendix, we derive the PEP expression for the CSI-assisted AaF relaying scheme assuming a fading $R \to D$ link. In this case, $d^2(\mathbf{x},\hat{\mathbf{x}})$ is given as

$$d^2(\mathbf{x},\hat{\mathbf{x}}) = \frac{\lambda E_{SD}}{M_S}\sum_{j=1}^{N}\sum_{i=1}^{M_S}\left|h_{SD,j}^{i}\right|^2 + \lambda\sum_{j=1}^{N}\alpha_j\sum_{m=1}^{M_T}\left|h_{RD,j}^{m}\right|^2\left(\sum_{m=1}^{M_R}\beta_{SR,m}\right)^2 \tag{4.62}$$

Under the assumption of $E_{SD}/N_0 = E_{RD}/N_0 >> 1$ with perfect power control and sufficiently large $E_{SR}/N_0 >> E_{SD}/N_0$ values, the scaling factor in (4.19) reduces to $\alpha_j = E_{SD}\left(M_T\left(\sum_{m=1}^{M_R}\beta_{SR,m}\right)^2\right)^{-1}$. Hence, (4.62) is simplified as

$$d^2(\mathbf{x},\hat{\mathbf{x}}) = \frac{\lambda E_{SD}}{M_S}\sum_{j=1}^{N}\sum_{i=1}^{M_S}\left|h_{SD,j}^{i}\right|^2 + \frac{\lambda E_{SD}}{M_T}\sum_{j=1}^{N}\sum_{m=1}^{M_T}\left|h_{RD,j}^{m}\right|^2 \tag{4.63}$$

(4.63) can be written in the same form as (4.48) where Y_1 and Y_2 are now defined by $Y_1 = \sum_{j=1}^{N}\sum_{i=1}^{M_S}\left|h_{SD,j}^{i}\right|^2$ and $Y_2 = \sum_{j=1}^{N}\sum_{m=1}^{M_T}\left|h_{RD,j}^{m}\right|^2$. Since $\left|h_{SD,j}^{i}\right|$ and $\left|\bar{h}_{SR}^{i}\right|$ are Rayleigh distributed, their characteristic functions are readily available. c.f., (4.51). Replacing those in (4.50), we find the PEP as

$$P(\mathbf{x},\hat{\mathbf{x}}) \le \left(\frac{E_{SD}}{4M_S N_0}\right)^{-N(M_S+M_T)} \lambda^{-N(M_S+M_T)} \tag{4.64}$$

C.4 Derivation of Eq. (4.36)

In this Appendix, we derive the PEP expression for the CSI-assisted AaF relaying scheme assuming the limiting case of $E_{SR}/N_0 \to 0$. Under this scenario, $d^2(\mathbf{x},\hat{\mathbf{x}})$ is given by (4.35). Substituting (4.35) in (4.22), we find the PEP expression as

$$P(\mathbf{x},\hat{\mathbf{x}}) \le \underset{|h^i_{SD,j}|}{\mathrm{E}}\left[\exp\left(-\frac{\lambda E_{SD}}{4M_S N_0}\sum_{j=1}^{N}\sum_{i=1}^{M_S}\left|h^i_{SD,j}\right|^2\right)\right] \times \underbrace{\lim_{E_{SR}/N_0\to 0}\underset{|\beta_{SR,m}|}{\mathrm{E}}\left[\exp\left(-\frac{1}{\nu}\frac{\lambda N}{4M_R M_S}\frac{E_{SR}}{N_0}\left(\sum_{m=1}^{M_R}\beta_{SR,m}\right)^2\right)\right]}_{\kappa} \tag{4.65}$$

For the limiting case of $E_{SR}/N_0 \to 0$, it can be easily noticed that $\kappa \to 1$. Therefore, the first term in this case evidently dominates the performance. Performing the expectation with respect to $\left|h^i_{SD,j}\right|$, which is Rayleigh distributed, PEP is found as

$$P(\mathbf{x},\hat{\mathbf{x}}) \le \left(\frac{\lambda E_{SD}}{4M_S N_0}\right)^{-NM_S} \tag{4.66}$$

C.5 Derivation of Eq. (4.38)

In this Appendix, we derive the PEP expression for the CSI-assisted AaF relaying under the assumption of a non-fading $R \to D$ link. Replacing $\alpha_j = 1\Big/M_T\left(\sum_{m=1}^{M_R}\beta_{SR,m}\right)^2$ in (4.33), we have

$$d^2(\mathbf{x},\hat{\mathbf{x}}) = \frac{\lambda E_{SD}}{M_S}\sum_{j=1}^{N}\sum_{i=1}^{M_S}\left|h^i_{SD,j}\right|^2 + \lambda N E_{SD}\,. \tag{4.67}$$

Substituting (4.67) in (4.22) and taking the expectation with respect to $\left|h^i_{SD,j}\right|$ which is Rayleigh distributed, we find PEP as

$$P(\mathbf{x},\hat{\mathbf{x}}) \le \left(\frac{E_{SD}}{4M_S N_0}\right)^{-NM_S}\lambda^{-NM_S}\exp\left(-N\lambda\frac{E_{SD}}{4N_0}\right) \tag{4.68}$$

Chapter 5
Conclusions and Future Work

Introduction

In this final chapter, we summarize the contributions of the work presented in this dissertation and discuss several potential extensions to our work.

5.1 Research Contributions

Cooperative networks have recently attracted much attention and fundamental information-theoretic aspects of these networks have been already well documented. However, practical implementation of cooperative communication requires an in-depth investigation of several physical layer issues such as channel estimation and equalization integrating the underlying cooperation protocols and relaying modes. In this dissertation, we have designed and analyzed equalization and channel estimation schemes for cooperative communication and further investigated the deployment of multiple-antennas in cooperative networks. In further detail, we summarize our conclusions and main findings of this dissertation as follows:

In Chapter 2, we have proposed and analyzed time-domain and frequency-domain equalization for cooperative communication. The considered schemes D-TR-STBC, D-SC-STBC and D-OFDM-STBC are built upon the distributed implementation of STBCs with AaF re-

laying and allow low-complexity designs due to the underlying orthogonality of the code. Through PEP derivations, we have presented a diversity gain analysis for the three equalization schemes under consideration. Under the assumption of perfect power control for the relay terminal and high SNR for the underlying links, we have demonstrated that D-TR-STBC and D-SC-STBC schemes yield identical performance achieving a maximum diversity order of $L_1 + L_2 + 2$ for a non-fading $R \to D$ link and $L_3 + L_2 + 2$ for a non-fading $S \to R$ link, where L_1, L_2, and L_3 are the channel memory lengths for $S \to R$, $S \to D$ and $R \to D$ links, respectively. For the general case where all underlying links experience frequency selectivity, these two schemes achieve a diversity order of $\min(L_1, L_3) + L_2 + 2$. Under the same assumptions, the uncoded D-OFDM-STBC scheme achieves only a maximum diversity order of two since it is not able to exploit the underlying multipath diversity. However, by combining D-OFDM-STBC scheme with interleaving and a judiciously-designed outer code, we have demonstrated that it is able to provide the same diversity of D-TR-STBC and D-SC-STBC.

In Chapter 3, we have investigated non-coherent and mismatched-coherent receivers for distributed STBC operating in AaF relaying mode. First, we have studied ML sequence estimation for the distributed STBC scheme without assuming channel knowledge. Under quasi-static fading assumption, we have shown that the ML rule reduces to a simple form due to the orthogonality structure of STBC which allows us to develop a recursive expression. Through the PEP analysis, we have demonstrated that the proposed decoder achieves full diversity. As an alternative scheme, we have considered the mismatched-coherent receiver where channel estimation is carried through pilot symbols. We have demonstrated through PEP analysis that the mismatched-coherent receiver is able to collect the full diversity as its non-coherent competitor over quasi-static channels. We have further presented a comprehensive comparison of two competing schemes under various mobility scenarios.

In Chapter 4, we have investigated the effect of multiple antenna deployment assuming different relaying techniques. In particular, we have investigated the error rate performance of blind AaF, CSI-assisted AaF, and DaF schemes in a single-relay assisted transmission scenario where the source, relay, and destination terminals are equipped with M_S, $M_T = M_R$, and N antennas, respectively. Under the assumption of perfect power control for the relay terminal and high SNR for the underlying links, we have shown through the PEP analysis that the maximum diversity order is $\min(M_S, N) + M_S N$ for the underlying blind AaF scheme and $N(M_T + M_S)$ for both CSI-assisted AaF and DaF schemes. For the case of a non-fading $R \to D$ link, we have demonstrated that the considered blind AaF scheme is able to achieve a diversity order of $M_S(N+1)$. On the other hand, the maximum diversity order of CSI-assisted AaF and DaF schemes is large and can not be determined by an integer value.

5.2 Future Work

While several key results for cooperative communication have been reported in this dissertation, there are several possible research topics yet to be explored as extensions of the current work.

Our results in Chapter 2 are mainly limited to single-relay deployment. While we believe that our results can be extended in a straightforward manner to the general case of multiple relays through the deployment of G3, G4, H3, H4 STBCs [13] in a distributed fashion, further investigation is required to characterize how the diversity orders interact. It is also well known that space-time codes (conventional ones as well as their distributed versions) suffer a loss in throughput efficiency for more than two transmit antennas. To address transmission rate efficiency, so-called *quasi-orthogonal* STBCs (QO-STBCs) has been proposed in [101]. In QO-STBC, the orthogonality assumption is relaxed to achieve full transmission rate. In

[40], we have investigated time-domain equalization for QO-STBC over frequency-selective channels, exploiting the embedded quasi-orthogonal structure to design low-complexity receivers. Further application of QO-STBC to cooperative communication scheme still remains an interesting open problem. It would also be interesting to examine the performance for other fading distributions, such as Ricean and Nakagami fading.

In Chapter 2 of this dissertation, our performance analysis has assumed MLSE equalization although we did investigate the performance of MMSE equalizers via Monte-Carlo simulation. The complexity of MLSE equalizers is prohibitive for many applications particularly for long channel impulse responses and high order modulation. It would be of practical importance to investigate suboptimal techniques such as Zero-Forcing (ZF) [86], MMSE [86], and decision feedback (DF) [86] equalizers in the context of cooperative communication.

A key underlying assumption in this dissertation is that the cooperating terminals transmit with same power, i.e., equal power allocation. To improve overall performance and increase energy efficiency, the following two questions need to be addressed: 1) How much overall power should be shared between broadcasting and relaying phases?, 2) How much power should be allocated to relay-to-destination and source-to-destination links in the relaying phase? Recent results have shown that the performance of cooperative networks can be substantially improved by optimally distributing the power among cooperating terminals [99], [100]. However, the current results are mainly restricted to frequency-flat channels. Thus, a rich area for future research would be to investigate optimal power allocation rules for D-TR-STBC, D-SC-STBC, and D-OFDM-STBC schemes.

In Chapter 3, we have exploited the orthogonal structure of distributed STBCs to derive a non-coherent decoding rule which can be implemented in practice by a Viterbi-type algorithm. However, we have only considered Alamouti code which requires a single relay node

deployment, i.e., STBC designed for two transmit antennas [15]. Extension to multiple relays, design of a channel estimator without the imposed orthogonality assumption, and differential detection are possible further research areas on this topic. As for mismatched-coherent detection, there are several issues that can be addressed in the context of cooperative communication. For example, since for channel estimation purposes, pilot symbols are employed, there is a need for an optimal design. Recently, for non-cooperative scenarios, few results have emerged, which suggest that significant potential gain can be realized if pilot symbols are designed optimally and placed judiciously [102]-[105]. It is an open research question to determine the number of pilot symbols, the power allocated for pilot symbols, and the locations of these pilots for cooperative networks taking into account the relay location and relaying technique.

In chapter 4, we have analyzed the effects of multiple-antenna deployment over frequency flat fading channels. A potential future research area is to investigate multiple antenna deployment in broadband cooperative networks over frequency-selective channels and further consider the problem of power allocation for such a scenario.

Bibliography

[1] S. Y. Hui and K. H. Yeung, "Challenges in the Migration to 4G Mobile Systems," *IEEE Commun. Mag.*, vol. 41, pp. 54 - 59, December 2003

[2] T. S. Rappaport, *Wireless Communications: Principles and Practice*, Prentice Hall PTR, 2000.

[3] W. C. Jakes, *Microwave Mobile Communications*, New York: Wiley, 1974.

[4] D. Tse and P. Viswanath, *Fundamentals of Wireless Communication*, Cambridge University Press, 2005.

[5] A. Wittneben, "Base station modulation diversity for digital SIMULCAST," in *Proceedings of the IEEE Vehicular Technology Conference (VTC)*, pp. 848-853, May 1991.

[6] A. Wittneben, "A new bandwidth efficient transmit antenna modulation diversity scheme for linear digital modulation," in *Proceedings of the IEEE International Conference Communications (ICC)*, pp. 1630-1634, May 1993.

[7] J. H. Winters, "Diversity gain of transmit diversity in wireless systems with Rayleigh fading," *IEEE Trans. Veh. Technol.*, vol. 47, pp. 119-123, February 1998.

[8] V. Tarokh, N. Seshadri, and A.R. Calderbank, "Space-time codes for high data rates wireless communications: Performance criterion and code construction," *IEEE Trans. Inf. Theory*, vol. 44, pp. 744-765, 1998.

[9] J. G. Foschini, "Layered space-time architecture for wireless communication in a fading environment when using multi element antennas," *Bell Labs Tech. J.*, vol. 2, pp. 41-59, Autumn 1996.

[10] C. Kose and R. D. Wesel, "Universal space-time trellis codes," *IEEE Trans. Inf. Theory*, vol. 49, pp. 2717-2727, Oct. 2003.

[11] Z. Safar and K. J. R. Liu, "Systematic space-time trellis code construction for correlated Rayleigh-fading channels," *IEEE Trans. Inf. Theory*, vol. 50, pp. 2855-2865, Nov. 2004.

[12] L. Yonghui, B. Vucetic, Y. Tang, and Q. Zhang, "Space-time trellis codes with linear transformation for fast fading channels," *IEEE Signal Process. Lett.*, vol. 11, no. 11, pp. 895- 898, Nov. 2004.

[13] V. Tarokh, H. Jafarkhani, and A.R. Calderbank, "Space-time block coding from orthogonal designs," *IEEE Trans. Inf. Theory*, vol. 45, pp. 1456-1467, 1999.

[14] V. Tarokh, H. Jafarkhani, and A.R. Calderbank, "Space-time block coding for wireless communications: Performance results," *IEEE J. Sel. Areas Commun.*, vol. 17, pp. 451-460, 1999.1

[15] S. M. Alamouti, "Simple transmit diversity technique for wireless communications," *IEEE J. Sel. Areas Commun.*, vol. 16, pp. 1451-1458, 1998.

[16] H. Wang and X.-G. Xia, "Upper bounds of rates of complex orthogonal space-time block codes," *IEEE Trans. Inf. Theory*, vol. 49, no. 10, pp. 2788–2796, October 2003.

[17] S. Das, N. Al-Dhahir, and R. Calderbank, "Novel full-diversity high-rate STBC for 2 and 4 transmit antennas," *IEEE Commun. Lett.*, vol. 10, no. 3, pp. 171-173, March 2006.

[18] H. Jafarkhani and N. Seshadri, "Super-orthogonal space-time trellis codes", *IEEE Trans. Inf. Theory*, vol. 49, no. 4 , pp. 937-950, April 2003.

[19] B. Hassibi and B. Hochwald, "High-rate codes that are linear in space and time", *IEEE Trans. Inf. Theory*, vol. 48, no. 7 , pp. 1804-1824, July 2002.

[20] R. W. Heath and A. Paulraj, "Linear dispersion codes for MIMO Systems based on frame theory," *IEEE Trans. Signal Process.*, vol. 50, no. 10, 2429-2441, October 2002.

[21] B. Vucetic and J. Yuan, *Space-Time Coding*, John Wiley & Sons, May 2003.

[22] A. Paulraj, D. Gore and R. Nabar, *Introduction to Space-Time Wireless Communications*, Cambridge University Press, May 2003

[23] H. Jafarkhani, *Space-Time Coding: Theory and Practice*, Cambridge University Press, September 2005.

[24] A. Sendonaris, E. Erkip, and B. Aazhang, "User Cooperation Diversity – Part I: System Description," *IEEE Trans. Commun.*, vol. 51, pp. 1927-1938, Nov. 2003.

[25] A. Sendonaris, E. Erkip, and B. Aazhang, "User Cooperation Diversity – Part II: Implementation, Aspects and Performance Analysis," *IEEE Trans. Commun.*, vol. 51, pp 1939-1948, Nov. 2003

[26] J. N. Laneman, D. N. C. Tse, and G. W. Wornell, "Cooperative Diversity in Wireless Networks: Efficient Protocols and Outage Behavior," *IEEE Trans. Inf. Theory*, vol. 50, no. 12, pp. 3062-3080, Dec. 2004.

[27] J. N. Laneman, G. W. Wornell, and D. N. C. Tse, "An Efficient Protocol for Realizing Cooperative Diversity in Wireless Networks," in *Proceedings of the IEEE International Symposium on Information Theory (ISIT)*, Washington, DC, June 2001.

[28] J. N. Laneman and G. W. Wornell, "Distributed Space-Time Coded Protocols for Exploiting Cooperative Diversity in Wireless Networks," *IEEE Trans. Inf. Theory*, vol. 49, no. 10, pp. 2415-2525, Oct. 2003.

[29] E. V. D. Meulen, "Three-terminal communication channels," *Advances in Applied Probability*, vol. 3, pp. 120-154, 1971.

[30] T. M. Cover and A. A. El Gamal. "Capacity theorems for the relay channel," *IEEE Trans. Inf. Theory*, vol. 25, pp. 572-584, Sept. 1979.

[31] T. E. Hunter and Aria Nosratinia, "Cooperation diversity through coding" *in Proceedings of the IEEE International Symposium on Information Theory (ISIT)*, Lausanne, Switzerland, June 2002.

[32] T. E. Hunter and Aria Nosratinia, "Diversity through coded cooperation," *IEEE Trans. Wireless Commun.*, vol. 5, no. 2, pp. 283-289, Feb. 2006.

[33] R. U. Nabar, H. Bölcskei, and F. W. Kneubühler, "Fading relay channels: Performance limits and space-time signal design", *IEEE J. Sel. Areas Commun.*, vol. 22, no. 6, pp. 1099-1109, August 2004.

[34] K. Azarian, H. El Gamal, and P. Schniter, "On the achievable diversity multiplexing tradeoff in half-duplex cooperative channels," *IEEE Trans. Inf. Theory*, vol. 51, pp. 4152–4172, Dec. 2005.

[35] N. Al-Dhahir, "Single Carrier Frequency Domain Equalization for Space Time Block Coded Transmissions over Frequency Selective Fading Channels," *IEEE Commun. Lett.*, vol. 5, no. 7, pp. 304-306, July 2001.

[36] Z. Liu, G. B. Giannakis, A. Scaglione, and S. Barbarossa, "Block Precoding and Transmit-Antenna Diversity for Decoding and Equalization of Unknown Multipath Channels," *in Proceedings of the of 33rd Asilomar Conference Signals, Systems, and Computers*, Nov. 1999

[37] E. Lindskog and A. Paulraj, "A Transmit Diversity Scheme for Channel with ISI," in *Proceedings of the International Conference on Communications (ICC)*, June 2000.

[38] H. Mheidat, M. Uysal and N. Al-Dhahir, "Comparative Analysis of Equalization Techniques for STBC with Application to EDGE", in *Proceedings of the IEEE Vehicular Technology Conference (VTC)*, Milano, Italy, May 2004.

[39] H. Mheidat, M. Uysal and N. Al-Dhahir, "Time-and Frequency-Domain Equalization for Quasi-Orthogonal STBC over Frequency-Selective Channels", in *Proceedings of the International Conference on Communications (ICC)*, Paris, France, July 2004.

[40] H. Mheidat, M. Uysal, and N. Al-Dhahir, "Quasi-Orthogonal Time-Reversal Space-Time Block Coding for Frequency-Selective Fading Channels", to appear in *IEEE Trans. Signal Process.*

[41] S. Yatawatta and A. P. Petropulu, " A Multi-user OFDM System with User Cooperation," *38th Asilomar Conference on Signals, Systems, and Computers*, Nov. 2004.

[42] P. A. Anghel and M. Kaveh, "Exact symbol error probability of a Cooperative network in a Rayleigh-fading environment", *IEEE Trans. Wireless Commun.*, vol. 3, no. 5, p. 1416 – 1421, Sept. 2004

[43] P. A. Anghel and M. Kaveh, "Relay assisted uplink communication over frequency-selective channels", in *Proceedings of the 4th IEEE Workshop on Signal Processing Advances in Wireless Communications (SPAWC)*, June, 2003.

[44] X. Li, F. Ng, J. Hwu and M. Chen, "Channel equalization for STBC-encoded cooperative transmissions with asynchronous transmitters," in *Proceedings of the 39th Asilomar Conference on Signals, Systems and Computers*, Pacific Grove, CA, Oct. 30-Nov. 2, 2005.

[45] G. Scutari and S. Barbarossa, "Distributed Space–Time Coding for Regenerative Relay Networks," *IEEE Trans. Wireless Commun.*, vol. 4, no. 5, pp.2387-2399, September 2005

[46] H. Mheidat, M. Uysal, and N. Al-Dhahir, "Equalization Techniques for Distributed Space-Time Block Codes with Amplify-and-Forward Relaying", accepted for publication in *IEEE Trans. Signal Process*.

[47] H. Mheidat, M. Uysal, and N. Al-Dhahir, "Equalization Techniques for Space-Time Coded Cooperative Systems", in *Proceedings of the IEEE Vehicular Technology Conference (VTC)*, Los Angeles, California, USA, September 2004.

[48] H. Mheidat, M. Uysal, and N. Al-Dhahir, "Distributed Space-Time Block Coded OFDM for Relay-Assisted Transmission", in *Proceedings of the IEEE International Conference on Communications (ICC)*, Istanbul, Turkey, June 2006.

[49] H. Mheidat, M. Uysal, and N. Al-Dhahir, "Time-Reversal Space-Time Equalization for Amplify-and-Forward Relaying", in *Proceedings of the IEEE International Conference on Communications (ICC)*, Istanbul, Turkey, June 2006.

[50] H. Mheidat, M. Uysal, and N. Al-Dhahir, "Single-Carrier Frequency Domain Equalization for Broadband Cooperative Communications", in *Proceedings of the IEEE Wireless Communications and Networking Conference (WCNC)*, Las Vegas, Nevada, USA, April 2006.

[51] D. Chen and J. N. Laneman, "Non-coherent Demodulation for Cooperative Wireless Systems," in *Proceedings of the IEEE Global Telecommunications Conference (GLOBECOM)*, Dallas, TX, Nov. 2004

[52] P. Tarasak, H. Minn, and V.K. Bhargava, "Differential Modulation for Two-User Cooperative Diversity Systems," *IEEE J-SAC: Differential and Non coherent Wireless Communications*, vol. 23, no. 9, pp. 1891-1900, Sept. 2005

[53] T. Wang, Y. Yao, and G. B. Giannakis, "Non-Coherent Distributed Space-Time Processing for Multiuser Cooperative Transmissions," in *Proceedings of the IEEE Global Telecommunications Conference (GLOBECOM)*, St. Louis, December 2005

[54] S. Yiu, R. Schober, and L. Lampe, "Distributed Space-Time Block Coding," *IEEE Trans. Commun.*, vol. 54, no.7, pp.1195-1206, July 2006.

[55] S. Yiu, R. Schober, and L. Lampe, "Non-coherent Distributed Space-Time Block Coding," in *Proceedings of the IEEE Vehicular Technology Conference (VTC)*, Dallas, USA, September 2005.

[56] R. Annavajjala, P. Cosman, and L. Milstein, "On the Performance of Optimum Non-coherent Amplify-and-Forward Reception for Cooperative Diversity," *IEEE Military Communications Conference (MILCOM 2005)*, Atlantic City, USA, Oct. 2005.

[57] H. Mheidat and M. Uysal, "Non-Coherent and Mismatched-Coherent Receivers for Distributed STBCs with Amplify-and-Forward Relaying", under second round review in *IEEE Trans. Wireless Commun.*

[58] M. Uysal and H. Mheidat, "Maximum-Likelihood Detection for Distributed Space-Time Block Coding", ," in *Proceedings of the IEEE Vehicular Technology Conference (VTC)*, Los Angeles, California, USA, September 2004.

[59] P. Gupta and P. R. Kumar, "The capacity of wireless networks," *IEEE Trans. Inf. Theory*, vol. 46, pp. 388–404, Mar. 2002.

[60] M. Gastpar and M. Vetterli, "On the capacity of wireless networks: The relay case," in *Proceedings of the IEEE INFOCOM*, New York, USA, June 2002.

[61] R. Pabst, B. H. Walke, D. C. Schultz, P. Herhold, H. Yanikomeroglu, S. Mukherjeee, H. Viswanathan, M. Lott, W. Zirwas, M. Dohler, H. Aghvami, D. D. Falconer, and G. P. Fettweis, "Relay-based deployment concepts for wireless and mobile broadband radio," *IEEE Commun. Mag.*, vol. 42, no. 9, pp. 80–89, Sep. 2004.

[62] P. Gupta, P.R. Kumar, "Towards an Information Theory of Large Networks: An Achievable Rate Region," *IEEE Trans. Inf. Theory*, vol. 49, pp. 1877-1894, August 2003.

[63] B. Wang, J. Zhang and A. Host-Madsen, "On the Capacity of MIMO Relay Channels," *IEEE Trans. Inf. Theory*, vol. 51, no. 1, pp. 29-43, Jan. 2005.

[64] Y. Jing B. Hassibi, "Cooperative Diversity in Wireless Relay Networks with Multiple-Antenna Nodes", *in IEEE International Symposium on Information Theory (ISIT)*, pp. 815 – 819, September 2005.

[65] S. Yiu and R. Schober, "On Distributed Space-Time Filtering," in *Proceedings of the IEEE Global Telecommunications Conference (GLOBECOM)*, St. Louis, USA, November 2005.

[66] S. Yiu, R. Schober, and L. Lampe, "Distributed Space-Time Block Coding for Cooperative Networks with Multiple-Antenna Nodes," in *Proceedings of IEEE Workshop on Computational Advances in Multi-Sensor Adaptive Processing (CAMSAP)*, Puerto Vallarta, Mexico, December 2005.

[67] H. Mheidat and M. Uysal "Impact of Receive Diversity on the Performance of Amplify-and-Forward Relaying under APS and IPS Power Constraints", *IEEE Commun. Lett.*, vol. 10, no. 6, p. 468-470, June 2006.

[68] H. Mheidat, M. Uysal, and M. M. Fareed "Cooperative Diversity with Multiple-Antenna Nodes in Fading Relay Channels," to be submitted to *IEEE Trans. Wireless Commun.*

[69] S. Zhou and G. B. Giannakis, "Single-Carrier Space-Time Block Coded Transmissions over Frequency-Selective Fading Channels", *IEEE Trans. Inf. Theory*, vol. 49, no. 1, pp. 164-179, January 2003

[70] G. Forney Jr., "Maximum-Likelihood Sequence Estimation of Digital Sequence in the Presence of Intersymbol Interference," *IEEE Trans. Inf. Theory*, vol. 18, pp. 363-378, May 1972.

[71] I. S. Gradshteyn and I. M. Ryzhik, *Table of Integrals, Series and Products*, Academic Press, 2000.

[72] H. Sari, G. Karam and I. Jeanclaude, "Transmission Techniques for Digital Terrestrial TV Broadcasting", *IEEE Commun. Mag.*, no. 2, February 1995.

[73] E. Biglieri, D. Divsalar, M. K. Simon and P. J. McLane, *Introduction to Trellis-Coded Modulation with Applications,* Macmillan Publishing, 1991.

[74] S. M. Alamouti, V. Tarokh and P. Poon, "Trellis coded modulation and transmit diversity: Design criteria and performance evaluation", in *Proceedings of IEEE International Conference on Universal Personal Communications (ICUPC),* pp. 703-707, October 1998.

[75] M. Uysal and C. N. Georghiades, "Analysis of Concatenated Trellis Coded STBC Schemes over Rician Fading Channels", in *Proceedings of the 39th Allerton Conference on Communication, Control and Computing*, Monticello, USA, October 2001.

[76] Y. Gong and K. B. Letaief, "Concatenated Space-Time Block Coding with Trellis Coded Modulation in Fading Channels", *IEEE Trans. Wireless Commun.*, vol. 1, no. 4 , p.580-590, October 2002.

[77] M. Uysal and C. N. Georghiades, "Upper Bounds on the BER Performance of MTCM-STBC Schemes over Shadowed Rician Fading Channels", *Eurasip Journal on Applied Signal Processing*, vol. 4, no. 9, p. 1238-1245, Aug. 2004.

[78] Y. Gong and K. B. Letaief, "An Efficient Space-Frequency Coded OFDM system for Broadband Wireless Communications", *IEEE Trans. Commun.*, vol. 51, no.12, p. 2019-2029, December 2003.

[79] Z. Liu, Y. Xin, and G. B. Giannakis, "Space-Time-Frequency Coded OFDM over Frequency-Selective Fading Channels," *IEEE Trans. Signal Process.*, vol. 50, no. 10, pp. 2465-2476, October 2002**.**

[80] S. Zhou and G. B. Giannakis, "Space-Time Coding with Maximum Diversity Gains over Frequency-Selective Fading Channels," *IEEE Signal Process. Lett*., vol. 8, no. 10, pp. 269-272, October 2001.

[81] A. Bletsas, A. Khisti, D. Reed, A. Lippman, "A simple Cooperative diversity method based on network path selection", *IEEE J. Sel. Areas Commun.* vol. 24, no. 3, pp. 659 - 672, March 2006.

[82] E. Baccarelli and S. Galli, "New results about analysis and design of TCM for ISI channels and combined equalization/decoding", *IEEE Trans. Commun.*, vol .46, no. 4, p. 417-420, April 1998.

[83] K. A. Hamied and G. L. Stuber, "Performance of trellis-coded modulation for equalized multipath fading ISI channels", *IEEE Trans. Veh. Technol.*, vol. 44, no. 1, p.50–58, Feb. 1995.

[84] M. K. Simon and M. S. Alouini, *Digital Communication Over Fading Channels: A Unified Approach to Performance Analysis,* New York: Wiley-Interscience, 2000.

[85] A. Stuart and J. K. Ord, *Kendall's Advanced Theory of Statistics*, 5th ed., Griffin and Co., London, 1987

[86] J. G.Proakis, *Digital Communications*, 2nd ed. , New York: McGraw-Hill, 1989.

[87] X. Yu and S. Pasupathy, "Innovations-based MLSE for Rayleigh fading channels", *IEEE Trans. Commun.*, vol. 43, no. 2/3/4, pp. 1534-1544, Feb./Mar./Apr. 1995.

[88] R. A. Horn and C.R. Johnson, *Matrix Analysis*, Cambridge University Press, Cambridge, 1990.

[89] M. Uysal and C. N. Georghiades, "Efficient Implementation of a Maximum-Likelihood Detector for Space-Time Coded Systems", *IEEE Trans. Commun.*, vol. 51, no.4, p. 251-254, April 2003.

[90] B. M. Hochwald and T. L. Marzetta, "Unitary Space-Time Modulation for Multiple-Antenna Communications in Rayleigh Flat Fading," *IEEE Trans. Inf. Theory*, vol. 46, no. 2, pp. 543-564, Mar. 2000.

[91] P. Stoica and R. Moses, *Introduction to Spectral Analysis*. Upper Saddle River, NJ: Prentice-Hall, 1997.

[92] S. M. Kay, *Fundamentals of Statistical Signal Processing: Estimation Theory*, Prentice-Hall, New Jersey, 1993.

[93] J. K. Cavers, "An analysis of pilot symbol assisted modulation for Rayleigh fading channels", *IEEE Trans. Veh. Technol.*., vol. 40, pp. 686-693, Nov.1991.

[94] M. Uysal, "Diversity Analysis of Space-Time Coding in Cascaded Rayleigh Fading Channels", *IEEE Commun. Lett.*, vol. 10, no. 3, pp. 165 – 167, March 2006.

[95] M. Brehler and M. K. Varanasi, "Asymptotic error probability analysis of quadratic receivers in Rayleigh-fading channels with applications to a unified analysis of coherent and non-coherent space-time receivers," *IEEE Trans. Inf. Theory*, vol. 47, no. 6, pp. 2383-2399, Sep. 2001.

[96] V. Tarokh, A. Naguib, and N. Seshadri, "Space-Time codes for high data rate wireless communication: performance criteria in the presence of channel estimation errors, mobility, and multiple paths," *IEEE Trans. Commun.*, vol. 47, no. 2, pp. 199–207, Feb. 1999.

[97] E. G. Larsson, "Diversity and channel estimation errors," *IEEE Trans. Commun.*, vol. 52, no. 2, pp. 205–208, Feb. 2004.

[98] K. Ahmed, C. Tepedelenlioglu, and A. Spanias, "PEP-based optimal training for MIMO systems in wireless channels," in *Proceedings of the IEEE International Conference on Acoustics, Speech, and Signal Processing* (*ICASSP)*, Philadelphia, USA, March 2005

[99] M. M. Fareed and M. Uysal, "BER-optimized power allocation for fading relay channels," *IEEE Trans. Wireless Commun.*, submitted to publication.

[100] Y. Jing and B. Hassibi, "Distributed space-time coding in wireless relay networks – Part I: Basic diversity results," *IEEE Trans. Wireless Commun.*, submitted for publication.

[101] H. Jafarkhani, "A Quasi-Orthogonal Space-Time Block Code," *IEEE Trans. Commun.*, vol. 49, pp. 1-4, Jan. 2001.

[102] S. Adireddy and L. Tong, "Optimal placement of known symbols for slowly varying frequency selective channels," *IEEE Trans. Wireless Commun.*, vol. 4, no. 4, pp. 1292- 1296, July 2005.

[103] B. Hassibi and B. Hochwald, "How much training is needed in multiple antenna wireless links," *IEEE Trans. Inf. Theory*, vol. 49, no. 4, pp. 951–963, 2003.

[104] J. Baltersee, G. Fock, and H. Meyr, "An information theoretic foundation of synchronized detection," *IEEE Trans. Commun.*, vol. 49, no. 12, pp. 2115–2123, 2001.

[105] X. Ma, G. Giannakis, and S. Ohno, "Optimal training for block transmission of doubly selective wireless fading channels," *IEEE Trans. Signal Process.*, vol. 51, no. 5, pp. 1351–1366, 2003.